VOLUME 84 NO. EM1
JANUARY 1958

JOURNAL of the

Engineering Mechanics Division

PROCEEDINGS OF THE
AMERICAN SOCIETY
OF CIVIL ENGINEERS

Journal of the
ENGINEERING MECHANICS DIVISION
Proceedings of the American Society of Civil Engineers

CONTENTS

January, 1958

Papers

Paper 1494 January, 1958 EM 1

Journal of the
ENGINEERING MECHANICS DIVISION
Proceedings of the American Society of Civil Engineers

MATRIX ANALYSIS OF BEAMS

Ray W. Clough,[1] A.M. ASCE
(Proc. Paper 1494)

SUMMARY

Matrix formulation of the general theory of structures has been the subject of several recent papers. In the present paper, the application of a matrix procedure to the analysis of structures consisting of flexural members is presented. The procedure may be applied to non-uniform as well as uniform beams, and permits consideration of shear distortion effects. Four examples demonstrate the application of the method to various types of structures.

Notation

Symbols are defined where they are first introduced in the text, and the most important ones are also listed here for convenience. Underlining indicates that the symbol represents a matrix. A "prime" indicates a transposed matrix.

$\underline{f_n}$	= flexibility of element "n"
$\underline{f}$	= flexibility of complete system of elements
$\underline{b_0}$	= element forces in the primary system due to unit external loads
$\underline{b_1}$	= element forces in the primary system due to unit redundants
$\underline{D}$	= deflection of redundants due to unit redundants

Note: Discussion open until June 1, 1958. A postponement of this closing date can be obtained by writing to the ASCE Manager of Technical Publications. Paper 1494 is part of the copyrighted Journal of the Engineering Mechanics Division, Proceedings of the American Society of Civil Engineers, Vol. 84, No. EM1, January, 1958.

1. Associate Prof. of Civ. Eng., Univ. of California, Berkeley, Calif.

$\underline{X}$ = values of redundants due to unit external loads

$\underline{F}$ = flexibility matrix of the complete structure

$\underline{b}$ = stress matrix of the complete structure

$\underline{R}$ = external load system

ℓ = length of beam segment

ϕ = rotation of end of beam segment

$\theta = \phi \ell_o$ = linearized rotation of end of beam segment

M = moment at end of beam segment

$\mathcal{M} = M/l_o$ = linearized moment

EI = beam flexural stiffness

G = modules of rigidity

A' = effective shear area of beam

$\alpha = \frac{EI_o}{EI} \frac{l}{l_o}$ = bending flexibility factor

$\beta = \frac{6EI_o/l_o^2}{GA'} \frac{l}{l_o}$ = shear flexibility factor

$\gamma = \frac{6EI_o/l_o^3}{k}$ = elastic support flexibility factor

k = spring constant of elastic support

p = force acting in elastic support

P = external force applied to structure

m = external moment applied to structure

$\mu = m/l_o$ = linearized external moment

i,c,j, = superscripts referring to left end, center, and right end of a beam segment respectively

1,2,3, ... n = subscript indicating the number of the element considered

o = subscript indicating reference quantity

(It will be noted that the subscripts in the symbols $\underline{b_o}$ and $\underline{b_1}$ are exceptions to the above usage, but this should not cause any confusion.)

INTRODUCTION

At least two general approaches are available for the systematic analysis of beam flexibility and stresses. One of these is essentially an extension of the Holzer method of evaluating the critical frequencies of shaft vibrations. The initial developments in this method were made by Myklestad,(1) while

Thomson[2] and Marguerre[3] have concerned themselves with matrix formulations of procedure. This approach is well suited to the study of vibrations of beam systems, but is somewhat awkward to apply to static analyses.

On the other hand, the standard procedures of structural analysis, such as the virtual work (or dummy unit load) method provide very convenient means for evaluating stresses or deflections under static conditions. The method presented herein may be considered as a matrix systemizing of the virtual work procedure. The numerical operations which are involved correspond exactly to those which would be performed in the standard virtual work solution. The advantage of the matrix formulation lies in the fact that all problems may be treated by an efficient standardized procedure. Moreover, the mathematical operations necessary after the original matrices have been established are of such routine nature that they can be carried out by persons having no knowledge of structural analysis, or preferably by an electronic digital computer.

The direct results of this matrix procedure are two influence coefficient matrices: the first of these, the stress matrix, represents the forces in each of the members of the structure due to successive applications of unit values of the external loads; while the second, the flexibility matrix, represents the deflections at the points of loading due to unit values of the external loads. When these two matrices have been evaluated, it is a simple operation to obtain stresses or deflections due to any system of externally applied concentrated loads. (As is true of influence coefficient procedures in general, this method does not, without modification, make possible the analysis for distributed loads. Usually the simplest manner of handling a distributed load is to replace it by an equivalent system of concentrated loads applied at points for which influence coefficients have been obtained.)

The matrix formulation of structural theory which forms the basis for this paper was pioneered by Langefors[4] and recently was given a very thorough and effective treatment by Argyris.[5] The purpose of this paper is to demonstrate the application of the Argyris matrix equations to the analysis of stresses and deflections of various types of beam systems. A convenient approximate procedure for taking account of non-uniform beam stiffness is also presented and shown to give good results.

General Outline of the Method

In this presentation, the Argyris notation, as summarized by Hunt[6] will be used to represent the various matrices involved in the analysis. The principal matrix equations will be restated here for purposes of clarity.

The procedure involves first establishing a flexibility matrix $\underline{f}$ and two force transformation matrices $\underline{b_0}$ and $\underline{b_1}$. The flexibility matrix is diagonal matrix of submatrices $\underline{f_1}$, $\underline{f_2}$, $\underline{f_3}$, . . . $\underline{f_n}$, thus

$$\underline{f} = \begin{bmatrix} \underline{f_1} & 0 & 0 & \cdot & 0 \\ 0 & \underline{f_2} & 0 & \cdot & 0 \\ 0 & 0 & \underline{f_3} & \cdot & 0 \\ \cdot & \cdot & \cdot & \cdot & \cdot \\ 0 & 0 & 0 & \cdot & \underline{f_n} \end{bmatrix} \qquad \text{(a)}$$

where the submatrices f_1, etc., represent the flexibility of the "n" elements into which the structure is considered to be divided for purposes of analysis.

To establish the force transformation matrices, it is first necessary to make the system statically determinate in the usual way, by selecting a set of redundant forces (one for each degree of static in determinacy). The force transformation matrix b_0 then represents the static equilibrium relationships between the external loads applied to the structure and the forces developed in each element, the redundants being assigned arbitrary values (usually zero). Similarly, b_1 represents the equilibrium relationship between the redundant forces in the structure and the element forces. The b_1 matrix exists only for statically indeterminate structures, of course. Generally several different b_1 matrices could be set up for a given structure depending upon the particular set of forces which are selected as redundants. As is well known, the conditioning of the matrix which must be inverted in the solution of the structure will be influenced greatly by the choice of the redundants, but such considerations are not a part of the present discussion.

When the flexibility of the elements and force transformation matrices have been established, the analysis of the structure is carried out by a series of matrix operations as follows:

1) Evaluate the displacements corresponding to the redundants*

$$\underline{D} = \underline{b_1'}\,\underline{f}\,\underline{b_1} \qquad \text{(A-1)}$$

2) Compute the values of the redundants due to application of unit external loads

$$\underline{X} = -\underline{D^{-1}}\,\underline{b_1'}\,\underline{f}\,\underline{b_0} \qquad \text{(A-2)}$$

3) Compute the stress matrix, i.e. the total forces in all the elements of the structure due to unit external loads

$$\underline{b} = \underline{b_0} + \underline{b_1}\,\underline{X} \qquad \text{(A-3)}$$

4) Compute the flexibility matrix of the structure, i.e. the displacements corresponding to the external loads due to application of unit external loads

$$\underline{F} = \underline{b_0'}\,\underline{f}\,\underline{b} \qquad \text{(A-4)}$$

5) Check the structural continuity at the redundants when unit external loads are applied

$$\underline{b_1'}\,\underline{f}\,\underline{b} \stackrel{?}{=} \underline{0} \qquad \text{(A-5)}$$

After the stress and flexibility matrices have been obtained from Eqs. A-3 and A-4, the stresses $\underline{S}$ and deflections $\underline{r}$ due to any system of applied loads $\underline{R}$ may be calculated from following equations

$$\underline{S} = \underline{b}\,\underline{R} \qquad \text{(A-6)}$$

*The structure of this equation is discussed in the Appendix.

$$\underline{r} = \underline{F}\,\underline{R} \tag{A-7}$$

It will be noted that the procedure involves only matrix multiplications and additions except for the inversion of the matrix $\underline{D}$. This operation is equivalent[1] to the solution of the set of simultaneous equations obtained from the conditions of continuity imposed at the redundants. There will be as many conditions as there are redundants, hence the analysis of a structure indeterminate to the degree "m" will require the inversion of a matrix of order "m." Generally this inversion will cause little difficulty if the calculation is carried out on an automatic digital computer, but if the analysis is to be done by desk calculator the inversion may represent a large part of the total work to be done. In this case a reduction in the size of the matrix to be inverted may be very desirable. Langefors has pointed out(7) that such a reduction may be accomplished by analyzing parts of the structure first, and then combining these parts in a subsequent operation. (G. Kron has also made use of this concept in his "tearing" procedure, described in References 10 and 11.) In effect, the flexibility matrix of each subsection is obtained by following the procedure outlined in Eqs. A-1 to A-5. Then the subsections are joined by repeating the procedure, the subsections now being considered as structural elements. In order to carry out this joining operation, the forces acting at the points of contact of the subsections must be included in their flexibility matrices. In other words, the interconnection forces between the subsections must be considered as part of the external force systems acting on the subsections, even though these forces may not be required in the combined flexibility matrix. An analysis of this type is demonstrated in Example IV of this paper.

Flexibility of the Beam Segments

Since this presentation is limited to the analysis of beam type structures, only the flexibility of beam segments (and possible elastic supports) need be considered here. For the purposes of this discussion, it is convenient to define the flexibility of a beam segment in terms of the rotations at the ends of the segment developed by unit moments applied at the ends (see Fig. 1). Rotations and moments are considered positive in the directions shown in the figure. In matrix notation, the rotations of a beam segment in terms of the moments, are as shown in Eqs. 1, in which $\tilde{f}_n$ is the flexibility matrix of this beam segment. When flexural elements are combined with linear elements, such as elastic supports, it is somewhat more convenient to express the flexibility in terms of linear forces and displacements; accordingly

$$\begin{Bmatrix} \phi^i \\ \phi^j \end{Bmatrix}_n = \begin{bmatrix} \tilde{f}^{ii} & \tilde{f}^{ij} \\ \tilde{f}^{ji} & \tilde{f}^{jj} \end{bmatrix}_n \begin{Bmatrix} M^i \\ M^j \end{Bmatrix}_n \tag{1}$$

or

$$\underline{\phi_n} = \underline{\tilde{f}_n}\ \underline{M_n} \tag{1a}$$

1. Further discussion of this point is given under "Discussion" at the end of the paper.

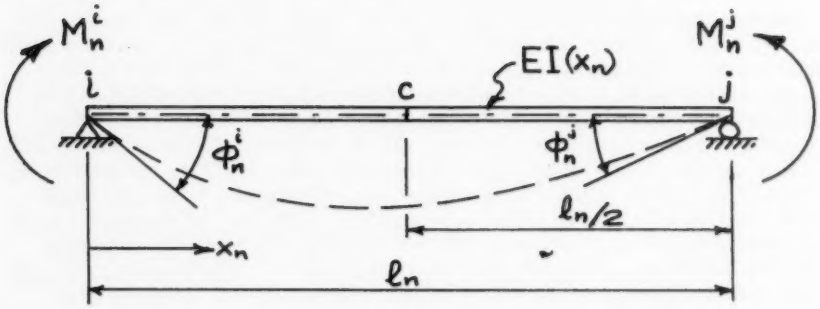

Fig. 1 Typical Beam Segment "n"

Eq. 1 will be written as shown in Eqs. 2. In Eqs. 2b, l_o is any convenient reference length.

$$\begin{Bmatrix} \Theta^i \\ \Theta^j \end{Bmatrix}_n = \begin{bmatrix} f^{ii} & f^{ij} \\ f^{ji} & f^{jj} \end{bmatrix}_n \begin{Bmatrix} m^i \\ m^j \end{Bmatrix}_n \tag{2}$$

or

$$\underline{\Theta_n} = \underline{f_n}\ \underline{m_n} \tag{2a}$$

where

$$\left.\begin{aligned} \Theta_n &= \Phi_n \ell_o \\ m_n &= M_n/\ell_o \end{aligned}\right\} \tag{2b}$$

For calculation purposes, the flexibility f_n may be expressed as the sum of two matrices: flexibility due to bending $\underline{f_{B_n}}$ and flexibility due to shear $\underline{f_{S_n}}$, thus

$$\underline{f_n} = \underline{f_{B_n}} + \underline{f_{S_n}} \tag{3}$$

The elements of these matrices represent the rotation at the ends of the segment due to unit moments applied at the ends of the segment. The bending flexibility terms may be calculated from the expressions of Eqs. 4. The values of these terms will depend, of course, upon the manner of variation of the stiffness EI(x). Various assumptions may be made regarding how this quantity varies, with corresponding differences in the results; however, only two cases will be considered here. If an average value for the stiffness EI_n is assumed constant through the length of the segment, the flexibility matrix will take the form of Eqs. 5. The symbols l_o and EI_o in Eq. 5a represent any convenient reference values of length and stiffness.

$$\left.\begin{aligned} f_B^{ii} &= \int_0^{\ell_n} \frac{(\ell_n - x_n)^2}{EI(x_n)}\, dx_n \\ f_B^{ij} = f_B^{ji} &= \int_0^{\ell_n} \frac{x_n(\ell_n - x_n)}{EI(x_n)}\, dx_n \\ f_B^{jj} &= \int_0^{\ell_n} \frac{x_n^2}{EI(x_n)}\, dx_n \end{aligned}\right\} \tag{4}$$

$$\underline{f_{Bn}} = \frac{\ell_o^3}{6EI_o}\,\alpha_n \begin{bmatrix} 2 & 1 \\ 1 & 2 \end{bmatrix} \tag{5}$$

where

$$\alpha_n = \frac{\ell_n}{\ell_o}\,\frac{EI_o}{EI_n} \tag{5a}$$

On the other hand, if it is assumed that the flexibility $\frac{1}{EI}$ varies parabolically through the length of the segment the flexibility matrix is given by Eq. 6. $EI_n^{\,i}$, $EI_n^{\,c}$ and $EI_n^{\,j}$ being

$$\underline{f_{Bn}} = \frac{\ell_o^3}{EI_o} \begin{bmatrix} (0.9\alpha_n^i + 1.2\alpha_n^c - 0.1\alpha_n^j) & (0.1\alpha_n^i + 0.8\alpha_n^c + 0.1\alpha_n^j) \\ (0.1\alpha_n^i + 0.8\alpha_n^c + 0.1\alpha_n^j) & (-0.1\alpha_n^i + 1.2\alpha_n^c + 0.9\alpha_n^j) \end{bmatrix} \tag{6}$$

where

$$\left.\begin{aligned} \alpha_n^i &= \frac{\ell_n}{\ell_o}\,\frac{EI_o}{EI_n^i} \\ \alpha_n^c &= \frac{\ell_n}{\ell_o}\,\frac{EI_o}{EI_n^c} \\ \alpha_n^j &= \frac{\ell_n}{\ell_o}\,\frac{EI_o}{EI_n^j} \end{aligned}\right\} \tag{6a}$$

values of the stiffness of the beam segment at the left end, middle, and right end respectively, and l_o and EI_o being reference values as before. Eq. 6 gives much better results than Eq. 5 if there is an appreciable variation of stiffness within the beam segment, and for such cases the extra effort involved in its evaluation is generally worthwhile.

Elements of the shear flexibility matrix may be evaluated similarly as shown in Eq. 7 in which G is the modulus of rigidity of the material and A[1]

$$f_{Sn}^{ii} = f_{Sn}^{jj} = -f_{Sn}^{ij} = -f_{Sn}^{ji} = \int_0^{\ell_n} \frac{1}{GA'(x_n)}\, dx_n \tag{7}$$

represents the effective shear area of the cross-section, (see for example, W.M. Fife and J. B. Wilbur, "Theory of Statistically Indeterminate Structures," McGraw-Hill, New York, 1937, p. 29). For a rectangular beam section A^1 is 5/6 of the total area, while for flanged beams it may be taken equal to the web area. As is apparent from Eq. 7, the shear flexibility matrix depends only upon the average value of the shear flexibility, $\frac{1}{GA^1}$, and may be expressed as shown in Eq. 8.

$$\underline{f_{s_n}} = \frac{\ell_o^3}{6EI_o}\,\beta_n \begin{bmatrix} 1 & -1 \\ -1 & 1 \end{bmatrix} \tag{8}$$

where

$$\beta_n = \frac{6EI_o/\ell_o^2}{GA'_n}\,\frac{\ell_n}{\ell_o} \tag{8a}$$

For a parabolic variation of the shear flexibility, the average value within the segment is given by Eq. 9 in which the superscripts have the same meaning as before.

$$\frac{1}{GA'_n} = \frac{1}{6}\left[\left(\frac{1}{GA'}\right)^i + \left(\frac{4}{GA'}\right)^c + \left(\frac{1}{GA'}\right)^j\right] \tag{9}$$

Eqs. 5 and 8 may be combined to give the total flexibility of the beam segment. Where bending flexibility may be represented by an average value, the combined flexibility matrix takes the form shown in Eq. 10a while a parabolic variation of the bending flexibility yields the matrix of Eq. 10b.

$$\underline{f_n} = \frac{\ell_o^3}{6EI}\begin{bmatrix} (2\alpha_n + \beta_n) & (\alpha_n - \beta_n) \\ (\alpha_n - \beta_n) & (2\alpha_n + \beta_n) \end{bmatrix} \tag{10a}$$

$$\underline{f_n} = \frac{\ell_o^3}{6EI_o}\begin{bmatrix} (0.9\alpha_n^i + 1.2\alpha_n^c - 0.1\alpha_n^j + \beta_n) & (0.1\alpha_n^i + 0.8\alpha_n^c + 0.1\alpha_n^j - \beta_n) \\ (0.1\alpha_n^i + 0.8\alpha_n^c + 0.1\alpha_n^j - \beta_n) & (-0.1\alpha_n^i + 1.2\alpha_n^c + 0.9\alpha_n^j + \beta_n) \end{bmatrix} \tag{10b}$$

Eq. 10a or 10b provides the only type of element flexibility matrix needed for the analysis of structures composed of beam or girder elements. In cases where the beams are mounted on elastic supports, however, the flexibility of the supports must also be considered. A linear elastic support of any type may be represented by a spring as shown in Fig. 2. The deflections of such an element may be represented as shown in the following equation,

$$\delta_n = f_{s_n}\,\rho_n \qquad \text{where} \qquad f_{s_n} = \frac{1}{k_n} \tag{b}$$

k_n being the spring constant. Since only one type of displacement is contemplated, the flexibility matrix for such an element consists of a single term. In order to facilate the combination of elastic supports into a beam

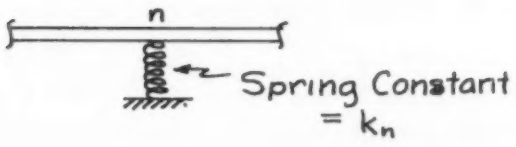

Fig. 2 Elastic Support "n"

system, it is convenient to express the spring flexibility in the form given in Eq. 11, EI_o

$$\underline{f_{\varepsilon_n}} = \frac{\ell_o^3}{6EI} \gamma_n \tag{11}$$

where

$$\gamma_n = \frac{6EI_o/\ell_o^3}{k_n} \tag{11a}$$

and l_o being reference values as before. The analysis of any type of beam system may now be carried out using the element flexibilities represented by Eq. 10a or 10b and Eq. 11.

Examples of Beam Analysis

I. Uniform Simple Beam

As an introductory example the deflections and rotations will be evaluated at a series of equally spaced points across the span of a uniform beam, due to vertical forces and moments applied at these points, as shown in Fig. 3.

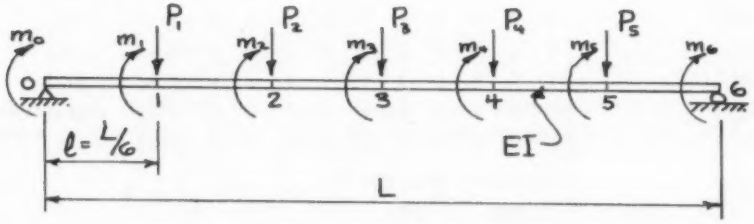

Fig. 3 Uniform Simple Beam

Flexibility Matrix:

In this uniform structure, all beam segments have the same flexibility, as shown in Eq. 12a (shear deformations being neglected).

$$\underline{f_1} = \underline{f_2} = \cdots = \underline{f_6} = \frac{\ell^3}{6EI}\begin{bmatrix} 2 & 1 \\ 1 & 2 \end{bmatrix} \tag{12a}$$

The complete flexibility matrix for all beams then becomes

$$\underline{f} = \frac{\ell^3}{6EI}\begin{bmatrix} 2 & 1 & 0 & 0 & . & . & 0 & 0 \\ 1 & 2 & 0 & 0 & . & . & 0 & 0 \\ 0 & 0 & 2 & 1 & . & . & 0 & 0 \\ 0 & 0 & 1 & 2 & . & . & 0 & 0 \\ . & . & . & . & . & . & . & . \\ . & . & . & . & . & . & . & . \\ 0 & 0 & 0 & 0 & . & . & 2 & 1 \\ 0 & 0 & 0 & 0 & . & . & 1 & 2 \end{bmatrix} \tag{12b}$$

Force Transformation:

For this statically determinate system, the redundant force matrix b_1 does not exist. Thus, the matrix b_0 represents the complete relationship between the applied loads and the member forces in terms of which the flexibility matrix has been expressed, as shown in Eq. 13a.

$$\begin{Bmatrix} m_1^i \\ m_1^j \\ m_2^i \\ m_2^j \\ m_3^i \\ m_3^j \\ m_4^i \\ m_4^j \\ m_5^i \\ m_5^j \\ m_6^i \\ m_6^j \end{Bmatrix} = \left(\frac{1}{6}\right)\begin{bmatrix} 0 & 0 & 0 & 0 & 0 & 6 & 0 & 0 & 0 & 0 & 0 & 0 \\ 5 & 4 & 3 & 2 & 1 & 5 & -1 & -1 & -1 & -1 & -1 & -1 \\ 5 & 4 & 3 & 2 & 1 & 5 & 5 & -1 & -1 & -1 & -1 & -1 \\ 4 & 8 & 6 & 4 & 2 & 4 & 4 & -2 & -2 & -2 & -2 & -2 \\ 4 & 8 & 6 & 4 & 2 & 4 & 4 & 4 & -2 & -2 & -2 & -2 \\ 3 & 6 & 9 & 6 & 3 & 3 & 3 & 3 & -3 & -3 & -3 & -3 \\ 3 & 6 & 9 & 6 & 3 & 3 & 3 & 3 & 3 & -3 & -3 & -3 \\ 2 & 4 & 6 & 8 & 4 & 2 & 2 & 2 & 2 & -4 & -4 & -4 \\ 2 & 4 & 6 & 8 & 4 & 2 & 2 & 2 & 2 & 2 & -4 & -4 \\ 1 & 2 & 3 & 4 & 5 & 1 & 1 & 1 & 1 & 1 & -5 & -5 \\ 1 & 2 & 3 & 4 & 5 & 1 & 1 & 1 & 1 & 1 & 1 & -5 \\ 0 & 0 & 0 & 0 & 0 & 0 & 0 & 0 & 0 & 0 & 0 & -6 \end{bmatrix}\begin{Bmatrix} P_1 \\ P_2 \\ P_3 \\ P_4 \\ P_5 \\ \mu_0 \\ \mu_1 \\ \mu_2 \\ \mu_3 \\ \mu_4 \\ \mu_5 \\ \mu_6 \end{Bmatrix} \tag{13a}$$

where $m_n = M_n/\ell$

$\mu_n = m_n/\ell$

In matrix symbols this equation may be written simply

$$\underline{m} = \underline{b_0}\ \underline{R} \tag{13b}$$

Solution:

The flexibility matrix for a statically determinate system is given by the matrix operation

$$\underline{F} = \underline{b}_o' \, \underline{f} \, \underline{b}_o \qquad (c)$$

which is equivalent to Eq. A-4 since $\underline{b}_o = \underline{b}$ in this case. Carrying out this operation yields the matrix shown in Eq. 14. Rows and Columns of this matrix are arranged in the sequence specified by the column matrix of external loads $\underline{R}$ in Eq. 13a. It may be used to evaluate the bending displacements and rotations induced by any system of applied loads and moments $\underline{R}$, as shown by Eq. A-5.

$$\underline{F} = \frac{L^3}{(216)^2 EI} \begin{bmatrix} 300 & 456 & 468 & 372 & 204 & 330 & 240 & 78 & -48 & -138 & -192 & -210 \\ & 768 & 828 & 672 & 372 & 480 & 408 & 192 & -60 & -240 & -348 & -384 \\ & & 972 & 828 & 468 & 486 & 432 & 270 & 0 & -270 & -432 & -486 \\ & & & 768 & 456 & 384 & 348 & 240 & 60 & -192 & -408 & -480 \\ & & & & 300 & 210 & 192 & 138 & 48 & -78 & -240 & -330 \\ & & & & & 432 & 234 & 72 & -54 & -144 & -198 & -216 \\ & & & & & & 252 & 90 & -36 & -126 & -180 & -198 \\ & & & & & & & 144 & 18 & -72 & -126 & -144 \\ & & & & & (\text{Symmetrical}) & & & 108 & 18 & -36 & -54 \\ & & & & & & & & & 144 & 90 & 72 \\ & & & & & & & & & & 252 & 234 \\ & & & & & & & & & & & 432 \end{bmatrix} \qquad (14)$$

Shear Flexibility:

To demonstrate the effect of shear distortions on the beam flexibility, a second calculation was made in which the shear terms were incorporated into the flexibility matrix of the beam segments. For this example, it was assumed that the beam under consideration was a 24" I 100# rolled section on a total span of 18 feet (1=3 ft.) for which the shear flexibility factor is given by

$$\beta = \frac{GEI/\ell^2}{GA'} = 1.528$$

making the total flexibility matrix of a single beam segment as shown in Eq. 15. Since the geometry of the system has not been changed, the force transformation matrix remains as shown in Eq. 13a. The flexibility of the beam was calculated as before, with partial results as shown in Eq. 14a below (only the vertical displacement due to vertical loads being shown, to save space).

$$\underline{f} = \underline{f}_B + \underline{f}_S = \frac{\ell^3}{GEI} \begin{bmatrix} 3.528 & -0.528 \\ -0.528 & 3.528 \end{bmatrix} \qquad (15)$$

$$\underline{F} = \frac{L^3}{(216)^2 EI} \begin{bmatrix} 345.8 & 492.7 & 495.5 & 390.3 & 213.2 \\ & 841.3 & 883.0 & 708.7 & 390.3 \\ & & 1054.5 & 883.0 & 495.5 \\ & & & 841.3 & 492.7 \\ & & & & 345.8 \end{bmatrix} \qquad (14a)$$

Comparing this with the corresponding portion of Eq. 14 it is evident that shear distortions have a significant effect on the deflections in this beam.

II. Tapered Cantilever Beam

Application of the suggested approximate procedure for treating non-uniform beams will be demonstrated by analysis of the flexibility of the tapered cantilever beam shown in Fig. 4, for which an exact solution has been published by Bisplinghoff.[8] Only vertical loads will be considered and shear distortion will be neglected.

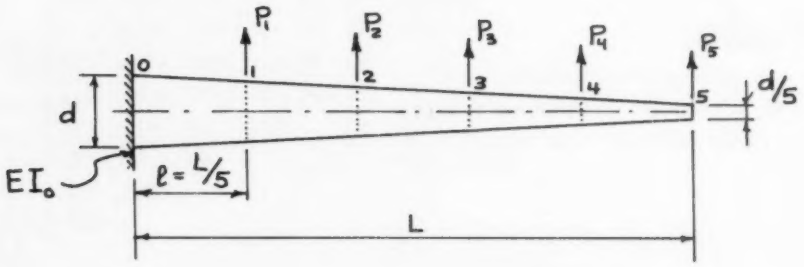

Fig. 4 Tapered Cantilever

Flexibility Matrix:

Since the depth of the beam varies continously it was necessary to evaluate the relative stiffness at the ends and center of each segment. The stiffness at the support was taken as the reference value EI_0. The flexibility matrix of each segment was then calculated according to Eq. 6. The flexibility matrix of the complete set of beam segments is given in Eq. 16a.

Force Transformation:

For this statically determinate system the relationship between the applied loads and the moments in the segments is found easily to be as shown in Eq. 17a. At this point it may be noted that the size of the matrices (Eqs. 16a and 17a) may be reduced for this type of loading, due to the fact that the moments at adjacent ends of the segments are equal. ($M_n^j = M_n^{i}{}_{+1}$). For this case the force transformation matrix of Eq. 17a can be reduced to the form in Eq. 17b.

$$\underline{f} = \frac{\ell^3}{6EI_o}\begin{bmatrix} 2.27 & 1.30 & 0 & 0 & 0 & 0 & 0 & 0 & 0 & 0 \\ 1.30 & 2.96 & 0 & 0 & 0 & 0 & 0 & 0 & 0 & 0 \\ 0 & 0 & 3.94 & 2.31 & 0 & 0 & 0 & 0 & 0 & 0 \\ 0 & 0 & 2.31 & 5.42 & 0 & 0 & 0 & 0 & 0 & 0 \\ 0 & 0 & 0 & 0 & 7.70 & 4.73 & 0 & 0 & 0 & 0 \\ 0 & 0 & 0 & 0 & 4.73 & 11.64 & 0 & 0 & 0 & 0 \\ 0 & 0 & 0 & 0 & 0 & 0 & 18.37 & 12.25 & 0 & 0 \\ 0 & 0 & 0 & 0 & 0 & 0 & 12.25 & 32.68 & 0 & 0 \\ 0 & 0 & 0 & 0 & 0 & 0 & 0 & 0 & 61.18 & 51.00 \\ 0 & 0 & 0 & 0 & 0 & 0 & 0 & 0 & 51.00 & 164.76 \end{bmatrix} \quad (16a)$$

$$\begin{Bmatrix} m_1^i \\ m_1^j \\ m_2^i \\ m_2^j \\ m_3^i \\ m_3^j \\ m_4^i \\ m_4^j \\ m_5^i \\ m_5^j \end{Bmatrix} = \begin{bmatrix} 1 & 2 & 3 & 4 & 5 \\ 0 & 1 & 2 & 3 & 4 \\ 0 & 1 & 2 & 3 & 4 \\ 0 & 0 & 1 & 2 & 3 \\ 0 & 0 & 1 & 2 & 3 \\ 0 & 0 & 0 & 1 & 2 \\ 0 & 0 & 0 & 1 & 2 \\ 0 & 0 & 0 & 0 & 1 \\ 0 & 0 & 0 & 0 & 1 \\ 0 & 0 & 0 & 0 & 0 \end{bmatrix} \begin{Bmatrix} P_1 \\ P_2 \\ P_3 \\ P_4 \\ P_5 \end{Bmatrix} \quad (17a)$$

where $m_n = M_n/\ell$

or

$$\underline{m} = \underline{b_o}\ \underline{R}$$

$$\begin{Bmatrix} m_1^i \\ m_2^i \\ m_3^i \\ m_4^i \\ m_5^i \end{Bmatrix} = \begin{bmatrix} 1 & 2 & 3 & 4 & 5 \\ 0 & 1 & 2 & 3 & 4 \\ 0 & 0 & 1 & 2 & 3 \\ 0 & 0 & 0 & 1 & 2 \\ 0 & 0 & 0 & 0 & 1 \end{bmatrix} \begin{Bmatrix} P_1 \\ P_2 \\ P_3 \\ P_4 \\ P_5 \end{Bmatrix} \quad (17b)$$

The flexibility matrix, Eq. 16a, may be put in the corresponding form by adding the rows (and columns) which correspond to the duplicated rows in Eq. 17a, i.e. 2 + 3, 4 + 5, 6 + 7, and 8 + 9. The last row (and column) may be dropped because no moments are developed corresponding to these terms. The reduced flexibility matrix thus takes the form of Eq. 16b. When the calculations are to be done by automatic computers, there is generally no great advantage to be gained by this type of reduction, and the matrices may

$$\underline{f} = \frac{\ell^3}{6EI_o}\begin{bmatrix} 2.27 & 1.30 & 0 & 0 & 0 \\ 1.30 & 6.90 & 2.31 & 0 & 0 \\ 0 & 2.31 & 13.12 & 4.73 & 0 \\ 0 & 0 & 4.73 & 30.01 & 12.25 \\ 0 & 0 & 0 & 12.25 & 93.86 \end{bmatrix} \tag{16b}$$

as well be left in their original form. However, if the operations are to be performed with desk calculators, the reduced form is considerably more convenient to use. The remaining examples in this paper are expressed in the reduced form to save space.

Results:

Performing the required matrix multiplications (Eq. c) the flexibility matrix for this tapered beam was found to be as shown in Eq. 18a. For comparison purposes, the exact values given by Bisplinghoff, and values

$$\underline{F} = \frac{\ell^3}{6EI_o}\begin{bmatrix} 2.27 & 5.84 & 9.41 & 12.98 & 16.55 \\ & 21.18 & 38.83 & 56.48 & 74.13 \\ & & 85.99 & 137.88 & 189.77 \\ & (\text{Symmetrical}) & & 258.75 & 391.87 \\ & & & & 712.33 \end{bmatrix} \tag{18a}$$

obtained by assuming a constant average value of $\frac{1}{EI}$ for each section are given in Eqs. 18b and 18c below. (The average value for each segment was computed by a formula analogous to Eq. 9).

From Bisplinghoff (8):

$$\underline{F} = \frac{\ell^3}{6EI_o}\begin{bmatrix} 2.29 & 5.86 & 9.43 & 13.01 & 16.58 \\ & 21.21 & 38.85 & 56.48 & 74.12 \\ & & 86.02 & 137.93 & 189.90 \\ & (\text{Symmetrical}) & & 259.10 & 392.40 \\ & & & & 716.95 \end{bmatrix} \tag{18b}$$

Assuming Constant Segment Stiffness:

$$\underline{F} = \frac{\ell^3}{6EI_o}\begin{bmatrix} 2.6 & 6.5 & 10.4 & 14.4 & 18.3 \\ & 22.9 & 41.7 & 60.5 & 79.1 \\ & & 91.9 & 146.8 & 201.8 \\ & (\text{Symmetrical}) & & 277.6 & 421.0 \\ & & & & 799.9 \end{bmatrix} \tag{18c}$$

It is clear that the parabolic flexibility approximation is quite accurate in this case, whereas the assumption of uniform stiffness in each segment leads to sizable errors.

III. Beam Continous over Several Supports

The application of this matrix method to a statically indeterminate system will be demonstrated first by the analysis of a uniform beam continous over four supports, as shown in Fig. 5.

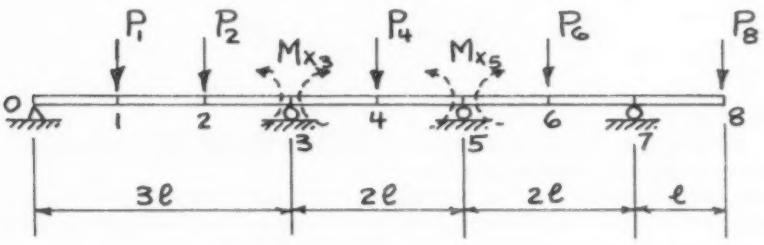

Fig. 5 Uniform Continuous Beam

Flexibility Matrix:

Since the beam is divided into segments of equal length, the flexibility of each segment is the same, and the reduced form of the flexibility matrix of the elements (neglecting shear distortion) is given by Eq. 19. This may be

$$\underline{f} = \frac{\ell^3}{6EI} \begin{bmatrix} 4 & 1 & 0 & 0 & 0 & 0 & 0 \\ 1 & 4 & 1 & 0 & 0 & 0 & 0 \\ 0 & 1 & 4 & 1 & 0 & 0 & 0 \\ 0 & 0 & 1 & 4 & 1 & 0 & 0 \\ 0 & 0 & 0 & 1 & 4 & 1 & 0 \\ 0 & 0 & 0 & 0 & 1 & 4 & 1 \\ 0 & 0 & 0 & 0 & 0 & 1 & 4 \end{bmatrix} \tag{19}$$

compared with the unreduced form of the matrix shown in Eq. 12b. Note that the first and last row and column have been omitted because no moments are developed at the ends of the beam.

Force Transformations:

Moments in the beam over the supports at points 3 and 5 are taken as the redundants (M_{x3} and M_{x5}). On this basis, the force transformation matrices take the reduced form indicated in Eq. 20.

$$\begin{Bmatrix} m_2^i \\ m_3^i \\ m_4^i \\ m_5^i \\ m_6^i \\ m_7^i \\ m_8^i \end{Bmatrix} = \frac{1}{6} \left[\begin{array}{ccccc:cc} 4 & 2 & 0 & 0 & 0 & 2 & 0 \\ 2 & 4 & 0 & 0 & 0 & 4 & 0 \\ 0 & 0 & 0 & 0 & 0 & 6 & 0 \\ 0 & 0 & 3 & 0 & 0 & 3 & 3 \\ 0 & 0 & 0 & 0 & 0 & 0 & 6 \\ 0 & 0 & 0 & 3 & -3 & 0 & 3 \\ 0 & 0 & 0 & 0 & -6 & 0 & 0 \end{array}\right] \begin{Bmatrix} P_1 \\ P_2 \\ P_4 \\ P_6 \\ P_8 \\ \hdashline X_3 \\ X_5 \end{Bmatrix} \quad \text{where } m_n = M_n/\ell \quad X_n = M_{x_n}/\ell \tag{20}$$

or $$\underline{m} = [b_0 \vdots b_1] \begin{Bmatrix} R \\ \hdashline X \end{Bmatrix}$$

Results:

Following the matrix operations of Eqs. A-1 through A-4, the results shown in Eqs. 21 were obtained.

$$\underline{D} = \frac{\ell^3}{3EI} \begin{bmatrix} 5 & 1 \\ 1 & 4 \end{bmatrix} \tag{21a}$$

$$\underline{X} = \frac{1}{228} \begin{bmatrix} 64 & 80 & 27 & -9 & 12 \\ -16 & -20 & 36 & 45 & -60 \end{bmatrix} \tag{21b}$$

$$\underline{b} = \frac{1}{1368} \begin{bmatrix} 784 & 296 & -54 & 18 & -24 \\ 200 & 592 & -108 & 36 & -48 \\ -384 & -480 & -162 & 54 & -72 \\ -144 & -180 & 495 & -108 & 144 \\ 96 & 120 & -216 & -270 & 360 \\ 48 & 60 & -108 & 549 & -504 \\ 0 & 0 & 0 & 0 & -1368 \end{bmatrix} \tag{21c}$$

$$\underline{F} = \frac{1}{49248} \frac{\ell^3}{EI} \begin{bmatrix} 15744 & 11472 & -2592 & 864 & -1152 \\ & 12288 & -3240 & 1080 & -1440 \\ & & 4806 & -1944 & 2592 \\ & \text{(Symmetrical)} & & 5778 & -9072 \\ & & & & 44928 \end{bmatrix} \tag{21d}$$

Eqs. 21c and 21d may be used to evaluate the forces and deflections in the beam produced by any system of applied loads $\underline{R}$ as shown by Eqs. A-6 and A-7.

IV. Continous Beam on Elastic Supports

As an example of the procedure for treating flexible supports, the stress and flexibility matrices will be calculated for the beam system shown in Fig. 6. The beam is uniform throughout its length, and all supporting springs

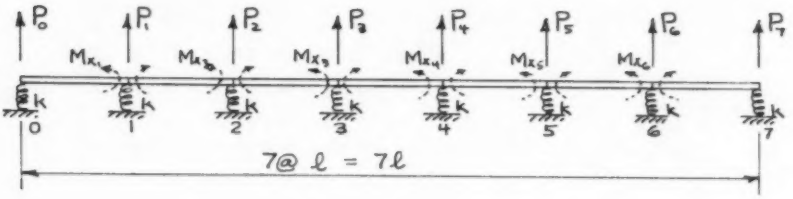

Fig. 6 Beam on Elastic Supports

have the same stiffness. This example will also be used to demonstrate how a multiply redundant system may be analyzed by parts to avoid the inversion of a large matrix. The standard solution will be outlined first for comparison.

Standard Solution:

For this uniform system, the flexibility matrices for the beam segments and the elastic supports are as shown in Eq. 22a. Thus the flexibility matrix of the complete system of elements takes the reduced form of Eq. 22b.

$$\left.\begin{aligned} f_B &= \frac{\ell^3}{6EI}\begin{bmatrix} 2 & 1 \\ 1 & 2 \end{bmatrix} \\ f_E &= \frac{\ell^3}{6EI}(1.5) \end{aligned}\right\} \qquad (22a)$$

Selecting the moments in the beam over the interior supports as the redundant forces, the force transformation matrices take the (reduced) form shown in Eq. 23.

The flexibility and force transformation matrices of Eqs. 22b and 23 having been established, the system could now be analyzed by the matrix operations of Eqs. A. In the process, because this structure is indeterminate to the sixth degree, it would be necessary to invert a sixth order matrix $\underline{D}$. This would offer no great difficulties in the present case, but for the illustrative purposes the analysis will be carried out here by parts. (It may be noted that considerable simplification could also be achieved in the analysis of this structure using the concepts of symmetry and anti-symmetry, but such ideas are not pertinent to the present discussion).

$$\underline{f} = \frac{1}{2}\cdot\frac{\ell^3}{6EI}\begin{bmatrix} 8 & 2 & 0 & 0 & 0 & 0 & 0 & 0 & 0 & 0 & 0 & 0 & 0 \\ & 8 & 2 & 0 & 0 & 0 & 0 & 0 & 0 & 0 & 0 & 0 & 0 \\ & & 8 & 2 & 0 & 0 & 0 & 0 & 0 & 0 & 0 & 0 & 0 \\ & & & 8 & 2 & 0 & 0 & 0 & 0 & 0 & 0 & 0 & 0 \\ & & & & 8 & 2 & 0 & 0 & 0 & 0 & 0 & 0 & 0 \\ & & & & & 8 & 0 & 0 & 0 & 0 & 0 & 0 & 0 \\ & & & & & & 3 & 0 & 0 & 0 & 0 & 0 & 0 \\ & & & & & & & 3 & 0 & 0 & 0 & 0 & 0 \\ & & & & & & & & 3 & 0 & 0 & 0 & 0 \\ & & & & & & & & & 3 & 0 & 0 & 0 \\ & & & & (\text{Symmetrical}) & & & & & & 3 & 0 & 0 \\ & & & & & & & & & & & 3 & 0 \\ & & & & & & & & & & & & 3 \end{bmatrix} \tag{22b}$$

$$\begin{Bmatrix} m_1^i \\ m_2^i \\ m_3^i \\ m_4^i \\ m_5^i \\ m_6^i \\ m_7^i \\ \beta_0 \\ \beta_1 \\ \beta_2 \\ \beta_3 \\ \beta_4 \\ \beta_5 \\ \beta_6 \\ \beta_7 \end{Bmatrix} = \left[\begin{array}{cccccccc:cccccc} 0 & 0 & 0 & 0 & 0 & 0 & 0 & 0 & 1 & 0 & 0 & 0 & 0 & 0 \\ 0 & 0 & 0 & 0 & 0 & 0 & 0 & 0 & 0 & 1 & 0 & 0 & 0 & 0 \\ 0 & 0 & 0 & 0 & 0 & 0 & 0 & 0 & 0 & 0 & 1 & 0 & 0 & 0 \\ 0 & 0 & 0 & 0 & 0 & 0 & 0 & 0 & 0 & 0 & 0 & 1 & 0 & 0 \\ 0 & 0 & 0 & 0 & 0 & 0 & 0 & 0 & 0 & 0 & 0 & 0 & 1 & 0 \\ 0 & 0 & 0 & 0 & 0 & 0 & 0 & 0 & 0 & 0 & 0 & 0 & 0 & 1 \\ 1 & 0 & 0 & 0 & 0 & 0 & 0 & 0 & -1 & 0 & 0 & 0 & 0 & 0 \\ 0 & 1 & 0 & 0 & 0 & 0 & 0 & 0 & 2 & -1 & 0 & 0 & 0 & 0 \\ 0 & 0 & 1 & 0 & 0 & 0 & 0 & 0 & -1 & 2 & -1 & 0 & 0 & 0 \\ 0 & 0 & 0 & 1 & 0 & 0 & 0 & 0 & 0 & -1 & 2 & -1 & 0 & 0 \\ 0 & 0 & 0 & 0 & 1 & 0 & 0 & 0 & 0 & 0 & -1 & 2 & -1 & 0 \\ 0 & 0 & 0 & 0 & 0 & 1 & 0 & 0 & 0 & 0 & 0 & -1 & 2 & -1 \\ 0 & 0 & 0 & 0 & 0 & 0 & 1 & 0 & 0 & 0 & 0 & 0 & -1 & 2 \\ 0 & 0 & 0 & 0 & 0 & 0 & 0 & 1 & 0 & 0 & 0 & 0 & 0 & -1 \end{array}\right] \begin{Bmatrix} P_0 \\ P_1 \\ P_2 \\ P_3 \\ P_4 \\ P_5 \\ P_6 \\ P_7 \\ \hline X_1 \\ X_2 \\ X_3 \\ X_4 \\ X_5 \\ X_6 \end{Bmatrix} \tag{23}$$

or

$$\underline{m} = \left[b_0 \vdots b_1\right]\left\{\frac{R}{X}\right\}$$

Analysis by Parts:

For this example, the structure will be analyzed by dividing it into two parts, analyzing them separately, and then rejoining them. This symmetrical structure will be divided into two identical parts, as shown in Fig. 7; thus only one subsection need by analyzed. In the analysis it will be observed that the process of joining the two subsections together is identical with the

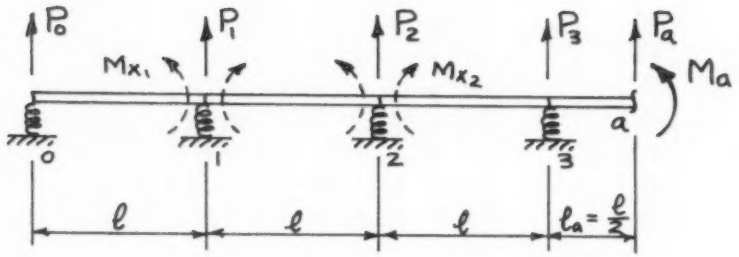

Fig. 7 Left-hand Subsection

standard indeterminate analysis, except that the "primary" structure is indeterminate and therefore requires a preliminary analysis.

The flexibility matrix for the subsection involves one element which is different from those representated in Eq. 22 b – the half length beam segment at the right end. For this segment, the flexibility matrix is given by Eq. 24a. The complete flexibility matrix of the subsection elements then

$$\underline{f_a} = \frac{\ell^3}{6EI}\left(\frac{1}{2}\right)\begin{bmatrix} 2 & 1 \\ 1 & 2 \end{bmatrix} \tag{24a}$$

may be written in the reduced form of Eq. 24b. Selecting the beam moments over support 1 and 2 as redundants, the force transformation matrix takes

$$\begin{Bmatrix} \theta_a^i \\ \theta_b^i \\ \theta_a^j \\ \theta_b^j \\ \delta_0 \\ \delta_1 \\ \delta_2 \\ \delta_3 \end{Bmatrix} = \frac{1}{2}\cdot\frac{\ell^2}{6EI}\begin{bmatrix} 8 & 2 & 0 & 0 & 0 & 0 & 0 & 0 \\ 2 & 8 & 2 & 0 & 0 & 0 & 0 & 0 \\ 0 & 2 & 6 & 1 & 0 & 0 & 0 & 0 \\ 0 & 0 & 1 & 2 & 0 & 0 & 0 & 0 \\ 0 & 0 & 0 & 0 & 3 & 0 & 0 & 0 \\ 0 & 0 & 0 & 0 & 0 & 3 & 0 & 0 \\ 0 & 0 & 0 & 0 & 0 & 0 & 3 & 0 \\ 0 & 0 & 0 & 0 & 0 & 0 & 0 & 3 \end{bmatrix}\begin{Bmatrix} m_a^i \\ m_b^i \\ m_a^j \\ m_b^j \\ P_0 \\ P_1 \\ P_2 \\ P_3 \end{Bmatrix} \tag{24b}$$

the reduced form shown in Eqs. 25. In Eq. 25a, the subscript "L" indicates that the moments and forces are referred to the left hand section. It should be noted that the forces P_a and M_a which will be needed later to satisfy the continuity conditions between the two subsections have been included as part of the external force system acting on the subsection. Also it is seen that only two redundants are included in this subsection, hence its analysis requires the inversion of only a second order matrix.

$$\begin{Bmatrix} m_2^i \\ m_3^i \\ m_a^i \\ m_a^i \\ \theta_0 \\ \theta_1 \\ \theta_2 \\ \theta_3 \end{Bmatrix} = \left[\begin{array}{cccccc:cc} 0 & 0 & 0 & 0 & 0 & 0 & 1 & 0 \\ 0 & 0 & 0 & 0 & 0 & 0 & 0 & 1 \\ 0 & 0 & 0 & 0 & \frac{1}{2} & 1 & 0 & 0 \\ 0 & 0 & 0 & 0 & 0 & 1 & 0 & 0 \\ 1 & 0 & 0 & 0 & 0 & 0 & -1 & 0 \\ 0 & 1 & 0 & 0 & 0 & 0 & 2 & -1 \\ 0 & 0 & 1 & 0 & -\frac{1}{2} & -1 & -1 & 2 \\ 0 & 0 & 0 & 1 & \frac{3}{2} & 1 & 0 & -1 \end{array}\right] \begin{Bmatrix} P_0 \\ P_1 \\ P_2 \\ P_3 \\ P_a \\ m_a \\ \hdashline X_2 \\ X_3 \end{Bmatrix} \tag{25}$$

or

$$\underline{m_L} = \left[b_0 \vdots b_1\right]_L \left\{\begin{array}{c} R_L \\ \hdashline X_L \end{array}\right\} \tag{25a}$$

The flexibility of the subsection, obtained by applying the matrix operations of Eqs. A, is found to be as shown in Eq. 26.

$$\underline{F_L} = \frac{1}{576}\frac{\ell^3}{6EI}\begin{bmatrix} 747 & 189 & -27 & -45 & -39 & 12 \\ & 459 & 243 & -27 & -153 & -252 \\ & & 459 & 189 & -9 & -396 \\ & & & 747 & 1065 & 636 \\ & & (\text{Symmetrical}) & & 2111 & 2236 \\ & & & & & 4064 \end{bmatrix} \tag{26}$$

In order to join the subsections together, the flexibility matrix of the elements of the complete structure is formed, as usual, as the diagonal matrix of the element flexibilities (subsections, in this case), as shown in Eq. 27. For this case, $\underline{F_R} = \underline{F_L}$ because the two subsections are identical.

$$\underline{f} = \begin{bmatrix} \underline{F_L} & 0 \\ 0 & \underline{F_R} \end{bmatrix} \tag{27}$$

The force transformation matrix required for combining the subsections takes the particularly simple form shown in Eq. 28 (this is typical of force transformations relating previously analyzed subsections). It should be noted how the force transformation takes account of the reversal of sequence in numbering between the left and right hand sections. In this equation, the external forces acting on the right hand subsection just to the right of the center joint are identified by "primes," (e.g. P_a'), while the redundant interconnection forces are designated X_p and X_m.

Analysis of this system also requires the inversion of only a second order matrix. Carrying out the standard matrix operations on these flexibility and force transformation matrices, yields the flexibility coefficient matrix of the complete beam shown in Eq. 29. This matrix gives the vertical deflections of the beam due to unit loads, and is arranged in the sequence indicated by the external load matrix $\underline{R}$ of Eq. 28.

$$\begin{Bmatrix} P_0 \\ P_1 \\ P_2 \\ P_3 \\ P_a \\ m_a \\ P_7 \\ P_6 \\ P_5 \\ P_4 \\ P'_a \\ m'_a \end{Bmatrix} = \left[\begin{array}{cccccccc:cc} 1 & 0 & 0 & 0 & 0 & 0 & 0 & 0 & 0 & 0 \\ 0 & 1 & 0 & 0 & 0 & 0 & 0 & 0 & 0 & 0 \\ 0 & 0 & 1 & 0 & 0 & 0 & 0 & 0 & 0 & 0 \\ 0 & 0 & 0 & 1 & 0 & 0 & 0 & 0 & 0 & 0 \\ 0 & 0 & 0 & 0 & 0 & 0 & 0 & 0 & 1 & 0 \\ 0 & 0 & 0 & 0 & 0 & 0 & 0 & 0 & 0 & 1 \\ 0 & 0 & 0 & 0 & 0 & 0 & 0 & 1 & 0 & 0 \\ 0 & 0 & 0 & 0 & 0 & 0 & 1 & 0 & 0 & 0 \\ 0 & 0 & 0 & 0 & 0 & 1 & 0 & 0 & 0 & 0 \\ 0 & 0 & 0 & 0 & 1 & 0 & 0 & 0 & 0 & 0 \\ 0 & 0 & 0 & 0 & 0 & 0 & 0 & 0 & -1 & 0 \\ 0 & 0 & 0 & 0 & 0 & 0 & 0 & 0 & 0 & 1 \end{array}\right] \begin{Bmatrix} P_0 \\ P_1 \\ P_2 \\ P_3 \\ P_4 \\ P_5 \\ P_6 \\ P_7 \\ \hdashline X_p \\ X_m \end{Bmatrix} \tag{28}$$

or $$\begin{Bmatrix} R_L \\ R_R \end{Bmatrix} = [b_0 \vdots b_1] \begin{Bmatrix} R \\ \hdashline X \end{Bmatrix} \tag{28a}$$

The stress matrix b_S obtained (using Eq. A-3) during the joining of the subsections represents, of course, the relationship between the applied loads

$$\underline{F} = \frac{\ell^3}{600EI} \begin{bmatrix} 129.62 & 32.63 & -4.60 & -6.27 & -1.87 & 0.12 & 0.31 & 0.06 \\ & 77.37 & 40.00 & 5.44 & -3.28 & -2.07 & -0.39 & 0.31 \\ & & 76.33 & 38.59 & 4.99 & -3.35 & -2.07 & 0.12 \\ & & & 74.41 & 38.00 & 4.99 & -3.28 & -1.87 \\ & & & & 74.41 & 38.59 & 5.44 & -6.27 \\ & & (\text{Symmetrical}) & & & 76.33 & 40.00 & -4.60 \\ & & & & & & 77.37 & 32.63 \\ & & & & & & & 129.62 \end{bmatrix} \tag{29}$$

and the subsection force system, as shown in Eq. 30a. In order to obtain the forces in the beam segments of the subsections, it is necessary to go back to

$$\begin{Bmatrix} R_L \\ R_R \end{Bmatrix} = \underline{b_S}\ \underline{R} \tag{30a}$$

the stress matrices b_L and b_R relating the subsection applied loads to the segment forces. This relationship is indicated in the matrix Eq. 30b. Thus the segment forces may be expressed in terms of the external load system

$$\begin{Bmatrix} m_L \\ m_R \end{Bmatrix} = \begin{bmatrix} \underline{b_L} & 0 \\ 0 & \underline{b_R} \end{bmatrix} \begin{Bmatrix} R_L \\ R_R \end{Bmatrix} \tag{30b}$$

applied to the entire beam as shown in Eq. 30c. Carrying out the operation, the stress matrix of the complete beam is obtained, as shown in Eq. 31. Only half of the matrix for this symmetrical structure is presented, in order to save space.

$$\left.\begin{aligned} \begin{Bmatrix} m_L \\ m_R \end{Bmatrix} &= \begin{bmatrix} \underline{b_L} & 0 \\ 0 & \underline{b_R} \end{bmatrix} \underline{b_S}\ \underline{R} \\ \text{i.e.} \qquad \underline{b} &= \begin{bmatrix} b_L & 0 \\ 0 & b_R \end{bmatrix} \underline{b_S} \end{aligned}\right\} \tag{30c}$$

$$\begin{Bmatrix} m_a^i \\ m_a^j \\ m_b^i \\ m_b^j \\ \rho_0 \\ \rho_1 \\ \rho_2 \\ \rho_3 \end{Bmatrix} = 10^{-4} \begin{bmatrix} 1359 & -2175 & 307 & 418 & 125 & -8 & -21 & -4 \\ 542 & 491 & -2053 & 473 & 468 & 123 & 15 & -29 \\ 31 & 491 & 498 & -2044 & 479 & 477 & 129 & -61 \\ -15 & 310 & 487 & -782 & -782 & 487 & 310 & -15 \\ 8641 & 2175 & -307 & -418 & -125 & 8 & 21 & 4 \\ 2175 & 5158 & 2667 & 362 & -218 & -138 & -26 & 21 \\ -307 & 2667 & 5089 & 2572 & 332 & -223 & -138 & 8 \\ -418 & 362 & 2572 & 4960 & 2533 & 332 & -219 & -125 \end{bmatrix} \begin{Bmatrix} P_0 \\ P_1 \\ P_2 \\ P_3 \\ P_4 \\ P_5 \\ P_6 \\ P_7 \end{Bmatrix} \tag{31}$$

where $m_n = M_n/\ell$

DISCUSSION

The matrix method presented herein provides a convenient and efficient means of calculating the flexibility and stresses of structures composed of beam type elements. After the basic flexibility and force transformation matrices of the elements of the structure have been set up (a relatively simple task for beam systems) the matrix manipulations required are of a routine nature which may be carried out by technicians having no training in structural analysis, or they may be handled in a routine manner by an electronic digital computer. It should be emphasized, however, that an electronic computer is not at all an essential requirement of the method, however. All the calculations in the examples presented herein were carried out in 20 to 30 hours on a desk calculator.

One of the convenient features of this approach is that all the elastic characteristics of the structure are contained in the flexibility matrix, while the geometric characteristics are presented separately in the force transformation matrices. Thus changing the stiffness of any of the members requires only that the appropriate portion of the flexibility matrix be changed. Similarly, it is possible to determine the effects of shear and flexural distortions separately, simply by using the proper flexibility matrices. Non-uniform members require the use of a special formula for evaluating the segment flexibilities, but introduce no other complications into the analysis.

In the general description of this method given at the beginning of the paper, the statement was made that the inversion of the matrix $\underline{D}$ is equivalent to the solution of a set of simultaneous equations. Actually, of

course, the inversion of a matrix is equivalent to the solution of the equations for many different loading conditions. Consequently, if only a single loading condition is contemplated for the beam system under consideration, it will be simpler to solve the simultaneous equations than to obtain the inverse of the matrix. In such a case, the inversion operation indicated in Eq. A-2 may be considered merely as a symbol of the solution of the set of equations. On the other hand, if the complete set of flexibility coefficients is required (as for example, for subsequent use in a vibration analysis) then the actual inversion operation must be performed. Langefors has presented a thorough discussion of this point in Reference 9.

ACKNOWLEDGMENT

The results presented in this paper were obtained during the course of a research program carried out at the Ship Research Institute of Norway, Trondheim, under the sponsorship of the U.S. Educational Foundation in Norway (Fulbright Fellowship). The wholehearted cooperation of Director Jan R. Getz and the staff of the Institute which made it possible to carry out this work is gratefully acknowledged. It is expected that a paper describing the application of these techniques to the analysis of box girders, such as a ship's hull, will be published in the near future.

APPENDIX

Note on the Displacement Matrix Equations

The dual function performed by the force transformation matrix $\underline{b}_1$ in Eq. A-1 (or b_0 in Eq. 13c) may appear somewhat surprising at first. However, the validity of the expression may be demonstrated easily by considering it as a statement of the principle of virtual work. By this principle, the deflection at a specified point of a structure, may be obtained by applying a unit load at the location and in the direction of the desired deflection and obtaining the product of the resulting force in each member multiplied by its specified deformation. The sum of these products for all members in the structure then equals the desired deflection.

In Eq. A-1, the matrix product $\underline{F}\underline{b}_1$ represents the internal deformations of the elements, while the matrix $\underline{b}'_1$ is the (transposed) matrix of forces in the members due to unit loads applied individually at points where the deflections are to be found. The matrix product $\underline{b}'_1 (\underline{f}\underline{b}_1)$ thus gives the sum of the member force-deformation products as required to obtain the desired deflection. The matrix $\underline{b}_1$ enters the expression twice because deflections are being calculated at the same points as the loads are being applied to.

It may also be worthwhile to note that Eq. A-1 is a typical equation of coordinate transformation expressed in matrix form. (See for example "Elementary Matrices" by R. A. Frazer, W. J. Duncan, and A. R. Collar, Cambridge University Press, 1955, p. 29). In this case, the transformation is from the deformation coordinates of the individual elements as exemplified by $\underline{f}$ to the deformation coordinates of the combined (primary) system represented by $\underline{D}$.

REFERENCES

1. Myklestad, N. O. "A New Method of Calculating Natural Modes of Uncoupled Bending Vibrations of Airplane Wings and Other Types of Beams," Journal of the Aeronautical Sciences, Vol. 11, No. 2, April 1944, p. 153.

2. Thomson, W. T. "Matrix Solution for the Vibration of Non-Uniform Beams," Journal of Applied Mechanics, Trans. ASME, Vol. 72, 1950, p. 337.

3. Marguerre, K. "Vibration and Stability Problems of Beams treated by Matrices," Journal of Mathematics and Physics, Vol. 35, No. 1, April 1956, p. 28.

4. Langefors, B. "Analysis of Elastic Structures by Matrix Transformation," Journal of Aeronautical Sciences, Vol. 19, No. 7, July 1952, p. 451.

5. Argyris, J. H. "Energy Theorems and Structural Analysis, Part I General Theory" Aircraft Engineering Vol. XXVI, Oct, 1954 p. 343, Nov. 1954 p. 383 and Vol. XXVII, Feb. 1955 p. 42, March 1955 p. 80, April 1955 p. 125 and May 1955 p. 145.

6. Hunt, P. M. "The Electronic Digital Computer in Aircraft Structural Analysis" Aircraft Engineering, Vol. XXVIII, March 1956, p. 70.

7. Langefors, B. "Exact Reduction and Solution by Parts of Equations for Elastic Structures" Saab Technical Notes 24, Saab Aircraft Company, Linköping, Sweden, 1953.

8. Bisplinghoff, R. L., Ashley, H. and Halfman, R. L. "Aeroelasticity," Addison-Wesley Publishing Company Inc., Cambridge, Massachusetts, 1955, p. 145.

9. Langefors, B. "On the Practical Solution of Linear Equations" Saab Technical Notes 35, Saab Aircraft Co., Linköping, Sweden, 1955.

10. Kron, G. "Solving Highly Complex Elastic Structures in Easy Stages," Journal of Applied Mechanics, Vol. 22, No. 2, June 1955, p. 235.

11. Kron, G., "Solution of Complex Non-Linear Plastic Structures by the Method of Tearing," Journal of the Aeronautical Sciences, Vol. 23, No. 6, June 1956, p. 557.

Paper 1495 January, 1957 EM 1

Journal of the
ENGINEERING MECHANICS DIVISION
Proceedings of the American Society of Civil Engineers

PLASTIC DESIGN OF COVER PLATED CONTINUOUS BEAMS

E. P. Popov* A.M. ASCE and J. A. Willis** J. M. ASCE
(Proc. Paper 1495)

SYNOPSIS

A non-prismatic continuous beam may be considered well designed by the plastic method if at the ultimate load a plastic hinge forms throughout the beam. Significantly, according to the plastic method of design, an infinite number of alternative designs to carry the same applied load is possible. The material of a beam may be distributed quite differently to achieve the same ultimate carrying capacity. This situation is entirely different from that found in elastic design where theoretically, once the type of cross-section is fixed, there is only one solution of a given problem. In this paper alternative plastic designs for a two-span continuous beam loaded with concentrated forces are discussed. Experimental evidence is submitted to serve as a justification for the simple plastic method of design of non-prismatic members and to show some of the shortcomings in the simple plastic theory.

INTRODUCTION

For ductile materials, such as structural steel, plastic methods of analysis and design are applicable. Realistic estimates of the carrying capacities of structures may be obtained on this basis. Convenient analytical procedures have been developed[1,2] for the design of structures based on this method. Reliable experimental verification of the theory is also available[3] for many practically significant cases. However, so far some aspects of the problem received insufficient emphasis. One of these deals with the fact that the plastic method of design permits an infinite flexibility in the manner of proportioning the various members of a structure. The material may be distributed differently to achieve the same ultimate carrying capacity. For example, in a simple portal frame fixed at the base a variety of column and beam sizes may

Note: Discussion open until June 1, 1958. A postponement of this closing date can be obtained by writing to the ASCE Manager of Technical Publications. Paper 1495 is part of the copyrighted Journal of the Engineering Mechanics Division, Proceedings of the American Society of Civil Engineers, Vol. 84, No. EM 1, January, 1958.

* Prof. of Civ. Eng., Univ. of California, Berkeley, Calif.

** Structural Designer, Thomas G. Atkinson, Structural Engr., San Diego, Calif., formerly graduate student at the Univ. of California, Berkeley, Calif.

be shown to be adequate for a given loading condition. By making columns stronger the beam may be reduced in size, or vice versa, provided of course, that the combined plastic strength of the system suffices to carry the applied load. Several adequate practical designs are possible even though the beam and columns are limited to constant cross-section throughout their respective lengths. An optimum design to achieve the minimum weight of such a portal frame has been discussed.(4)

Greater possibilities open up for the weight optimization of a structure if the cross-section of each member is permitted to vary along the length. For I-beams and wide-flange sections this is effectively accomplished by means of cover plates. Theoretical possibilities of this variation for uniformly loaded fixed-ended beams has been considered.(5) In the interest of weight economy the practical necessity for varying the cross-section of beams and columns is apparent in the recommended design procedures.(6,7,8) This possibility of having numerous designs for indeterminate structures to choose from when the plastic design method is used is unique. According to the elastic theory, whether the structure is determinate or indeterminate, there is one and only one solution of the problem for a given load system.

In this paper, several designs of a two-span continuous beam loaded by concentrated forces in the middle of each span are considered first. A somewhat analogous case of a three-span continuous beam is also discussed. Then, since most of the experimental research in plastic design of continuous beams and frames has been confined to prismatic members, experiments on the designed beams were performed. These experiments may serve in some measure in justification of predictions of the ultimate capacity of non-prismatic members based on the simple plastic theory.

Design of a Continuous Beam

As an example of plastic design of a continuous beam, consider the beam loaded as shown in Fig. 1a. Here it is evident that if the beam were not continuous over the center support, the moment diagram in each span would be triangular in shape with a maximum ordinate of +PL/4. The same diagrams may be considered as a part of a total bending moment diagram for a continuous beam, except that for a continuous beam the base line is a line ABC, Fig. 1b.

It should be noted particularly that the ordinates PL/4 in each span are based entirely on the conditions of statics and that irrespective of the magnitude of P these expressions remain the same. In plastic design, the ordinate for the moment diagram at the center support may be chosen arbitrarily. In terms of the notation shown in Fig. 1b, this means that the value of a dimensionless parameter α may be chosen arbitrarily. Actually, α may vary between the values of zero and two.(9) At both limits the continuous beam ceases to exist. For $\alpha = 0$, two simple spans are obtained; for $\alpha = 2$, the beam becomes a cantilever.

After a definite value of α is selected, the moment diagram becomes fixed. If, further, P is considered as an ultimate load, P_{ult}, sections along the beam may be proportioned following the rules of plastic design for the corresponding values of M_x. A beam of continuously varying size selected on this basis would be efficient from the point of view of plastic design. At an ultimate load a hinge continuous across the entire span would form all at

once. In an actual design of such a beam, portions of the span where the bending moment is small must be modified to care for the shear requirements.

The arbitrary choice of α is permissible only on the basis of plastic analysis. For the beam considered, when material behaves elastically, the general shape of the moment diagram remains the same. However, there is only one particular value of α which will satisfy the conditions of continuity at the middle support. The proportions of the beam influence the magnitude of α. A beam made stiff over the center support will develop there a large moment; a beam which is flexible over this support would develop there a smaller moment. Theoretically it is possible to select a continuous beam of constant strength for a given shape of a cross-section. This solution would be unique.(10) By contrast, for the same conditions an infinite number of designs is possible according to the plastic theory. Therein lies one of the fundamental differences between the elastic and plastic methods of design.

In structural work where rolled sections are normally used, a continuous variation in the size of a beam is not practical. Instead, a certain minimum size beam may be selected and by using cover-plates the bending moment requirements may be approximated step-wise. On this basis four two-span continuous beams of different cross-sections to carry the same loads P were designed and tested.

One of the continuous beams was made prismatic. For such a case the moment resisting capacity of the beam at the applied forces P and at the center support is the same, i.e. $\alpha = \frac{2}{3}$. Hence equating moment at the applied load to the moment at the support, see Fig. 1b, one finds

$$\frac{P_{ult}L}{4} - 1/2\, M_p = M_p \text{ or } P_{ult} = \frac{6M_p}{L} \qquad (1)$$

where

P_{ult} is the ultimate transverse load

M_p is the ultimate plastic moment

L is the length of each span

Three additional beams were made with cover-plates in which the plastic moments were different at various sections. For the loading conditions considered, the basic equation, a generalization of Eq. 1, is

$$\frac{P_{ult}L}{4} = M_{pa} + 1/2\, M_{pb} \qquad (2)$$

where M_{pa} is the plastic moment at the applied loads

M_{pb} is the plastic moment at the middle support

A 6 in. 12.5 lb. I-beam 16 ft. long beam was selected as the prismatic specimen. Based on the assumption that the yield strength of structural steel is 40 ksi, from Eq. 1 it was found that P_{ult} should be 20.9 kips and that P_{ult} L/4 is very nearly 500 in. kips.

A 5-in. 10 lb. and a 5 in. 7.7 lb. continuous I-beam were coverplated in the

middle of each span to provide for very nearly the same P_{ult} as was determined for the 6 in. prismatic beam. With no cover plates over the middle support, M_{pb} is readily computed, and, from Eq. 2, the M_{pa}, the bending moment capacity at the applied loads, was found. By assuming the same yield strength for cover plates as for the rolled sections, the appropriate sizes of cover plates were determined. Another 5 in. 10 lb. I-beam with cover plates only over the middle support was designed to carry the same P_{ult}. The design results are summarized in Table I.

TABLE I

Member Size	Cover Plates Size (in.x.in.)	M_p (kip-in) without plates	M_p (kip-in.) with plates	$\frac{P_{ult}L}{4}$ kips-in	P_{ult} (kips)
6 I 12.5	none	334	---	501	20.9
5 I 10.0	3/16 x 4	222	378	489	20.4
4 I 7.7	$\frac{1}{4}$x 3$\frac{1}{2}$ and $\frac{1}{4}$ x3	138	430	499	20.8
5 I 10.0	7/16 x 3$\frac{1}{2}$	222	555	500	20.9

The beams selected were so chosen that shear would not be important. Further, assuming that 1.88 is the proper factor of safety(11) for obtaining working loads from the ultimate loads, it was found that at working loads in all cases the deflections of the selected beams did not exceed 1/360-th of the span. However, for the 4 in. 7.7 lb. beam having cover plates in the middle of each span (Beam No. 5) yielding over the center support takes place before the total working load is reached. In plastic designs such situations are possible.

A composite bending moment diagram for the four cases considered is shown in Fig. 2. A different baseline is applicable in each case. From such a diagram cut-off points for cover plates were determined. As a general rule, the cover plates were extended 6 in. beyond the theoretically required cut off points.

Besides the four continuous beams described above, another related continuous beam was analyzed and tested. The loading diagram for this three-span continuous beam is shown in Fig. 3a. If the end spans of this beam were rotated downward at B and C through 90°, a small portal frame would result. Hence this beam simulates approximately an unfolded portal frame. On the other hand, if the loading diagram is viewed upside-down, the loading arrangement resembles the case considered earlier. The principal difference between the two cases is in the shape of the collapse mechanism, compare Fig. 1c and Fig. 3c. For this case Eq. 2 does not apply, instead, as may be readily seen from Fig. 3b the basic equation should be

$$\frac{P_{ult}L}{4} = M_{pa} + M_{pb} \qquad (3)$$

Where M_{pa} is the plastic moment at the applied load

M_{pb} is the plastic moment at the interior supports.

A 5 in. 10 lb. I-beam with 7/16 in. by 3 1/2 in. cover plates which exactly duplicated on the previously designed beams having M_{pa} = 555 kip-in. and M_{pb} = 222 kip-in. (See Table I) was selected for the experiment. For this case the cover plates extended about 1/2 in. beyond the required cut off points based on plastic analysis. Significantly, the elastic analysis indicated first yield would take place at the edges of cover plates. Therefore, the elastic and plastic analyses lead to different requirements for the length of cover plates. Further research on this question appears to be necessary.

For control purposes, a 5 in. 10 lb. I-beam to span 3 ft. 6 in. and a 5 in. 10 lb. I-beam with 3/16 in. by 4 in. cover plates to span 4 ft. 2 in. were selected. These beams were made short in order to obtain gradients in the bending moments which would be comparable to those found in the selected continuous beams.

Details for the seven beams chosen for the experiments are shown in Fig. 4. Note that 5/16 in. stiffeners were provided at all supports and at all points of concentrated load application. A liberal amount of intermittent welding was specified to provide interconnection of all beam elements.

Experimental Procedure

All beams were fabricated by a local steel fabricator and were made of ordinary structural steel. Beams of the same size were made from the same lot and all coverplates of similar size were likewise taken from same lots. Beams were not annealed either before nor after welding.

After the specimens were delivered to the laboratory, cross-sectional dimensions were measured. At a later date, unreinforced portions of the beams were cut out and weighed. No significant discrepancy with the values given in the AISC Manual were found. Therefore, handbook values of section properties were used in the calculations.

To verify the assumed mechanical properties of the material, 1 1/2 in. by 8 in. gage length tensile coupons were made. Three coupons were taken from each size I-beam (one from each flange and one from the web) and one from each size of coverplate.

A study of the stress-strain diagrams for the coupons showed no anomalities, although well defined yield strengths varied from 32.4 ksi to 45.4 ksi. An average value for the yield point for a given cross-section was determined by using a weighted average based on the area and location in the beam. The average values used in the final analysis are tabulated in Table II.

The beams were tested in a 200,000 lb. Olsen testing machine which has a long horizontal bed plate as may be seen in Fig. 5. The two experimental simple beams were loaded at midspan. The four two-span continuous beams were loaded symmetrically at midspans with a concentrated load. This was accomplished by applying, by means of the machine of a single concentrated load to a heavy distributing beam. A spherical block was used between the distributing beam and the head of the testing machine. The arrangement for the three-span experiment is shown in Fig. 5. The central span was loaded by the machine in the middle; the end supports were not permitted to deflect by maintaining pressure in calibrated hydraulic jacks, (see Fig. 6). A record of the required pressures in the jacks provided information on the magnitude of end reactions.

In all experiments, beams were placed on rocker supports. Spherical

blocks and rollers were extensively employed. In addition to plates and shims, Hydrostone cement was applied at joints to assure good bearing surfaces.

To prevent sidewise buckling of the specimens at midspans of beams, long wire ropes were attached to the vertical bars which in turn were attached to the beam stiffeners, as may be seen in Figs. 7 and 8.

Deflections were measured at midspan in all cases except in the end spans of the three-span beam. In most instances such deflections were measured by means of dial gages as may be seen in Fig. 8; in others when a Sanborn Recorder was available, deflections were obtained by Bourns Linear Potentiometer. This set-up is shown in Fig. 7. For the two-span beam experiments some discrepancy between the deflection readings in the two spans were observed. The two readings varied from 3% to 22%. However only the average values of deflections are reported since it is believed that this discrepancy does not affect substantially the end results.

In several experiments strain measurements were made on the flanges on the side opposite the point of load application. These were recorded with the aid of the Sanborn Machine. In all cases the initial yielding occurred prior to the predicted values. It is believed that residual stresses may account for this observation.(12,13,14) The data obtained are not reported.

The appearance of the beams at the end* of the experiments may be seen in Fig. 9. The experiments usually were discontinued after the deflection exceeded 1/36-th of the span length. The wire rope bracing was considered unsafe beyond such a point. In any event, since a substantial leveling of the load-deflection curve occurs in this range of deflection, continuation of the experiments beyond this point, without much additional load, would precipitate some local collapse.

Prior to the load application, the beams were white-washed. This aided in the detection of yield lines which occurred during loading, (see Fig. 9).

Experimental Results and Conclusions

In Fig. 10 are plotted load-deflection diagrams for beams 1, 2, and 7; in Fig. 11, for beams 3, 4, 5, and 6, each of which according to the plastic theory should carry practically the same ultimate load. The load at the time when maximum deflection reached 1/36-th of the span length was used to define the ultimate load, P_{ult}. This amount of deflection is ten times greater than is currently permitted by AISC specifications. With the exception of beam 2, where the strength appears to decay around this amount of deflection, all beams still could have carried slightly higher loads. However, the lateral bracing was considered inadequate to continue loading until actual collapse of the beams would occur.

On the graphs in Figs. 10 and 11, in the plastic range, two points are usually shown corresponding to the same deflection. The higher points are for initial reading of the applied load; the lower points indicate the applied load after a lapse of time, which permitted the material to complete plastic flow. All reported ultimate loads P_{ult} are based on inter- and extrapolation of the curves passing through the lower points.

The principal results of the experiment as well as some derived quantities are summarized in Table II. For further clarification, the significant results

* These beams were tested and later re-tested, to obtain the load-deflection data reported in this paper.

are plotted on the bar graph of Fig. 12. The load carrying capacity of beams at the actual yield point strength of steel has been computed by conventional methods. The yield strength of steel was based on data obtained from tests of coupons.

Based on the results of these experiments and the analysis of the data, a number of conclusions appear to be warranted:

a) As anticipated by theoretical considerations, it is possible to design non-prismatic beams using the simple plastic theory.

b) Although the simple plastic theory appears to have led to a very consistent design of beams 3, 4, 5, and 6, due to strain hardening of the material, the real capacity of beams is higher than such a theory predicts. In literature dealing with plastic analysis it became customary to cite cases showing remarkable agreement between experimental results and predictions based on simple plastic theory. Such one-sided exposition does not seem to be entirely proper. The simple plastic theory expands our understanding of structural action and leads, in a very simple manner, to reasonable estimates of the ultimate capacity of structures. It should be recognized, however, that this theory does not give the complete picture.

c) In examining Fig. 12 it should be noted that the elastic theory is completely unable to predict the behavior of beams beyond the yield point load. The regions cross-hatched in the diagram simply cannot be even estimated using the elastic theory. A substantially equal ultimate performance of beams 3, 4, 5, and 6, may be contrasted with a rather varied predicted performance of the same beams based on elastic analysis. Plastic design should, therefore, promote greater consistency in design for strength.

d) It is significant to reiterate that in plastic design for the same ultimate load capacity different size members may be utilized. Material may be distributed quite differently to achieve the same ultimate carrying capacity. This has practical implications of economy by permitting a freer choice of members. Also, the total weight of construction may be minimized.

e) Direct experience with testing beams into the plastic range forcefully pointed to the dire necessity of bracing beams laterally. Therefore, it seems safe to say that in actual design, likewise, to assure the desired performance of a structure, at locations where plastic hinges may be anticipated, bracing must be introduced. Such a general rule seems wise to apply whether one designs using elastic or plastic method.

f) In the reported experiments, coverplates performed satisfactorily. However, further research is needed to determine the minimum amount of welding and the proper length of the coverplates for plastic design.

ACKNOWLEDGMENT

The authors wish to express their appreciation to the University of California for sponsoring this project as a part of the faculty-student research program. The cooperation of Professor H. D. Eberhart is gratefully acknowledged. Messrs. E. Brown, N. Haavik and D. Koenig of the Engineering Materials Laboratory staff offered valuable assistance. Herrick Iron Works of Oakland, California fabricated the beams.

BIBLIOGRAPHY

1. "Limit Design of Prismatic Beams" by E. P. Popov, Engineering News-Record, May 13, 1948.

2. "Recent Progress in the Plastic Methods of Structural Analysis" by P. S. Symonds and B. G. Neal, Journal of the Franklin Institute, Vol. 252, No. 5, Nov. 1951 and Vol. 252, No. 6 Dec. 1951.

3. "Plastic Strength of Steel Frames" by L. S. Beedle, Proceedings ASCE, Vol. 81, No. 764, Aug. 1955.

4. "Minimum-Weight Design of a Portal Frame" by William Prager, Journal of the Eng. Mech. Div. ASCE, Vol. 82, No. EM 4, Oct. 1956, Paper 1073.

5. "Determination of the Shape of Fixed-Ended Beams for Maximum Economy According to the Plastic Theory" by M. R. Horne, Preliminary Publication, and Final Report, International Association for Bridge and Structural Engineering, 4th Congress, Cambridge and London, 1953, pp. 111-112.

6. "A Moment Distribution Method for the Analysis and Design of Structures by the Plastic Theory" by M. R. Horne, Proc. Institution of Civ. Eng., Pt. III, Vol. 3, April 1954.

7. "Design of Frames by Relaxation of Yield-Hinges" by J. M. English, Proceedings ASCE, Vol. 79, No. 322, Nov. 1953.

8. "The Collapse Method of Design," British Constructional Steelwork Association, Publication No. 5, 1952.

9. "Soprotivlenie Materialov" (Resistance of Materials), by N. M. Belyaev, GITTL, Moscos, 1950, 6th Edition, p. 470.

10. "Theory of Elasticity," by S. Timoshenko and J. N. Goodier McGraw-Hill, New York, Second Edition, 1951, p. 236.

11. "Plastic Design in Structural Steel," Lynn S. Beedle, Bruno Thurlimann, Robert L. Ketter. Lecture Notes, Summer Course, September 1955, Lehigh University, Bethlehem, Pennsylvania and AISC, Inc., New York 17, N. Y.

12. "Plastic Deformation of Wide-Flange Beam-Columns" by R. L. Ketter, E. L. Kaminsky, and L. S. Beedle, Proceedings ASCE, Vol. 79, No. 330, Nov. 1953.

13. "Residual Stresses and the Yield Strength of Steel Beams" by C. H. Yang, L. S. Beedle and B. G. Johnston, Welding Journal Vol. 31, No. 4, p. 205, April 1952.

14. "Residual Stresses Introduced During Metal Fabrication" by Kent R. Van Horn, Journal of Metals, Vol. 6, No. 1, Sect. 2, p. 405, March 1953.

TABLE II

Beam No.	Description	Total Weight Lbs.	Ave. Yield Strength (ksi)	M_p* (kip-in)	$\frac{P_{ult}L}{4}$ (kip-in)	L (in)	P_{ult} Calculated (Kips)	P_{ult}** Exper. (Kips)	$\frac{(P_{ult})Exp.}{(P_{ult})Calc.}$
1	5 I 10.0	-	40.5	225	225	42	21.5	28.6	1.33
2	5 I 10.0 4 x 3/16 C.Pl.	-	40.5 37.2	225 370	370	50	29.6	38.0	1.28
3	6 I 12.5	200	39.3	329	494	96	20.6	26.3	1.28
4	5 I 10.0 4 x 3/16 C.Pl.	197	40.5 37.2	225 370	483	96	20.1	24.7	1.23
5	4 I 7.7 3 x ¼ C.Pl. 3½ x ¼ C.Pl.	226	39.3 41.2 41.2	136	504	96	21.0	24.8	1.18
6	5 I 10.0 3½ x 7/16 C.Pl.	195	40.5 37.9	225 540	495	96	20.6	24.5	1.19
7	5 I 10.0 3½ x 7/16 C.Pl.	-	40.5 37.9	225 540	765	96	31.9	36.4	1.14

* When two values of M_p are given, the upper number gives M_p for a beam without cover plate; the lower with coverplate.

** P_{ult} is the load carried by the beam at deflection equal to 1/36-th of the span length.

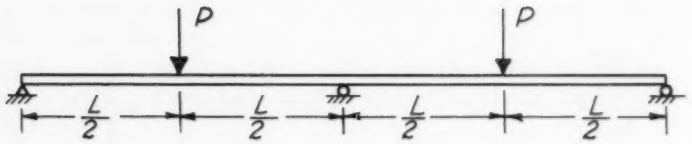

(a) Beam Loading Diagram

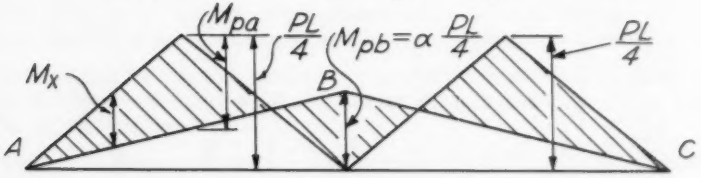

(b) Moment Diagram

(c) Collapse Mechanism

Fig. 1

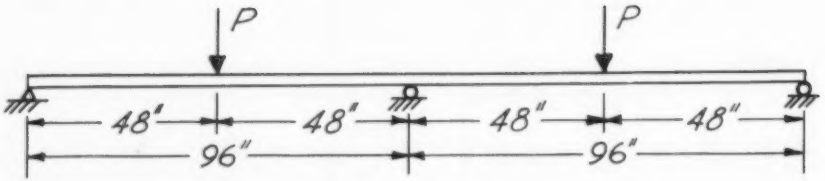

(a) Beam Loading Diagram

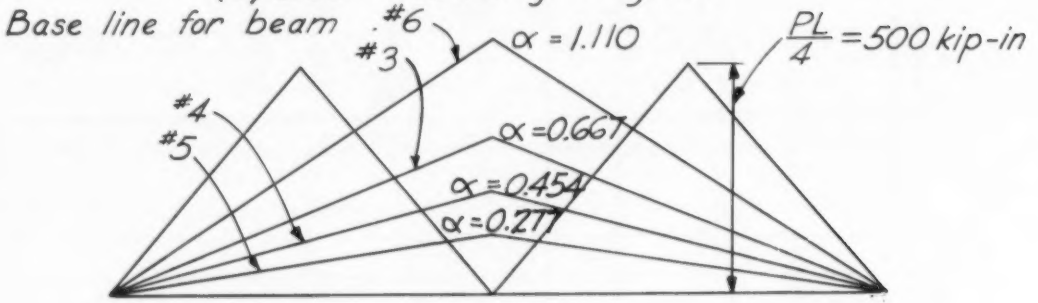

(b) Moment Diagram

Fig. 2

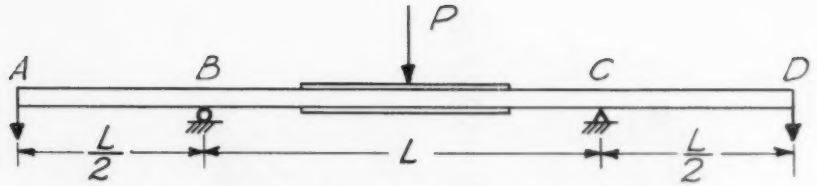

(a) Beam Loading Diagram

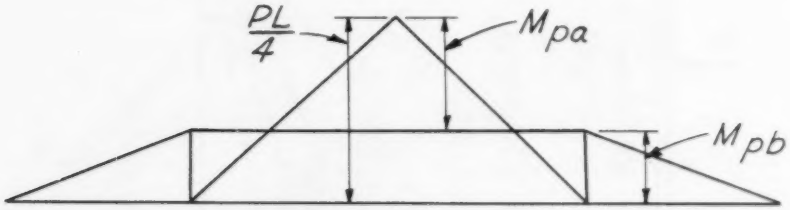

(b) Moment Diagram

(c) Collapse Mechanism

Fig. 3

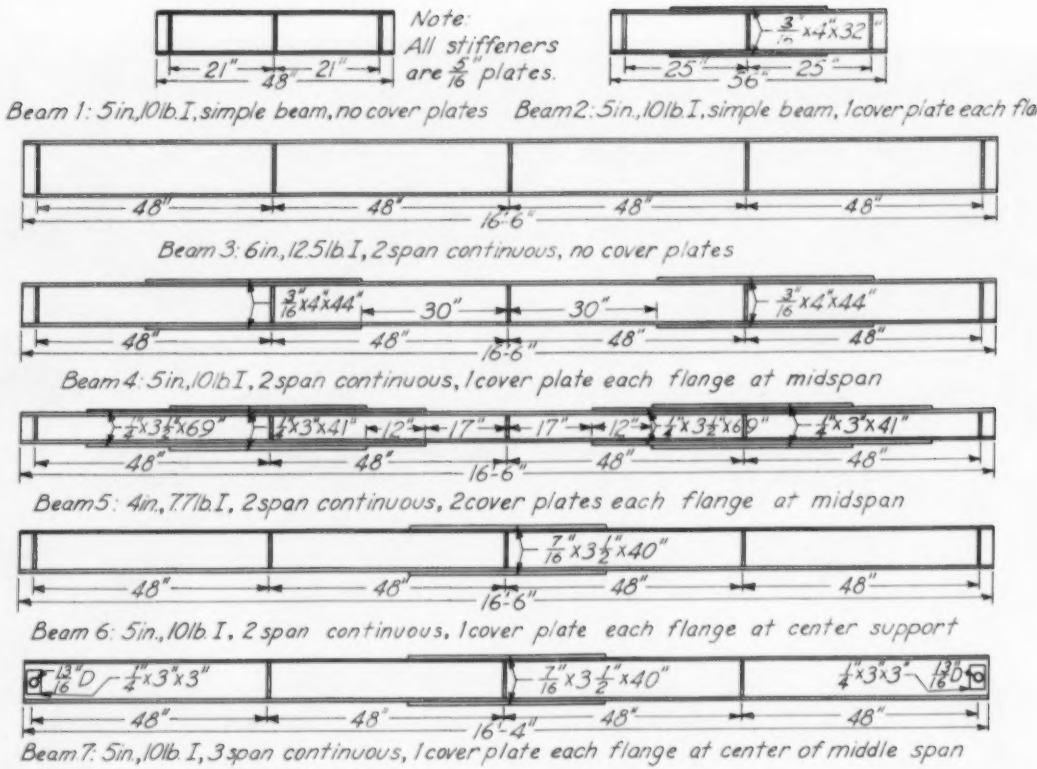
Note:
All stiffeners
are 5/16" plates.
21"
48"
21"
3/16" x 4" x 32"
25"
56"
25"
Beam 1: 5in, 10lb. I, simple beam, no cover plates
Beam 2: 5in., 10lb. I, simple beam, 1 cover plate each flange
48"
48"
48"
48"
16'-6"
Beam 3: 6in., 12.5lb. I, 2 span continuous, no cover plates
3/16" x 4" x 44"
30"
30"
3/16" x 4" x 44"
48"
48"
16'-6"
48"
48"
Beam 4: 5in., 10lb. I, 2 span continuous, 1 cover plate each flange at midspan
7/16" x 3 1/2" x 69"
1/4" x 3" x 41"
12"
17"
17"
12"
7/16" x 3 1/2" x 69"
1/4" x 3" x 41"
48"
48"
16'-6"
48"
48"
Beam 5: 4in., 7.7lb. I, 2 span continuous, 2 cover plates each flange at midspan
7/16" x 3 1/2" x 40"
48"
48"
16'-6"
48"
48"
Beam 6: 5in., 10lb. I, 2 span continuous, 1 cover plate each flange at center support
13/16" D
1/4" x 3" x 3"
7/16" x 3 1/2" x 40"
1/4" x 3" x 3"
13/16" D
48"
48"
16'-4"
48"
48"
Beam 7: 5in., 10lb. I, 3 span continuous, 1 cover plate each flange at center of middle span

Fig. 4

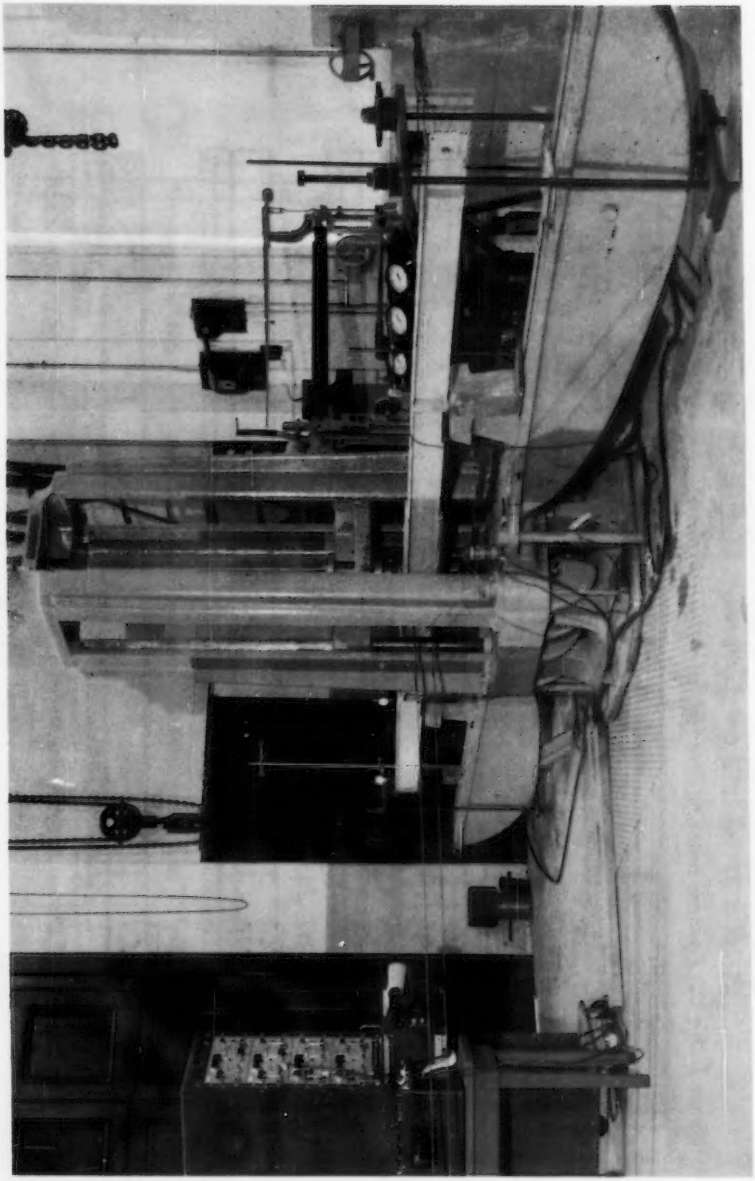

Fig. 5

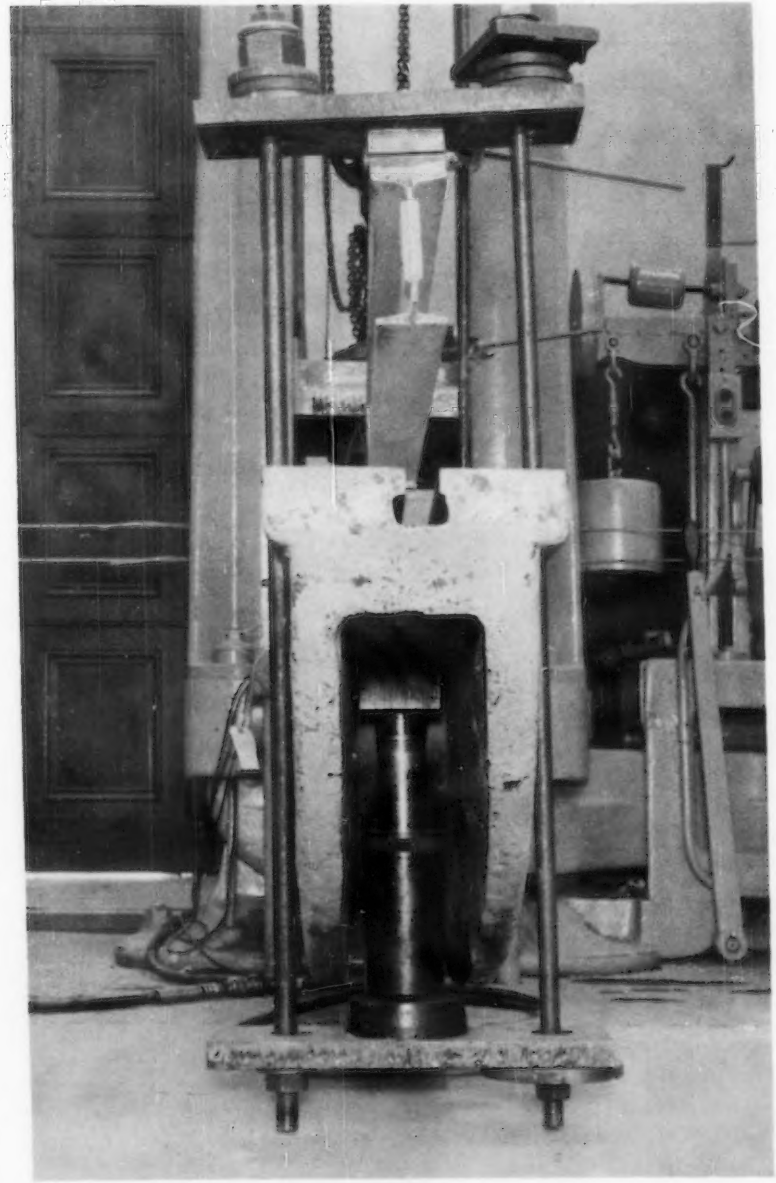

Fig. 6

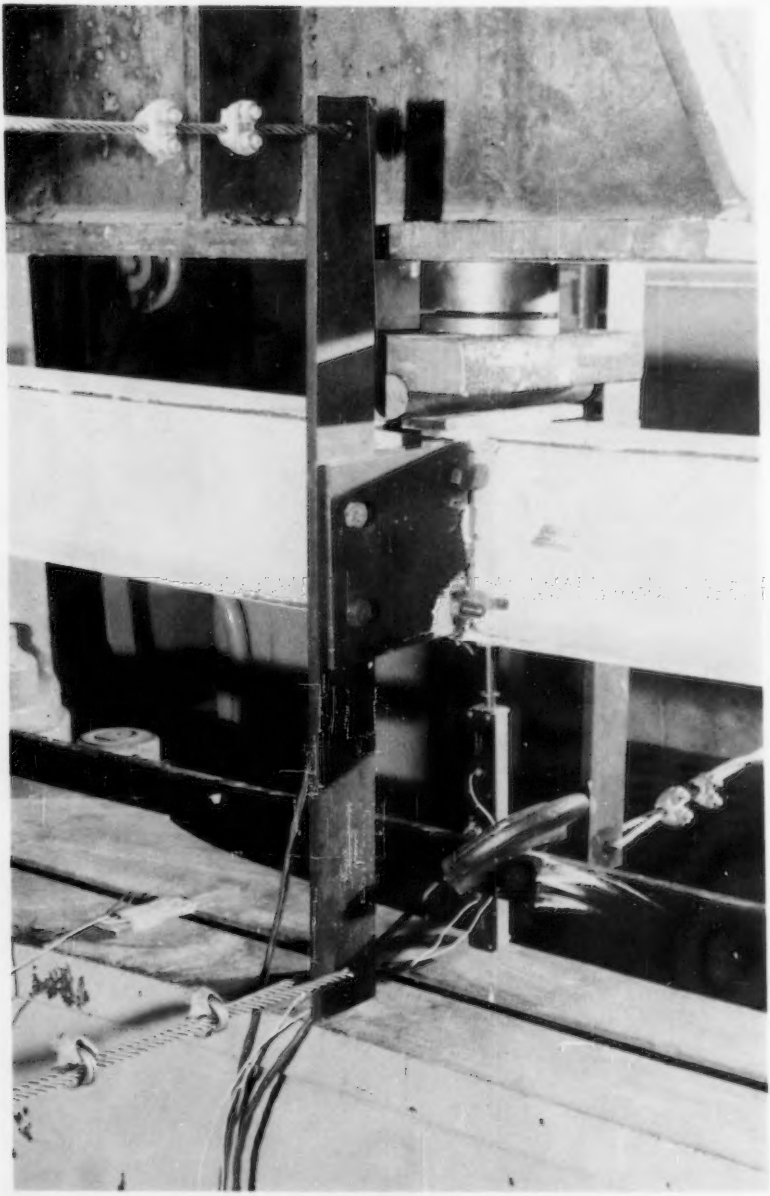

Fig. 7

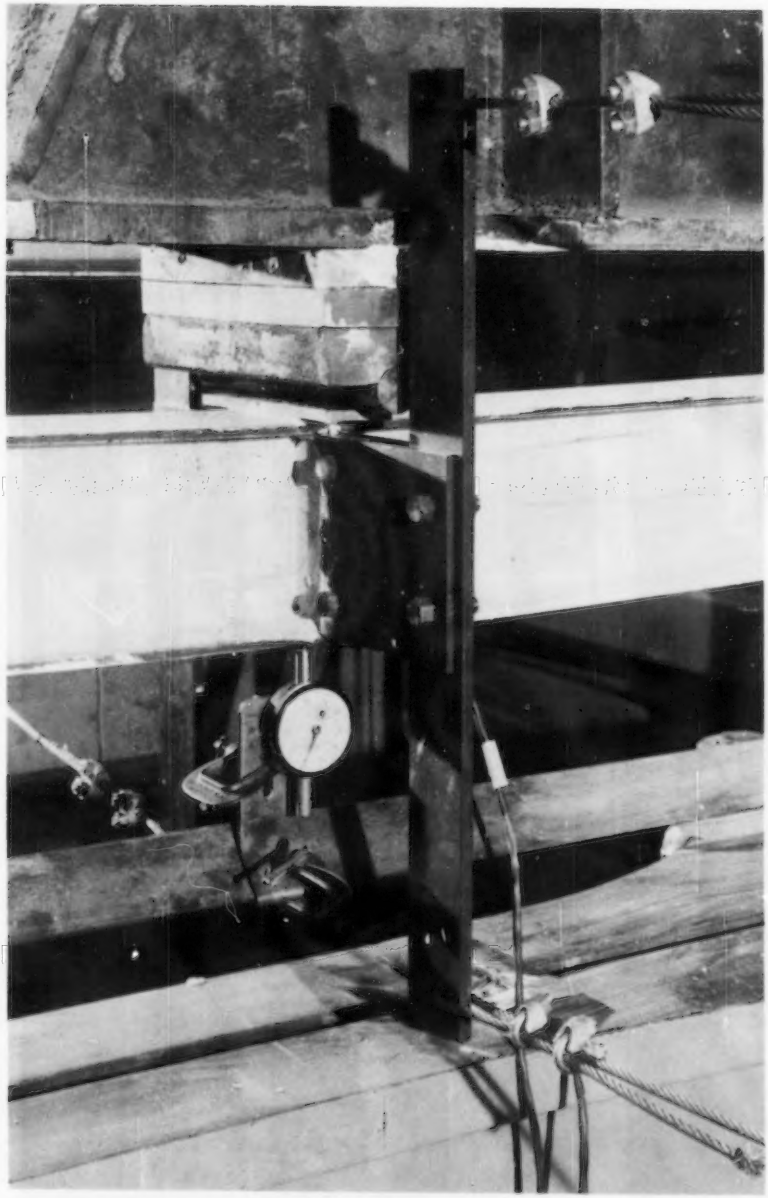

Fig. 8

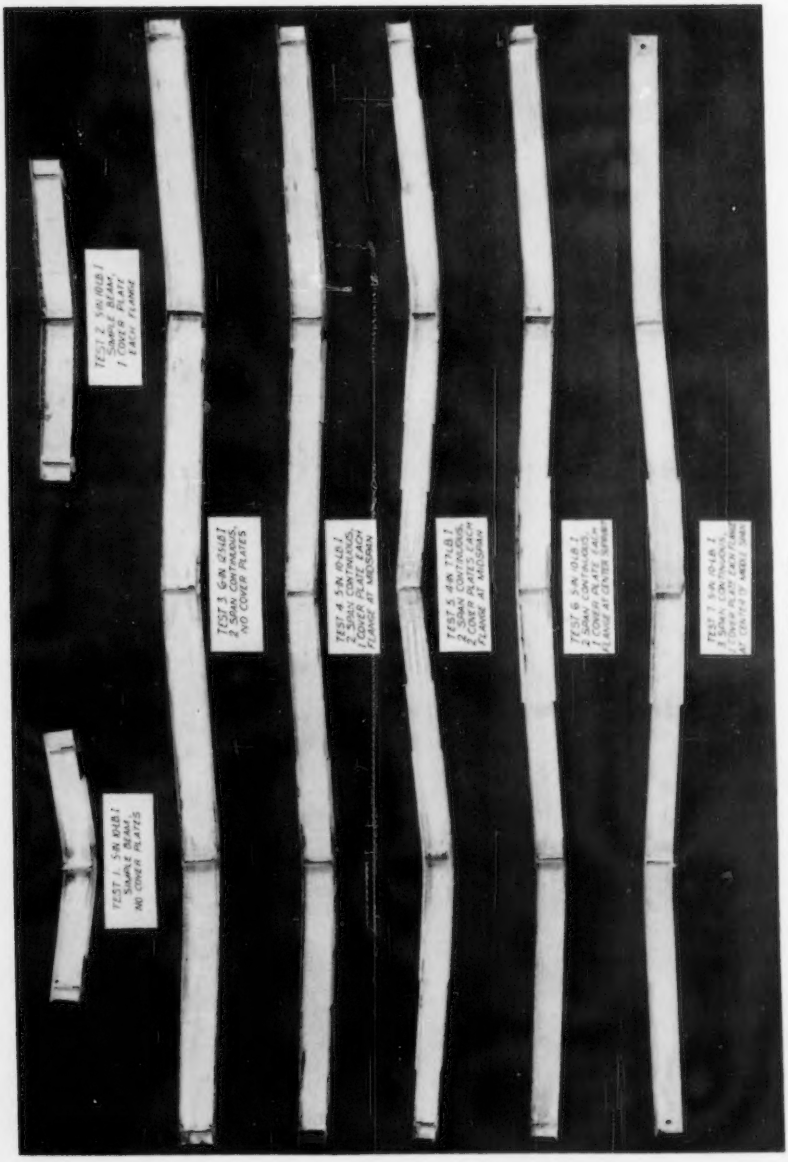
TEST 1 SPA EXHIBIT
SIMPLE BEAM
NO COVER PLATES
TEST 2 SPA EXHIBIT
SIMPLE BEAM
1 COVER PLATE
TEST 3 GPA EXHIBIT
2 SPANS
NO COVER PLATES
TEST 4 SPA EXHIBIT
2 SPAN CONTINUOUS
1 COVER PLATE EACH
FLANGE AT MIDSPAN
TEST 5 APA EXHIBIT
2 SPAN CONTINUOUS
1 COVER PLATE EACH
FLANGE AT MIDSPAN
TEST 6 SPA EXHIBIT
2 SPAN CONTINUOUS
1 COVER PLATE EACH
FLANGE AT CENTER SUPPORT
TEST 7 SPA EXHIBIT
2 SPAN CONTINUOUS
1 COVER PLATE EACH FLANGE
AT CENTER & ABOVE SUPPORT

Fig. 9

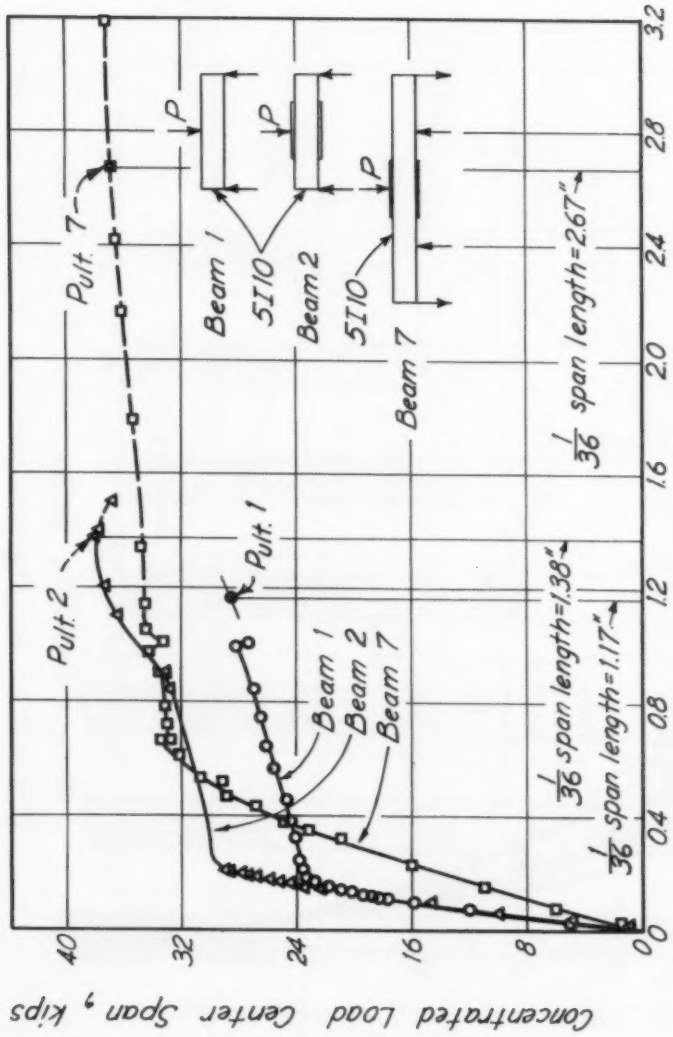
Concentrated Load Center Span, kips
Deflection Center Span, inches
Pult. 2
Pult. 1
Pult. 7
Beam 1
Beam 2
Beam 7
5I10
5I10
Beam 1
Beam 2
Beam 7
P
P
P
1/36 span length=1.38"
1/36 span length=1.17"
1/36 span length=2.67"
0
8
16
24
32
40
0.0
0.4
0.8
1.2
1.6
2.0
2.4
2.8
3.2

Fig. 10

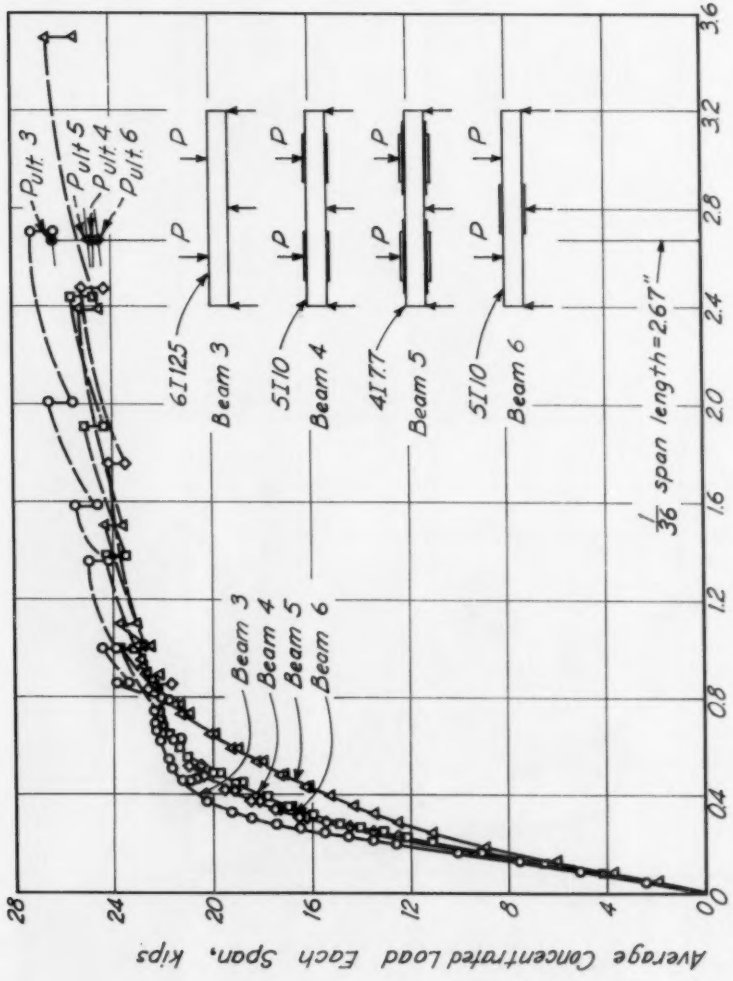
Average Concentrated Load Each Span, kips
Average Deflection Center Each Span, inches
Pult. 3
Pult. 5
Pult. 4
Pult. 6
Beam 3
Beam 4
Beam 5
Beam 6
6I125
Beam 3
5I10
Beam 4
4I7.7
Beam 5
5I10
Beam 6
P
1/36 span length=2.67"
0
4
8
12
16
20
24
28
0.0
0.4
0.8
1.2
1.6
2.0
2.4
2.8
3.2
3.6

Fig. 11

Percent of Predicted Pult.
140
120
100
80
60
40
20
0
1
2
3
4
5
6
7
Beam
Indicates test discontinued at deflection of 1/36 of span length
Pult. (calculated)
Yield Load
24 ksi
20 ksi
20 ksi

Fig. 12

Paper 1496 January, 1958 EM 1

Journal of the
ENGINEERING MECHANICS DIVISION
Proceedings of the American Society of Civil Engineers

SEA BOTTOM PRESSURE FIELDS PRODUCED BY YAWED VESSELS

P. M. Fitzpatrick*
(Proc. Paper 1496)

ABSTRACT

An understanding of the flow pattern about an ellipsoid immersed at rest in a parallel stream is often of value in aerodynamic and hydrodynamic studies. The steady flow, without circulation, about an ellipsoid immersed at rest in an infinite half-space of perfect fluid is discussed. A uniform stream flow is considered in which the centroid of the ellipsoid remains at a finite distance h from the plane boundary of the half-space. The major axis of the ellipsoid is taken to be parallel to the plane boundary and to make an angle θ with the direction of the undisturbed flow. Approximation equations are given for the velocity and pressure distributions on the plane boundary. These equations are based upon the method of images and the well-known theory of the flow pattern about a stationary ellipsoid in an infinite fluid medium. A procedure for obtaining the lines of equipressure change on the boundary is also described. The sea bottom pressure distribution produced by slowly moving yawed surface vessels in advance of the upstream hull-line may be approximated from computations based on formulae developed for the ellipsoid model. These approximations should hold when the ship proceeds through calm water of moderate depth at an angle of yaw sufficiently large to produce a wake, say θ greater than 20°. As an illustration of the application of the theory certain results of calculations of sea bottom pressure distributions and lines of equipressure change are given for a representative case.

INTRODUCTION

In certain areas of hydrodynamics it is important to be able to predict quantitatively the sea bottom pressure distribution associated with a surface ship or submarine moving slowly** in a calm sea. The most frequently

Note: Discussion open until June 1, 1958. A postponement of this closing date can be obtained by writing to the ASCE Manager of Technical Publications. Paper 1496 is part of the copyrighted Journal of the Engineering Mechanics Division, Proceedings of the American Society of Civil Engineers, Vol. 84, No. EM 1, January, 1958.

* Hydrodynamics Branch, Research Div., U. S. Navy Mine Defense Lab., Panama City, Fla.

** A conservative criterion for the validity of an assumption made later that the surface behaves as a rigid reflector is that the vessel proceed at a

encountered case is, of course, the one in which the longitudinal axis of the vessel moves approximately parallel to the track (i.e., the angle of yaw, θ, is less than say 3^{o}). For this case, which is amply treated in the literature, the pressure distribution functions are usually obtained either from a study in which the ship is represented by the source-sink technique or from a study of the flow pattern past an ellipsoid whose dimensions have been chosen to simulate the actual ship profile. Little information appears in the literature, however, on the methods which one may use to approximate the sea bed pressure distributions when a slowly moving surface (or subsurface) vessel proceeds at a constant angle of yaw greater than 3^{o}. These latter cases, although encountered infrequently, do on occasion find practical application and hence merit attention.

When a vessel proceeds through a calm sea at low speed, the magnitude of the angle of yaw, θ, affects the type of flow pattern which occurs. For values of θ less than approximately 3^{o} the usual treatments of the problem assume that a pure potential flow without circulation will hold. For values of θ, in the range $3^{o} < \theta < 15^{o}$ to 20^{o}, an approximation to the actual flow pattern about the ship profile may be obtained if one supplements a pure potential flow by the inclusion of circulation. This type of flow pattern is not treated in this paper. For values of θ which are greater than 20^{o}, a wake forms aft of the vessel and the methods of analysis presently available do not permit one to make quantitative predictions of the pressure distribution in this aft region. Nonetheless, a pressure distribution function obtained from pure potential flow theory (without circulation) should hold, as it does in the case that θ is less than 3^{o}. The region of validity of solutions based on this assumption must, however, be restricted to the neighborhood of the upstream hull line.

If θ is greater than 20^{o} it is possible to obtain a sea bottom pressure distribution function, which should hold approximately in the forward region, from a consideration of the pure potential flow (without circulation) about an ellipsoid. To this end a treatment of a yawed ellipsoidal body immersed at rest in an infinite fluid half-space has been made. Expressions which may be used to compute the velocity and pressure distributions on the plane boundary of the half-space are given. In addition, the problem of determining the curves of equipressure change on this boundary has been considered and a possible method of constructing these curves is developed and discussed.

Theoretical Procedures

Consider an ellipsoid form with semi-principal axes a, b, and c, (a>b>c). Let it be immersed at rest in an incompressible, nonviscous, infinite fluid medium which is moving with uniform total velocity $\sqrt{U^2 + V^2}$. An irrotational flow is assumed. Let the reference frame be fixed in the ellipsoid and so oriented that the Z-axis is perpendicular to the velocity vector $\sqrt{U^2 + V^2}$. The major axis of the ellipsoid (i.e., the X-axis) is assumed to make an angle θ with the direction of the uniform stream. Unless stated otherwise, in what follows, it is assumed that θ satisfies the condition $90^{o} \geq \theta > 20^{o}$. The velocity components of the uniform stream are designated as -U and -V

---

speed ($\sqrt{gh}$, where h is the depth of the water and g is the magnitude of the acceleration of gravity.

respectively and are directed along the negative X and Y-axes as shown in Figure (1).

For the system just described, the velocity potential ϕ, is given as[1]

$$\phi = UX + VY + \frac{abcUX}{2-\alpha_o}\int_\lambda^\infty \frac{d\lambda}{(a^2+\lambda)k_\lambda} + \frac{abcVY}{2-\beta_o}\int_\lambda^\infty \frac{d\lambda}{(b^2+\lambda)k_\lambda} \tag{1}$$

Here λ is an ellipsoidal coordinate which is related to the rectangular coordinates X, Y, and Z through the equation

$$\frac{(X/a)^2}{1+\lambda/a^2} + \frac{(Y/a)^2}{b^2/a^2+\lambda/a^2} + \frac{(Z/a)^2}{c^2/a^2+\lambda/a^2} = 1 \qquad (-c^2<\lambda>\infty) \tag{2}$$

The symbols k_λ, α_o and β_o which appear in Equation (1) are defined as follows:

$$k_\lambda = a^3\left[(1+\lambda/a^2)\,(b^2/a^2+\lambda/a^2)\,(c^2/a^2+\lambda/a^2)\right]^{1/2} = a^3 k'_\lambda \tag{3a}$$

$$\alpha_o = (b/c)\,(c/a)\int_o^\infty \frac{d(\lambda/a^2)}{(1+\lambda/a^2)\,k'_\lambda} \tag{3b}$$

$$\beta_o = (b/a)\,(c/a)\int_\lambda^\infty \frac{d(\lambda/a^2)}{(b^2/a^2+\lambda/a^2)k'_\lambda} \tag{3c}$$

The elliptic integrals which appear on the right-hand side of Equation (1) have been tabulated.[2]

Over the range of definition, Equation (2), regarded as a function of λ, represents a family of real confocal central ellipsoids. A nest of expanding quadric surfaces may be generated by successive substitution in Equation (2) of a monotonically increasing sequence of values of λ. In particular, for λ = 0, the quadric surface coincides with the elliptic form shown in Figure (1).

If the velocity components in the X, Y, and Z directions of the disturbed flow are designated by u, v, and w respectively, one finds by differentiation of Equation (1) that

$$u = -\partial\phi/\partial X = -U + 2\,(b/a)\,(c/a)\,\frac{(X/a)}{(1+\lambda/a^2)k'_\lambda\,\Lambda_o}\left\{\frac{K_1(X/a)}{(1+\lambda/a^2)} + \frac{K_2\,(Y/a)}{(b^2/a^2+\lambda/a^2)}\right\} - (b/a)\,(c/a)\,K_1\int_{\lambda/a^2}^\infty \frac{d(\lambda/a^2)}{(1+\lambda/a^2)k'_\lambda} \tag{4a}$$

$$v = -\partial\phi/\partial y = -V + 2\,(b/a)\,(c/a)\,\frac{(Y/a)}{(b^2/a^2+\lambda/a^2)k'_\lambda A_o}\left\{\frac{K_1\,(X/a)}{(1+\lambda/a^2)}\right. \tag{4b}$$

$$\left. + \frac{K_2\,(Y/a)}{(b^2/a^2+\lambda/a^2)}\right\} - (b/a)\,(c/a)\,K_2 \int_{\lambda/a^2}^{\infty} \frac{d\,(\lambda/a^2)}{(b^2/a^2+\lambda/a^2)k'_\lambda}$$

$$w = -\partial\phi/\partial Z = 2\,(b/a)\,(c/a)\,\frac{(Z/a)}{(c^2/a^2+\lambda/a^2)k'_\lambda\,A_o}\left\{\frac{K_1\,X/a}{(1+\lambda/a^2)} + \frac{K_2\,(Y/a)}{(b^2/a^2+\lambda/a^2)}\right\} \tag{4c}$$

The symbols K_1, K_2, and A_o are defined by the equations

$$K_1 = \frac{U}{2-\alpha_o} \tag{5a}$$

$$K_2 = \frac{V}{2-\beta_o} \tag{5b}$$

$$A_o = \frac{(X/a)^2}{(1+\lambda/a^2)^2} + \frac{(Y/a)^2}{(b^2/a^2+\lambda/a^2)^2} + \frac{(Z/a)^2}{(c^2/a^2+\lambda/a^2)^2} \tag{5c}$$

Equations (4a), (4b), and (4c), which are valid only for an infinite medium, may not be applied directly to the problem of an ellipsoid in an infinite fluid half-space. They must be modified to take account of the fact that the normal component of the fluid velocity across the plane boundary must vanish. This latter requirement may be satisfied if one considers the system to be composed of an ellipsoid and its image in the boundary. The introduction of the image while it satisfies the velocity criterion on the plane boundary results in a perturbation of the flow at the ellipsoid wall and on the plane Z = 0. If the ellipsoid is not too close to the plane boundary, however, this interaction effect is small. For the purpose of a rough approximation, this perturbation effect may be neglected* so that one may obtain the velocity function on the plane boundary by the simple process of doubling the velocity changes given through Equations (4a) and (4b).

If the plane $Z = +h$, $h > c$, is taken to be the boundary, the modified expressions for the velocity components on this plane become

---

* If a higher order of approximation is desired, a greater number of images may be employed. The general scheme for the positioning of images whose centroids lie on the Z-axis is given by the expression $Z = \pm 2nh$ $n = 1, 2, 3, \ldots$.

$$u_h = -U + 4\,(b/a)\,(c/a)\,\frac{(X/a)}{(1+\lambda/a^2)k'_\lambda A_h}\left\{\frac{K_1(X/a)}{(1+\lambda/a^2)} + \frac{K_2(Y/a)}{(b^2/a^2+\lambda/a^2)}\right\} \tag{6a}$$

$$-2\,(b/a)\,(c/a)\,K_1\int_{\lambda/a^2}^{\infty}\frac{d(\lambda/a^2)}{(1+\lambda/a^2)k'_\lambda}$$

$$v_h = -V + 4\,(b/a)\,(c/a)\,\frac{(Y/a)}{(b^2/a^2+\lambda/a^2)k'_\lambda A_h}\left\{\frac{K_1(X/a)}{(1+\lambda/a^2)} + \frac{K_2(Y/a)}{(b^2/a^2+\lambda/a^2)}\right\} \tag{6b}$$

$$-2\,(b/a)\,(c/a)\,K_2\int_{\lambda/a^2}^{\infty}\frac{d\,(\lambda/a^2)}{(b^2/a^2+\lambda/a^2)k'_\lambda}$$

$$w_h = 0 \tag{6c}$$

where $A_h = \dfrac{(X/a)^2}{(1+\lambda/a^2)^2} + \dfrac{(Y/a)^2}{(b^2/a^2+\lambda/a^2)^2} + \dfrac{(h/a)^2}{(c^2/a^2+\lambda/a^2)^2}$ and the additional subscript h on the velocity components denotes that they are to be evaluated on the plane Z = +h.

If the ellipsoid is immersed in a body of water sufficiently deep so that the effect of the surface may be neglected, Equations (6a), (6b), and (6c) may be applied to compute the velocity field on the sea bed forward of the ellipsoid. Equations (6a), (6b), and (6c) will also serve to describe the velocity distribution produced on the bottom in the forward region by a half ellipsoid moving in the surface of a body of calm water of moderate depth h if the plane Z = 0 may be treated as a symmetry plane. This latter condition is met approximately if the half ellipsoid is moving slowly through the fluid since for this case the surface of the water is essentially smooth. In many cases of practical interest which involve surface vessels it is possible to make a rough representation of the underwater hull by a half ellipsoid of suitable dimensions. When such a representation is used and within the limitations stated, Equations (6a), (6b), and (6c) may be used to compute the approximate sea bottom velocity distribution in the neighborhood of the upstream hull-line.

If the parameter a is chosen as the unit of length, one may for fixed values of the ratios a/c, b/c, and h/a express Equations (6a), (6b), and (6c) in a functional form which will prove to be convenient for the purpose of the subsequent discussion. If note is taken of the fact that V = U tan θ, one may write

$$u_h = U\,[\alpha\,(X,Y,\lambda) - 1] \tag{7a}$$

$$v_h = U\,[\beta\,(X,Y,\lambda) - \tan\,\theta] \tag{7b}$$

where α and β are defined by the relations:

$$\alpha = \alpha(X,Y,\lambda) = 4\,(b/a)\,(c/a)\,\frac{(X/a)}{(1+\lambda/a^2)k'_\lambda\,A_h}\left\{\frac{(X/a)}{(2-\alpha_o)\,(1+\lambda/a^2)}\right.$$

$$\left.+\,\frac{(Y/a)\tan\theta}{(2-\beta_o)\,(b^2/a^2+\lambda/a^2)}\right\} - \frac{2}{(2-\alpha_o)}\,(b/a)\,(c/a)\int_{\lambda/a^2}^{\infty}\frac{d\,(\lambda/a^2)}{(1+\lambda/a^2)k'_\lambda} \tag{8a}$$

$$\beta = \beta(X,Y,\lambda) = 4\,(b/a)\,(c/a)\,\frac{(Y/a)}{(b^2/a^2+\lambda/a^2)k'_\lambda\,A_h}\left\{\frac{(X/a)}{(2-\alpha_o)\,(1+\lambda/a^2)}\right.$$

$$\left.+\,\frac{(Y/a)\tan\theta}{(2-\beta_o)\,(b^2/a^2+\lambda/a^2)}\right\} - \frac{2\tan\theta}{(2-\beta_o)}\,(b/a)\,(c/a)\int_{\lambda/a^2}^{\infty}\frac{d\,(\lambda/a^2)}{(b^2/a^2+\lambda/a^2)k'_\lambda} \tag{8b}$$

Although λ is related to X and Y through the relation

$$\frac{(X/a)^2}{(1+\lambda/a^2)} + \frac{(Y/a)^2}{(b^2/a^2+\lambda/a^2)} = 1 - \frac{(h/a)^2}{(c^2/a^2+\lambda/a^2)} \tag{9}$$

it is convenient to think of α and β in the functional form given in Equations (8a) and (8b). Here, and in what follows, the parameters U and θ are considered to be fixed and, unless stated expressly otherwise, the velocity and pressure fields will be referenced to the plane boundary. Thus the velocity field at any arbitrary point (X', Y', h) is determined by the triplet of values (X', Y', λ') which satisfies Equation (9).

The pressure distribution function Δp, may be obtained from the Bernoulli equation for steady flow. For the case under consideration, the Bernoulli equation becomes

$$\Delta p = \rho U^2/2\,[\,1 + \tan^2\theta - (\alpha-1)^2 - (\beta-\tan\theta)^2\,] \tag{10}$$

In Equation (10) the units of Δp will be pounds per square foot when the velocities are expressed in ft/sec and the mass density, ρ, is expressed in slugs per cubic foot. It is more convenient to express Equation (10) in the dimensionless form,

$$\frac{\Delta p}{\rho U^2/2} = 2\,(\alpha+\beta\tan\theta) \tag{11}$$

in which, the squares of α and β have been neglected because α and β are small compared to unity.

In principle, a point-wise description of the pressure field has been given since the pressure change at any point (X, Y, h) may be calculated from Equation (11) after α and β have been determined from Equations (8a) and (8b). Of equal practical interest, however, is the determination of the lines of equipressure change. In the discussion which follows a procedure for obtaining these lines of equipressure change is described.

It is clear from an inspection of Equation (11) that at each point which lies on a line of given equipressure change, the following condition must be satisfied

$$(\alpha+\beta \tan \theta) = K \tag{12}$$

where K is a constant which has the same value at each point on the line. For a prescribed value of θ, one may write Equation (12) in functional form as

$$f(X,Y,\lambda) = K \tag{13}$$

If one were to express λ as an explicit function of X and Y, say $\lambda = g(X,Y)$, by solving Equation (9) for λ, and then were to substitute $g(X,Y)$ into Equation (13), the following relation would be obtained

$$f[X,Y,g(X,Y)] = K = F(X,Y) \tag{14}$$

where F is some other function of X and Y only. One might expect that F(X,Y) would represent a complicated curve in the Z = +h plane. Nonetheless, it would appear that the equation of a line of equipressure change could be easily constructed from the set of coordinate pairs obtained when one substitutes arbitrary values of Y into Equation (14) and solves for the corresponding values of X. While the foregoing development may be carried out in principle, a careful study of Equations (7a) and (7b) will show the difficulties which are inherent if one proceeds in such a fashion. These difficulties arise because of the complicated form of the expressions for α and β and because, for points which do not lie on the coordinate axes, Equation (9) represents a cubic equation in λ.

On the other hand, it is possible to express Equation (12) as a quadratic equation in Y which has as its solutions

$$Y = \frac{-rX \pm \sqrt{(r^2-4ls)X^2-4lt}}{2l} \tag{15}$$

where l, s, r, and t (to be defined) are functions only of λ and K, or λ alone. In terms of Y, Equation (9) yields

$$Y = \pm [m-nX^2]^{1/2} \tag{16}$$

where m and n are functions only of λ to be defined explicitly below. If Y is eliminated between Equations (15) and (16) one has, after performing two squaring operations to remove the radicals, a quadratic equation in x^2

$$X^2 = \frac{[2l(mnl-ms+nt)+(mr^2-2st)]}{2[n(nl^2+r^2-2sl)+s^2]} \pm \frac{\sqrt{[2l(mnl-ms+nt)+(mr^2-2st)]^2-4(ml+t)^2[n(nl^2+r^2-2sl)+s^2]}}{2[n(nl^2+r^2-2sl)+s^2]} \tag{17}$$

The functions l, s, r, t, m, and n introduced above are defined as follows:

$$l \equiv \frac{1}{a^2(b^2/a^2+\lambda/a^2)^2}\left[\frac{\tan^2\theta}{2-\beta_o} - \frac{k'_\lambda}{2}\left\{\frac{d}{2-\alpha_o} + \frac{e\tan^2\theta}{2-\beta_o}\right\} - 1/8\,(a/b)\,(a/c)\,k'_\lambda K\right] \tag{18a}$$

$$r \equiv \frac{\tan\theta}{a^4(1+\lambda/a^2)(b^2/a^2+\lambda/a^2)}\left\{\frac{1}{2-\beta_o} + \frac{1}{2-\alpha_o}\right\} \tag{18b}$$

$$s \equiv \frac{1}{a^2(1+\lambda/a^2)^2}\left[\frac{1}{2-\alpha_o} - \frac{k'_\lambda}{2}\left\{\frac{d}{2-\alpha_o} + \frac{e\tan^2\theta}{2-\beta_o}\right\} - 1/8\,(a/b)\,(a/c)\,k'_\lambda K\right] \tag{18c}$$

$$t \equiv -\left[\frac{(h/a)^2}{a^2(c^2/a^2+\lambda/a^2)^2}\,\frac{k'_\lambda}{2}\left\{\frac{d}{2-\alpha_o} + \frac{e\tan^2\theta}{2-\beta_o}\right\} + 1/8\,(a/b)\,(a/c)\,\frac{k'_\lambda}{a^2}\,\frac{K(h/a)^2}{(c^2/a^2+\lambda/a^2)^2}\right] \tag{18d}$$

$$n \equiv \frac{(b^2/a^2+\lambda/a^2)}{(1+\lambda/a^2)} \tag{18e}$$

$$m \equiv a^2(b^2/a^2+\lambda/a^2)\left[1 - \frac{(h/a)^2}{(c^2/a^2+\lambda/a^2)}\right] \tag{18f}$$

The symbols d and e which appear in Equations (18a), (18c), and (18d) are defined by the relations:

$$d \equiv \int_{\lambda/a^2}^{\infty} \frac{d(\lambda/a^2)}{(1+\lambda/a^2)k'_\lambda} \tag{19a}$$

$$e \equiv \int_{\lambda/a^2}^{\infty} \frac{d(\lambda/a^2)}{(b^2/a^2+\lambda/a^2)k'_\lambda} \tag{19b}$$

For a chosen value of λ and of K there are four values of X which satisfy Equation (17). These four values of X when substituted into Equation (16) serve to determine four corresponding values of Y. Thus to a single value of λ and of K there correspond four points of equal pressure change. By making successive choices of λ for a fixed value of K one can obtain a sufficient number of points of equal pressure change to use as the basis for the construction of a given line of equipressure change. If this procedure is repeated one may obtain, by varying K, any desired number of lines of equipressure change.

Certain limits must be placed on the value of λ which may be chosen if the four values of X obtained from Equation (17) are to be real. This restriction

on the permissible values of λ arises because a given curve of equipressure change will not, in general, intersect all of the ellipsoidal surfaces which would be generated if λ were permitted to vary over the range, $-c^2 < \lambda < \infty$. If the line of equipressure change neither pierces nor is tangent to the ellipsoidal surface which corresponds to a chosen value of λ, the values of X obtained from Equation (17) will be imaginary.

For values of λ less than $(h^2 - c^2)$, the confocal central ellipsoidal surfaces defined by Equation (2) will not intersect the plane Z = +h. Hence, for such values of λ, the roots of Equation (17) will be imaginary. When λ satisfies the condition that λ is greater than $(h^2 - c^2)$, the confocal central ellipsoids intersect the plane Z = +h in the real closed elliptic curves given by Equation (9). If now the value of λ is so chosen that the given line of equipressure change intersects the real closed elliptic curve associated with the value of λ, the roots of Equation (17) will be real.

The findings from theoretical studies and experimental measurements of flow patterns around ships will serve as a guide to the general location of the positive and negative regions of the pressure fields associated with ships. Thus, for a particular case under study, if an ellipsoidal representation of the vessel is used, it is a simple matter to choose the proper range of values of λ so that the roots of Equation (17) are real.

The results of certain computations which have been based on the use of the ellipsoid model, a:b:c = 10.50:1.11:1, are illustrated in Figure (2). The ratio h/a was taken to be 0.35. The ellipse shown in Figure (2) represents the projection on the plane of the bottom of the principal horizontal cross-section of the ellipsoid model.

Computations have been carried out for three different angles of yaw, (θ = 30^o, 45^o, and 60^o) and the line of zero pressure change to be associated with each angle is shown on Figure (2). For the value $\theta = 45^o$ the dimensionless quantity $\Delta p/\rho(U^2 + V^2)/2$ has been evaluated at a number of points which lie on the bottom in the region where the theory may be expected to apply. At each such point the value of $\Delta p/\rho(U^2 + V^2)2$ has been set forth on the figure.

Equation (9) defines the curves of intersection of the confocal central ellipsoidal surfaces given by Equation (2) with the plane Z = +h. These curves are real central ellipses (with respect to (0, 0, +h)) if λ satisfies the condition that λ is greater than or equal to $(h^2 - c^2)$. One may, through the use of Equation (9), select any number of coordinate pairs (X,Y) which satisfy the ellipse determined by a chosen value of $\lambda (\lambda \geqq h^2 - c^2)$. The value of λ and any desired number of corresponding corrdinate pairs may readily be chosen in such a fashion that the quantity $\Delta p/\rho(U^2 + V^2)/2$ will be evaluated at a fairly representative number of points in the region of interest. All such points will lie on the ellipse defined by the selected value of λ. If this process is repeated for several other choices of λ it is possible to obtain a reasonably complete picture of the magnitudes of the pressure changes associated with the pressure distribution. As will be seen by an inspection of Figure (2), this procedure has been followed in selecting nearly all of the coordinate points at which $\Delta p/\rho(U^2 + V^2)/2$ has been evaluated.

SUMMARY

In the foregoing an attempt has been made to set forth a procedure which may be employed to obtain a rough approximation of the sea bottom pressure

distributions produced in the neighborhood of the upstream hull line by a surface vessel yawed more than 20°. The vessel is considered to move at low speed in a calm sea of moderate depth. To this end a treatment of the flow pattern around an ellipsoid model in an infinite nonviscous fluid half-space is given. A brief derivation of the most important formulae for the velocity and pressure distributions produced by the ellipsoid on the plane boundary is presented. The mathematical complexities involved if one attempts to determine an analytical expression for the curves of equipressure change are pointed out and an alternative procedure for obtaining these curves is described. An application of the theory has been made to a special case. The results of certain calculations made in this regard have been presented to illustrate the principal features of the pressure distributions which may be expected.

ACKNOWLEDGMENT

The author is indebted to T. C. Watson, U. S. Navy Mine Defense Laboratory, for carrying out all of the lengthy computations from which the curves and data shown on Figure (2) have been obtained. Thanks are also due to Dr. M. R. Carstens of Georgia Tech Research Institute for his assistance in the preparation of this paper. Helpful discussions with Dr. G. B. Findley, U. S. Navy Mine Defense Laboratory, and Dr. J. P. Craven and J. Power of the David Taylor Model Basin are also appreciated. The work was suggested by J. A. Robertson, Civil Engineering Department, Washington State College.

REFERENCES

1. Milne-Thompson, L. M., Theoretical Hydrodynamics, The MacMillan Company, (1950), p. 453.

2. Byrd, P. F., and Friedman, M. D., Handbook of Elliptic Integrals for Engineers and Physicists, Lange, Maxwell and Springer Ltd., (1954), p. 84.

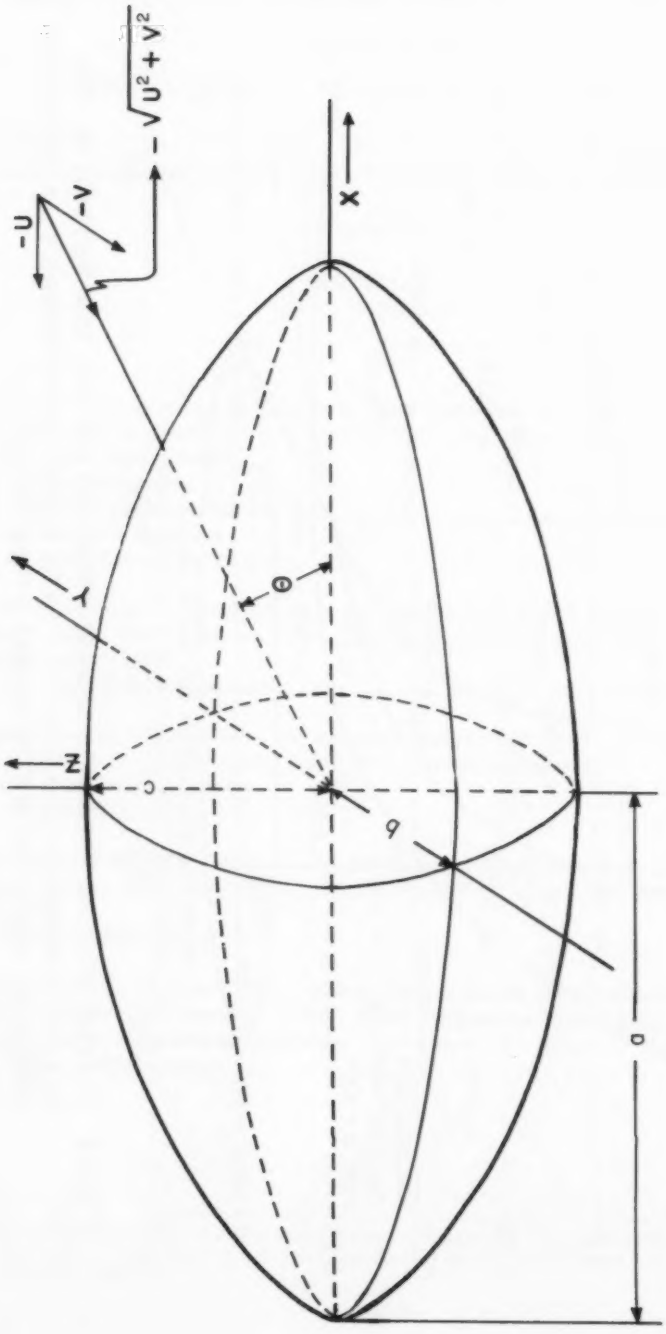

FIG. 1. REPRESENTATION OF THE ELLIPSOID (a>b>c) IN A UNIFORM STREAM

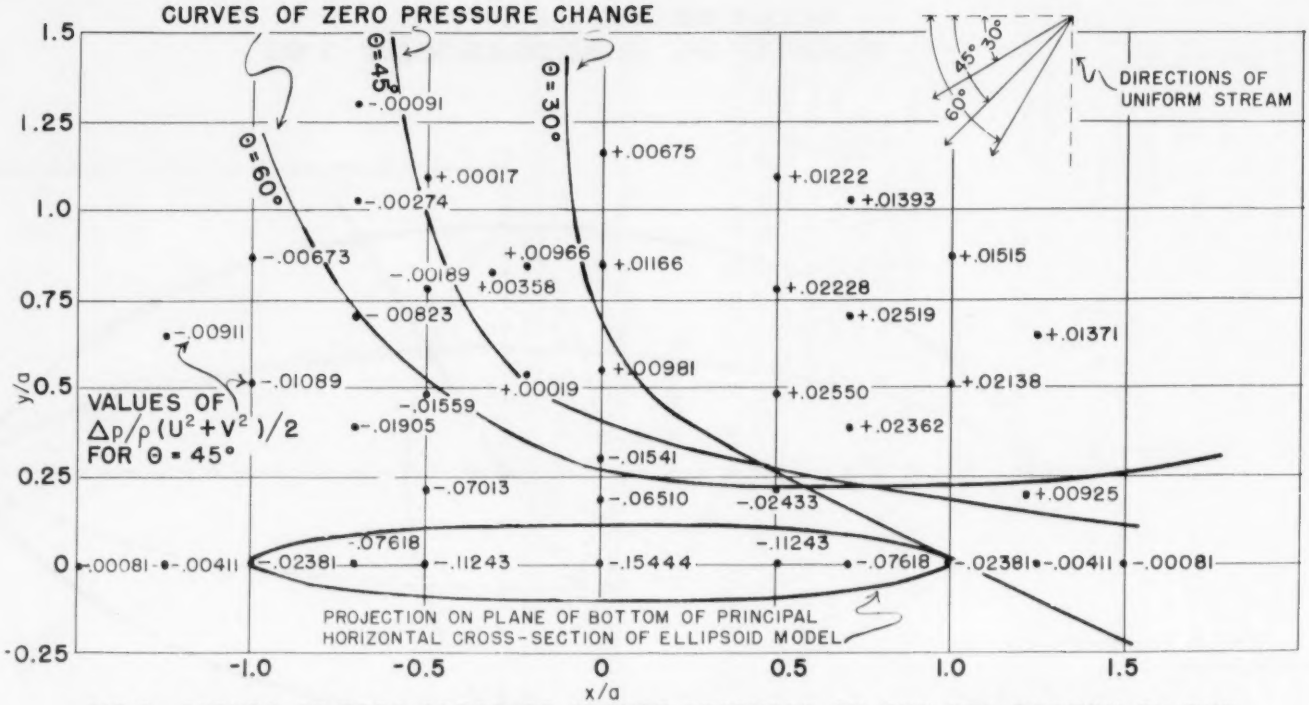

FIG. 2 CURVES OF ZERO PRESSURE CHANGE PRODUCED ON THE SEA BOTTOM BY THE ELLIPSOID MODEL, a:b:c:=10.50=1.11:1. EACH CURVE CORRESPONDS TO A DIFFERENT ANGLE OF YAW. THE RATIO h/a WAS TAKEN TO BE 0.35.

Paper 1520 January, 1958 EM 1

Journal of the
ENGINEERING MECHANICS DIVISION
Proceedings of the American Society of Civil Engineers

CONTENTS

DISCUSSION
(Proc. Paper 1520)

THE BOUNDARY LAYER DEVELOPMENT IN OPEN CHANNELS[a]

Discussion by Yoshiaki Iwasa, Alfred C. Ingersoll and Masashi Hom-ma
Closure by J. W. Delleur

YOSHIAKI IWASA.*—Prof. Delleur's study of the growth of the turbulent boundary layer in open-channel flows as well as that by Dr. Halbronn is most outstanding. The formulation of the dynamic principles of boundary layer and of the behavior of open channel flows will be shown in a different way. Use will be made of the one-dimensional approach of classical hydraulics in the light of modern hydro-dynamics.

The writer has studied for several years the problem of boundary layer growth associated with open channel flow; the results for a smooth channel are to be published in the Memoirs of the Fac. Eng., Kyoto University. This writers' study primarily with the hydraulic behavior of boundary layer growth for initially rapid flows, whereas Prof. Delleur was concerned with the flow on a horizontal bed and with the hydraulic behavior of the main flow near critical regime.

The writer wishes to show both theoretical and experimental results obtained from a study of boundary layer growth in open channel flow.

This earlier theoretical study has been presented to the Annual Convention of JSCE in Kwansai District held at Kobe University, Kobe, Japan in 1955; the experimental research has been conducted at the Hydraulics Laboratory, Kyoto University, with the use of a very smooth lucite flume 36 ft. long and of slope varying from 0° to 30°. The main part of the experimentation was conducted by Messrs. H. Matsunami and S. Kinukawa in 1956 when the writer was at the Hydrodynamics Laboratory, Massachusetts Institute of Technology.

Although our theoretical procedure is the same as that of Halbronn and Delleur, basic relationships of both main and boundary layer flows used by Prof. Delleur are hydrodynamically proved in what follows.

Dividing the flow into two parts: main and boundary layer, the principle of conservation of momentum or the integration of the Eulerian equation of motion for two dimensional main flow yields, under the assumption of hydrostatic distribution of pressure:

$$u_1 \frac{du_1}{dx} = g\left(\sin\theta - \cos\theta \frac{dh}{dx}\right) , \qquad (1)$$

where u_1 = velocity of main flow, x = distance along the channel bottom, h = fluid depth, g = acceleration of gravity, and θ = inclination angle of channel bed.

a. Proc. Paper 1138, January, 1957, by J. W. Delleur.

* Asst. Prof. of Hydraulics, Dept. of Civ. Eng., Kyoto University, Kyoto, Japan.

Integrating Eq. (1) with respect to x: to result in

$$E = \frac{u_1^2}{2g} + h\cos\theta - x\sin\theta \quad . \tag{2}$$

This is the well known equation of Bernoulli and the basic equation of Prof. Delleur.

The same principle used for boundary layer flow yields

$$\frac{\tau_0}{\rho} = g\delta(\sin\theta - \cos\theta\frac{dh_1}{dx}) - \frac{d}{dx}\int_0^\delta u^2 dy + u_1\frac{d}{dx}\int_0^\delta u\,dy \quad , \tag{3}$$

where T_0 = boundary shear and δ = boundary layer thickness.

In order to derive the usual form of the boundary layer equation in terms of displacement and momentum thicknesses, Eq. (1) is multiplied by δ, and then added to Eq. (3):

$$\frac{\tau_0}{\rho} = \frac{d}{dx}\int_0^\delta u(u_1 - u)\,dy + \frac{du_1}{dx}\int_0^\delta (u_1 - u)\,dy \quad . \tag{4}$$

With the aid of expressions of displacement and momentum thicknesses, Eq. (4) becomes

$$\frac{\tau_0}{\rho u_1^2} = \frac{d\vartheta}{dx} + \frac{1}{u_1}\frac{du_1}{dx}(2\vartheta + \delta_*) \quad . \tag{5}$$

Thus, basic relations used by Prof. Delleur are shown to be valid with the one dimensional procedure of approach from hydrodynamics.

The mutual relationship between the boundary layer approach and the usual one dimensional approach for mean flow, which was not explained by Prof. Delleur, can be established as follows:

Integrating Eq. (1) with respect to y throughout the whole region of main flow, and adding this relation to Eq. (4) yields

$$\frac{\tau_0}{\rho} = gh\sin\theta - gh\cos\theta\frac{dh}{dx} + \frac{\beta q^2}{h^2}\frac{dh}{dx} \quad , \tag{6}$$

where β = momentum correction factor. Therefore, with the use of normal depth h_0 and critical depth h_c, we can get

$$\frac{dh}{dx} = \tan\theta\,\frac{h^3 - h_0^3}{h^3 - h_c^3} \quad . \tag{7}$$

This is the hydraulic equation derived usually by the one dimensional approach

for mean flow. It means that the introduction of the boundary layer concept to open channel flows does not require any new knowledge for the hydraulic equation in classical hydraulics. However, the transitional behavior of flow near an entrance to a channel is more precisely expressed by solving simultaneously three basic equations for main flow, boundary layer, and constant discharge together.

At the entrance to the channel there is a reach where the assumption of flow without curvature is not valid as this hypothesis makes the velocity near the bottom faster than that in the upper flow. Therefore, to make the actual flow consistent with the mathematical assumption at the initiation of growth used by Prof. Delleur and the writer, a lucite guide vane was set up for our experiments to get a uniform velocity distribution at the entrance zone. Although the influence of setting the guide vane on flow characteristics is expected, the writer will only describe the following experimental results of velocity profile and its related skin friction law.

1. For a smooth boundary, the shape of the velocity profile of the turbulent layer is better approximated by the power type of law than the logarithmic law as Dr. Bauer* and Prof. Delleur concluded. Although the behavior of H expressed by $\delta_*/$ indicates a quite different character from the usual conclusion obtained by the unconfined theory, as seen in Fig. 1, it rapidly tends to a certain definite value determined by flow characteristics.

2. The local skin friction coefficient, $C_f = 2\,T_o/\rho\,u_o^2$, has slightly lower values than those derived from the curves of Blasius and Dr. Bauer (Fig. 2).

3. The Karman constant in the logarithmic velocity law decreases rapidly with the increase of Reynolds numbers and converges to a constant value of 0.40, as seen in Fig. 3.

Although the conclusion may be largely influenced by the guide vane, we can show the same behavior for steady uniform flow after the fluid has travelled downstream; this was shown by Dr. Keulegan and Prof. Powell.

The mathematical behavior in terms of a power law derived by three basic equations indicates that the expression has a singular point very near the origin of growth. However, as an approximation, the development of boundary layer will be expressed in a form of

$$\frac{\tan\theta}{\lambda\cdot H}\,\nu'^{m}\,\eta^{1-m} = \frac{1-m}{3+(1-m)(1+H)}\,r^{2+m}\left\{1-\left(\frac{r_o}{r}\right)^{\frac{3+(1-m)(1+H)}{7}}\right\} - \frac{\sigma}{1+H}\,r^{-1+m}\left\{1-\left(\frac{r_o}{r}\right)^{(1-m)(1+H)}\right\}. \qquad (8)$$

where λ = ratio of skin friction coefficient to mth power of Reynolds numbers, ν' = dimensionless parameter of kinematic viscosity and γ and σ = the same parameters as Prof. Delleur used. For the case of the Blasius 7th law,

$$\frac{\tan\theta}{\nu'^{\frac{5}{4}}}\,\eta^{\frac{5}{4}} = 0.00367\,r^{\frac{7}{4}}\left\{1-\left(\frac{r_o}{r}\right)^{\frac{41}{7}}\right\} - 0.007530\,r^{-\frac{5}{4}}\left\{1-\left(\frac{r_o}{r}\right)^{\frac{20}{7}}\right\}. \qquad (9)$$

Fig. 4 describes the growth of boundary layer calculated by several approaches. It is seen that for a smooth boundary the blasius 7th law indicates a close approximation of actual development.

Because we are concerned with the practical application to channel design,

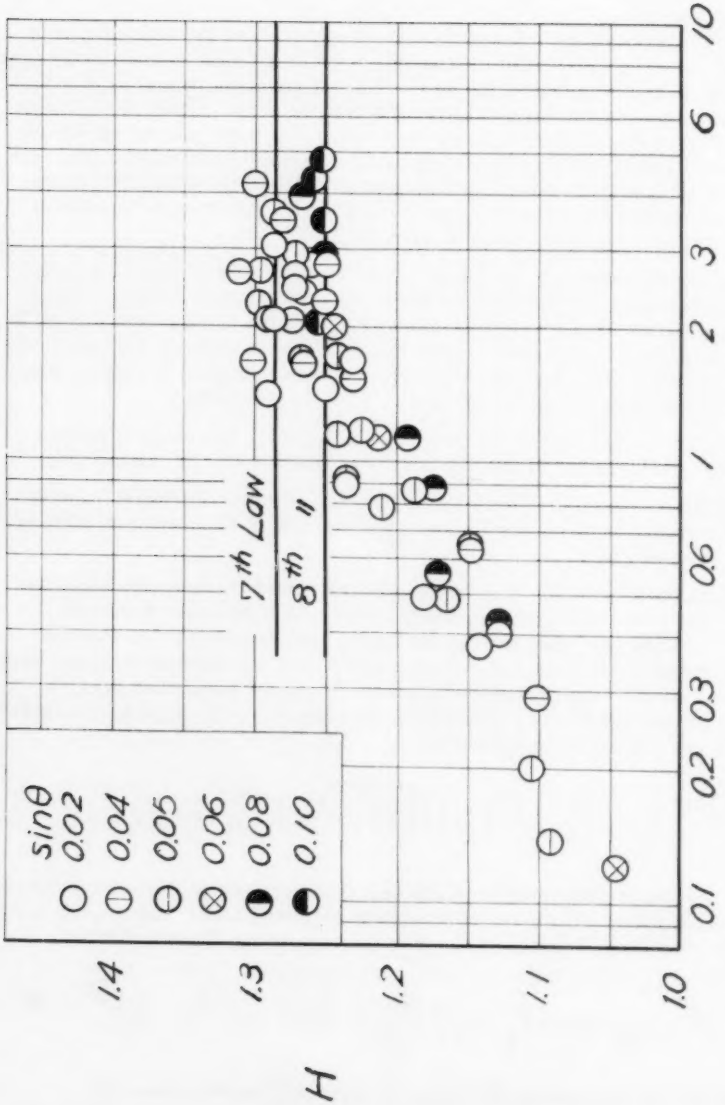

Fig. 1. Growth of H with the increase of Reynolds Numbers of Displacement Thickness.

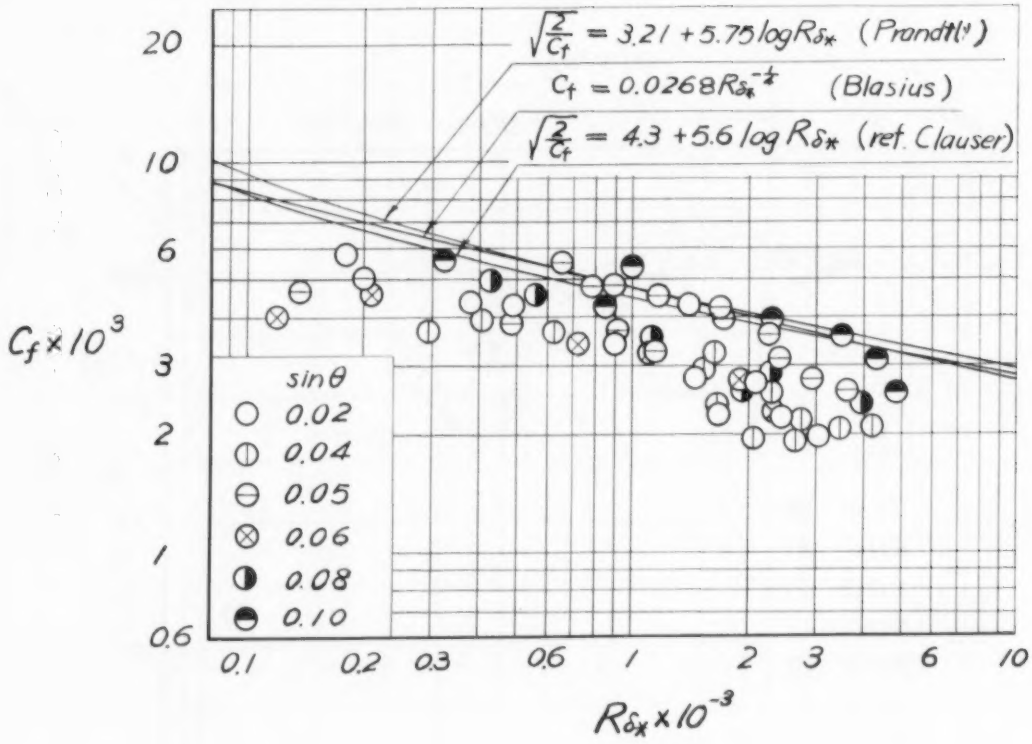

Fig. 2. Skin Friction Coefficient in Turbulent Boundary Layer.

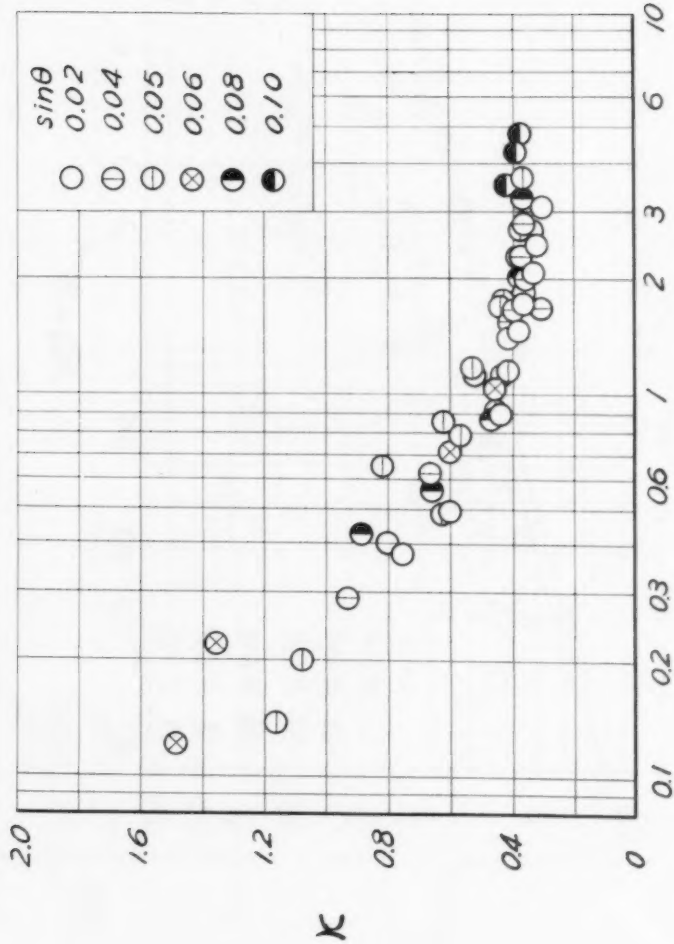

Fig. 3. Karman Constant in Turbulent Boundary Layer.

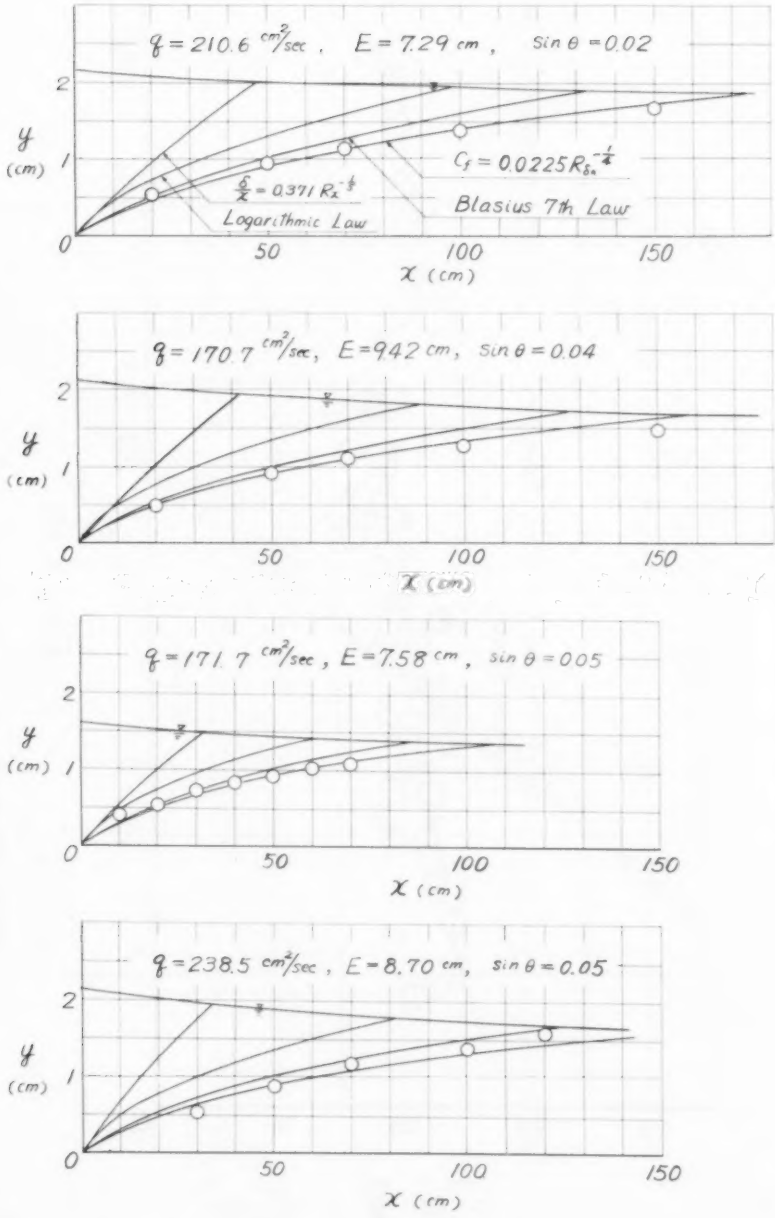

Fig. 4. Examples of Boundary Layer Growth.

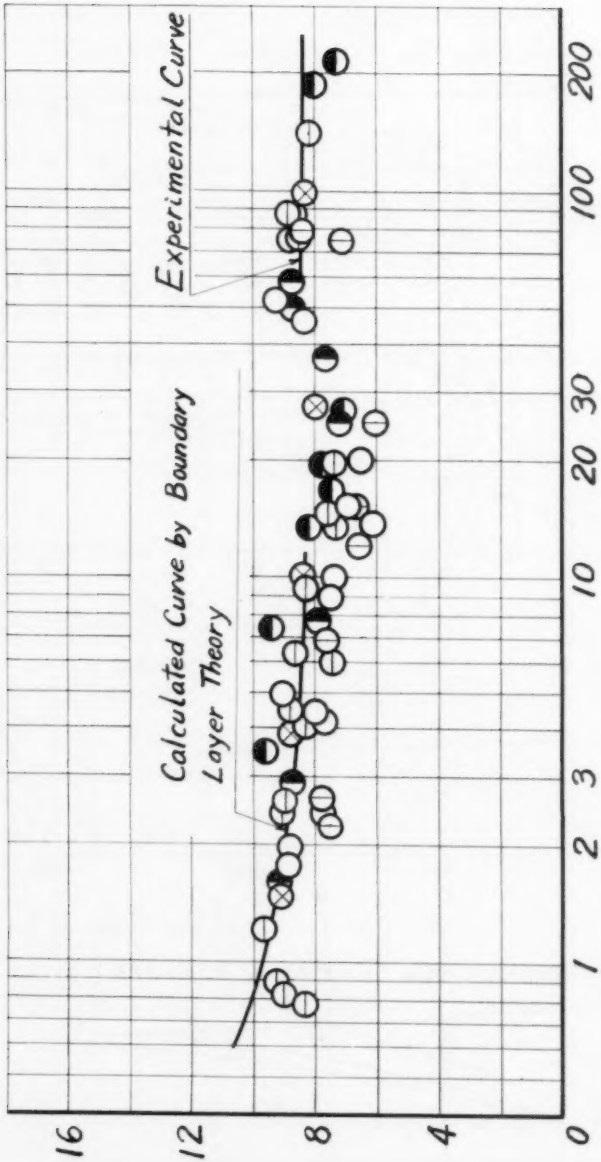

Fig. 5. Manning Roughness of a Very Smooth Lucite Bed.

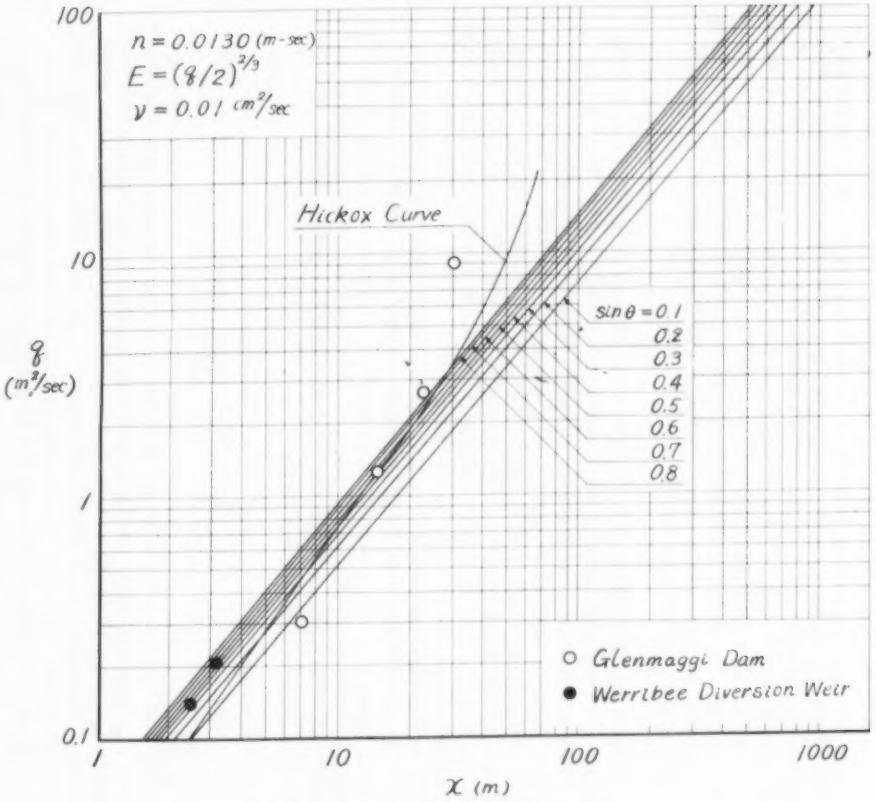

Fig. 6. Location of Critical Point.

the Manning roughness and the location of critical point where the boundary layer intersects the free surface should be considered. Fig. 5 indicates the behavior of the Manning roughness with an increase of distance and it is understood that the Manning roughness has a constant value determined by channel characteristics, while it has a large value at the earlier stage of development. Therefore, we may conclude that the channel is adequately designed by the usual method of one dimensional approach, as a close approximation.

The determination of the location of the critical point is also of importance for air-entrained flow and laboratory investigation. Fig. 6 describes the location of the critical point of flows over a concrete shute under the assumption of Manning roughness n = 0.013 and $E = (q/2)^{2/3}$. The plottings are obtained by field observation of Lovely and Michels.

It is hoped that much of the true nature of fluid motion still unsolved will be soundly clarified through the physical knowledge obtained by the boundary layer theory. However, a clear formulation of the boundary layer process is quite difficult because of the great difficulty with the mathematics and with the systematic experimentation.

ALFRED C. INGERSOLL,* M. ASCE.—One of the new horizons opened by this paper is the application of Mr. Delleur's boundary layer theory to the determination of bed shear stresses in open channels with movable beds. Knowing only the channel geometry, discharge, surface velocity and water temperature, it is possible to compute values of T_o without having any measurement of the slope of the energy gradient. This attack is especially helpful in the study of bed shears in settling tanks where the velocities are so low that no determination of slope can be made.

The writer has had occasion to test out this application in a glass-walled flume 1.27 ft. wide by 14 ft. long, at depths varying from 0.610 to 0.623 ft., the floor being partially covered with particles of gilsonite ranging from 0.0232 to 0.0328 in. in diameter. Surface velocities, u_1, were measured by timing confetti streamers. For the purpose of this computation Eq. (17) is written in the more convenient form,

$$\delta_* = R\left(1 - \frac{V}{u_1}\right) \qquad (1)$$

in which V is the mean velocity and R is the hydraulic radius. The bed shear stress, T_o, is computed from Eq. (7) with m = 1/8. The measurements reported below were all taken at a point 8 ft. downstream from the inlet to the channel, a perforated plate baffle with about 10 per cent free area. For comparison purposes, values of T_o are also computed from the relation, $T_o = fV^2/8$, where f is determined from the Moody chart of friction factor for pipes, (Ref. A) with Reynolds number equal to $4RV/\nu$, and relative roughness given by the size of gilsonite particles relative to 4R, or 0.0018.

* Associate Prof. of Civ. Eng., Calif. Inst. of Technology, Pasadena, Calif.

Mean Velocity V fps	Surface Velocity u_1 fps	Displacement Thickness δ_* ft.	Bed Shear by Eq. (7) τ_o psf	Bed Shear by Friction Factor τ_o psf
0.112	0.122	0.0270	0.925×10^{-4}	0.924×10^{-4}
0.116	0.127	0.0272	0.985	0.991
0.122	0.133	0.0258	1.093	1.094
0.128	0.140	0.0268	1.180	1.199

The remarkable agreement between the values of bed shear computed by these two methods is perhaps not surprising inasmuch as each method stems from the application of pipe flow formulas to open channels. The boundary layer approach, however, utilizes the Blasius formula and the concept of the virtual channel, while the friction factor method is based on the Colebrook-White function for flow in rough pipes.

The concept of the virtual channel is interesting and helpful. If the equation for the shaded corner areas if $y'z' = 9.312\delta_*^2$ as indicated in Fig. 1, however, the writer believes that the last term of Eq. (12) would come to $-23\,\delta_*^2$ instead of the $0.5\,\delta_*^2$ shown. Even with this value, however, the term would still be less than 5 per cent of A, which might justify its omission for many types of computations.

With reference to curve II in Fig. 3, the writer is confused by the statement that "r_1 is the value of r which satisfies Eq. (31)." Inasmuch as Eq. (31) is simply the equation of curve II, then all values of r will satisfy the equation for corresponding values of σ. The values of r_0, r_1, r_2, and r_3 in Fig. 3 all seem to be related to a value of $\sigma = 0.75$. Whether this is simply a representative value of σ or whether it has some special significance is not immediately clear.

In Table I it is not clear what the difference is between the first and third rows. In both cases, presumably, the values of δ_* have been computed from velocity profiles, but the values in the first row seem to be just 1.74 times those of the third row in each instance.

The writer finds the concept of the "vertical tangent" referred to in the section on general properties of the boundary layer development to be a very difficult one. Regardless of what the theory may predict, the physical concept of a boundary layer above a horizontal bed having a vertical tangent seems indeed remote from reality.

The author makes considerable use of H as a length parameter. As it is tied to the specific energy, E_S, it must vary along the length of a horizontal channel unless the reference value of E_S is fixed at one particular point. Similarly the author refers to "uniform flow" as that occurring in the horizontal channel after the boundary layer has pierced the surface. As it is commonly understood, uniform flow cannot occur at any time in a horizontal channel because the frictional losses cannot be equated to the drop in bed level. Clarification on these points will be helpful.

In the analysis of experiments the author remarks that σ is not a free parameter when E_S and L are given. Inspection of the summary data reveals that Series B and C have very closely the same energy (0.259 against 0.2505) while their values of σ vary widely (from 0.50 to 0.855). Considering Series A and C, on the other hand, reveals that the values of σ are almost the same

while the specific energies differ considerably. Is it not true that the tank length, L, was the same for all of these tests? If it was, as would appear to have been the case, how may these anomolous relations be accounted for?

This paper is a signal contribution to the understanding of open channel fluid mechanics, yielding as it does a means for computing the boundary layer development in rectangular channels. The writer hopes that the studies may be continued and extended to channels of other shapes, and especially to the very tranquil flows encountered in settling tanks. While still in the turbulent range, such flows would be characterized by values of the discharge parameter σ on the order of 0.01, far below the range of values presented here.

The writer wishes to acknowledge with thanks the assistance of Mr. A. R. Porush and Mr. H. J. Hansen in making the bed shear tests reported hereinbefore.

REFERENCE

A. Daugherty, R. L., and A. C. Ingersoll, Fluid Mechanics, p. 182, McGraw-Hill Book Company, New York, 1954.

MASASHI HOM-MA.[1]—The author's treatment of the problem is very interesting and valuable for the promotion of further research. The writer wishes to consider these phenomena and to suggest research on related problems.

The author's fundamental equations for the main flow may be written as,

$$(h - \delta_*) + \frac{u_1^2}{2g} = E_s - \delta_*$$

$$q = u_1 (h - \delta_*)$$

If we limit the problem to two-dimensional motion, these are the equations for the flow of an ideal fluid over a solid bottom, the height of which coincides with the displacement thickness in each section. Therefore, when we consider a flow which changes from subcritical to supercritical on this bottom, the control section must be the section where the value of $E_S - \delta_*$ is minimum. This fact shows that in such flow the displacement thickness must take its maximum at the control section.

Actually, the discharge of ideal fluid through the depth $h - \delta_*$ is not equal to q but is equal to $q - \Delta q$ (see figure 2). In the boundary layer there must occur the energy consumption which will cause the inflow of momentum from the main flow. (This must be the inflow of a certain mass of fluid from the main flow into the boundary layer). Thus the value of Δq will increase with the distance x from the inlet section.

In the subcritical flow, the decreasing of δ_* with the distance x is accompanied with the increasing of the depth $h - \delta_*$ and the decreasing of u_1 (see Fig. 1). This means that the increasing of Δq is impossible and also the decreasing of δ_* can't occur in the subcritical flow.

On the contrary, it is understood from Fig. 1 that the decreasing of δ_* can be accompanied with the increasing of Δq in the supercritical flow. Now the writer finds that the author's idea is reasonable and it will lead us to valuable results.

---

1. Prof. Dept. of Civ. Eng., Univ. of Tokyo, Tokyo, Japan.

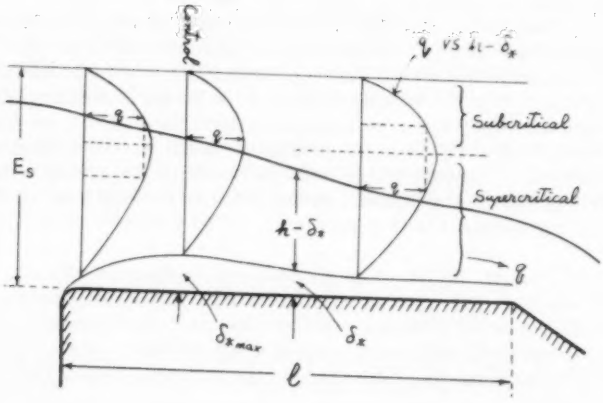

Figure 1

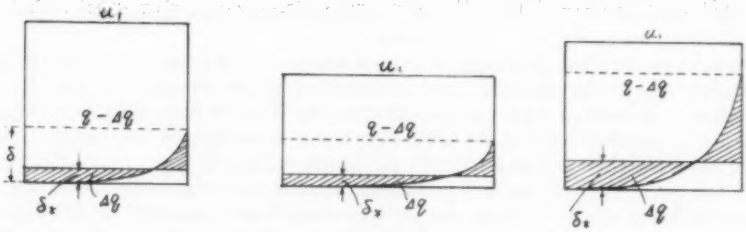

Figure 2

But a doubt still remains. If we consider the case when the length (ℓ) of the dam crest is very long, the author's result shows that δ_* continues to decrease until the amount of u_1 becomes extremely large. Such velocity seems not to take place. Also, in an inclined open channel, an uniform flow state of ideal fluid is impossible, because the ideal fluid must be accelerated constantly in the channel. Rarely can we observe a fairly long extent of undisturbed surface in a steep-sloped flow, but when the flow becomes uniform, the boundary layer must extend itself to the free surface. It seems to the writer that after a long run of flow the boundary layer grows with increasing Δq (discharge through the depth δ_*) even in supercritical flow. Here we will look back the theoretical analysis of the problem. In the writer's opinion, for the case of a long channel, a correction must be added to the pressure term in the equation (4) of the original paper, because the water depth above the boundary layer is not constant in this problem.

J. W. DELLEUR,* A.M. ASCE.—The discussions by Messrs. Blench, Ingersoll, Iwasa and Hom-ma were most stimulating. Professor Blench makes a number of inquiries from the point of view of the practicing engineer, whereas, Messrs. Ingersoll and Iwasa present some additional experimental data, and, as Professor Hom-ma, they discuss the problem from a fluid mechanics point of view.

Consider first Professor Blench's questions. A fully developed flow does not occur in the throat of a broad crested weir under usual conditions. The flow is critical, and the boundary layer reaches a maximum at a point near the brink. A fully developed flow can occur, however, in a horizontal open channel if it is long enough. The fully developed flow will start where the boundary layer reaches the surface. At this point, the value of the independent variable r is given by eq. (33), which replaced in (27) with the proper value of the flow parameter σ, will yield the corresponding value of m. The value of $m = 0.13$ has no particular significance.

Regarding Professor Blench's second and third questions, eq. (15) defines the energy E_S of the potential flow, and H; it does not compel critical flow. The theory developed does not require that the flow be very nearly critical. It is solely pointed out that the boundary layer development will reach a maximum when the flow is close to critical, as given by (34).

In his questions (iv) and (v) Professor Blench challenges the use of the boundary layer momentum eq. (4) for turbulent flows, because of the neglect of the turbulent shear-stress. Although the justifications for so doing were already briefly mentioned in the paper immediately after eq. (4), it may be added here that Ross(5) and Robertson(6) have integrated the complete Reynolds equations, and have obtained four corrective terms due to anisotropy of the turbulence normal stresses, to the second derivative of the shear stress, to the deviation of the mean flow from Prandtl's assumptions, and to the viscosity. Essentially these corrections are all connected with the fact that the pressure is not exactly constant across the boundary layer. With the first correction, which is the predominant one, the momentum equation reads

$$\frac{\tau_0}{\rho} = u_1^2 \frac{d\theta}{dx} + (2\theta + \delta_*) u_1 \frac{du_1}{dx} - \frac{1}{u_1} \int_0^\delta \frac{\partial}{\partial x} (\overline{u'^2} - \overline{v'^2})\, dy$$

* Associate Prof. of Hydr. Eng., School of Civ. Eng., Purdue University, Lafayette, Ind.

However, past experiments have shown that this correction may be neglected for zero or small pressure gradients.

Finally, it is not agreed, as Professor Blench states in his sixth question, that σ is $H^{3/2}$ divided by itself. σ has the form of a Froude number, and perhaps, is an unconventional one. However, there are many accepted forms of the Reynolds number, in which the length term may be a pipe diameter, a displacement thickness, a grain size, or the velocity term may be $\sqrt{\tau_o/\rho}$, etc. Similarly, there is no reason why different forms of the Froude number cannot be constructed, as long as its form and non-dimentionality are respected.

The discussion by Dr. Ingersoll is most interesting, in particular because of his novel use of the boundary layer approach to compute the bed shear stress in open channels with movable beds. He computes the boundary layer displacement thickness from

$$\delta_* = R\left(1 - \frac{V}{u_1}\right)$$

which is the same as (26) in which the hydraulic radius, R, replaces the depth. His comparison of the bed shear stress obtained by Blasius formula, eq. (7), and the Colebrook-White function for pipe flow is noteworthy.

One of the difficulties encountered in the computation of the virtual channel area is that of evaluating the zone of mutual interference of the displacement thicknesses in the corners of the channel. In view of the question asked by Dr. Ingersoll, the detail of the computation which was omitted in the paper for the sake of brevity, is given in what follows. Loitsianskii and Bolshakov[9] modified the 1/7th power law for the velocity distribution for the zone of interference of two boundary layers near the intersection of two plates, (fig. D-1), to

$$\frac{u}{u_1} = \left[\frac{y'z'}{a(x,\theta)}\right]^{1/7} \qquad \text{(D-1)}$$

and Blasius formula to

$$\frac{\tau_o}{\rho u_1^2} = 0.0225\left[\frac{\nu\, y'}{u\, a(x,\theta)\sin\theta}\right]^{1/4} \qquad \text{(D-2)}$$

where x is measured from the leading edge of the plates forming the corner in the direction of the flow, and θ is the angle of the corner. They show that the equation of the edge of the boundary layer is

$$y'z' = a(x,\theta) \qquad \text{(D-3)}$$

where

$$a(x,\theta) = \frac{K(\theta)}{\sin^2\theta}\,\delta_o^2(x) \qquad \text{(D-4)}$$

in which $K(\theta)$ is a certain non-dimensional constant parametrically dependent on the angle θ, and δ_o is the boundary layer thickness in the undistrubed region, away from the corner. The constant $K(\theta)$ has been determined by Loitsianskii and Bolshakov,[9] and for $\theta = 90^o$, $K(\theta) = 1.164$. Now, letting Zo(x) be the outside limit of the zone of interference, measured along the side or the bottom of the channel from the corner, at station x, as shown in fig. (D-1). For $y = Zo(x)$, $Z' = \delta(x)$, equations (D-3) and (D-4) yield

$$l_o(x) = \frac{a(x,\theta)}{\delta(x)} = \frac{K(\theta)\,\delta^2(x)}{y}$$

Since $K(90^o) = 1.164$ and since for the seventh power law $\delta = 8\delta_*$,

$$l_o(x) = 8 \times 1.164\,\delta_*(x) = 9.312\,\delta_*(x) \qquad \text{(D-5)}$$

Referring to figure (D-1) and calling A_T, the total area OAB'C'DO, A_L the "lost" area OABCDO, and A_N the net area BB'CC'B, it follows from the virtual channel concept that $A_N = A_T - A_L$, where A_N represents the area through which an ideal fluid flows with the same discharge as the real fluid through the total area. Thus

$$A_L = A_T - \frac{Q'}{u_1} \qquad \text{(D-6)}$$

where Q' is the discharge through A_T. The curved boundary B'C' of the zone of interference is defined by (D-3) which becomes

$$y'z' = a(x,\theta) = K(\theta)\,\delta^2(x) = 1.164 \cdot 8^2\delta_*^2 = 74.496\,\delta_*^2$$

Computing the area A_T:

$$A_T = 9.312\,\delta_* \cdot 8\delta_* + \int_{8\delta_*}^{9.312\delta_*}\int_o^{z_o'} dz'dy' = 85.808\,\delta_*^2$$

where

$$z_o' = \frac{74.496\,\delta_*^2}{y'}$$

and using the modified 7th power law (D-1) in (D-6)

$$A_L = A_T - \left\{\int_o^{8\delta_*}\int_o^{9.312\,\delta_*}\left[\frac{y'z'}{74.496\,\delta_*^2}\right]^{1/7} dz'dy' + \int_{8\delta_*}^{9.312\delta_*}\int_o^{z_o'}\left[\frac{y'z'}{74.496\delta_*^2}\right]^{1/7} dz'dy'\right\}$$

or

$$A_L = A_T - 74.496\delta_*^2 \cdot \frac{7}{8}\left[\frac{7}{8} + \ln(1.164)\right] = 18.874\,\delta_*^2$$

The cross section of the imaginary channel is thus

$$A = bh - (b - 18.624\delta_*)\delta_* - 2(h - 9.312\delta_*)\delta_* - 2 \times 18.874\,\delta_*^2$$

or

$$A = bh - b\delta_* - 2h\delta_* - 0.500\delta_*^2 \qquad \text{(D-7)}$$

With reference to the curves of fig. 3, the values of r_0, r_1, r_2, and r_3 are the values of r which satisfy equations (30), (31) and (35) for a given value of σ. For each discharge there is a particular value of σ for which there is a value of r_0, r_1, r_2 and r_3. These values are convenient for numerical computations, because they indicate the range of values that the independent variable r may take. The most reliable part of the curve of the growth of the boundary layer is that between its origin and its maximum—if it exits—that is for $r_0 < r < r_1$. It was stated after eq. (35), and is emphasized again that for $r > r_1$, the curve of growth of the boundary layer loses its accuracy, because of the curvature of the flow, which becomes important in that reach, was not considered in the derivation. As r approaches r_2, the theoretical curve ceases to represent accurately the physical phenomena. The plot of equations (27) and (28) see fig. 2) shows a point of vertical tangent, for $r = r_2$, which, as Dr. Ingersoll points out, is "remote from reality." Nevertheless, the important conclusion, which is confirmed by the experiments, is that beyond the maximum, for which $r = r_1$, the boundary layer decreases.

The length parameter H is tied to the specific energy E_S, (see eq. 15). For the purpose of the computations E_S was measured at the beginning of the turbulent boundary layer. In the experiments the value of E_S for series B and C are very close, but the value of the discharge parameter σ varies considerably. In Series B the flow was controlled by an adjustable weir at the downstream end of the channels, whereas in Series A the channel ended in a free fall. In all cases the length of the test flume was the same. The effect of the length of channel will be analyzed to show how E_S, σ, and L are related, and to show that there is no anomalous relation, as asked by Dr. Ingersoll.

It was stated that the equations (19) and (24) governing the development of the boundary layer do not contain explicitly the length L of the channel, because the energy E_S, the discharge parameter σ and the length of the channel are not independent. If E_S and L are given, σ may be computed. Two cases will be discussed, depending upon whether or not the maximum of the boundary layer exists (see eq. 34). Consider first the case of a broad crested weir, where the maximum exists. The length d between the origin and the point of maximum development may be obtained by integrating (28) between r_0 and r_1, assuming c = constant, and making use of (30) and (31) for the lower and upper limits respectively:

$$\frac{cd}{H} = \frac{1}{2}(2k+1)\ln\left(\frac{3}{2r_o^2} - \frac{1}{2}\right) + \frac{3}{4}\left[\frac{r_o(3-r_o^2)}{2}\right]^{2/3} + \frac{3}{4}r_o^2(2k+1) - \frac{3}{2}(k+1) \quad \text{(D-8)}$$

The dotted line in fig. 2 shows the locus of the maxima computed by the above equation, referred to as the approximate formula because of the approximation involved in taking c = constant. It should be noted here that c is very insensitive to changes in r and thus the approximation is a good one. On the other hand, d may be computed independently, by evaluating L - d, or the distance between the point of maximum boundary layer or point of critical flow and the free overfall. For this purpose the criteria developed by Rouse(A) may be used. If E_s and L are given, H may be computed from (15), L – d is estimated from the criteria, d is thus known; (D-8) may be solved for r_0, which, introduced in (30) will yield the value of σ. This reasoning may be used in developing a simple way of computing the discharge coefficient for flow over a broad crested weir.(16)

A similar argument may be developed when the boundary layer pierces the free surface if the length from the origin of the layer to the point of fully developed flow and the energy E_s are known, it may be shown that the discharge parameter σ may be evaluated.

Professor Iwasa's discussion is commended for rederiving the boundary layer momentum equation (4) from the one-dimensional analysis of open channel flow, and for tying the boundary layer principles to the classical Bresse formula (7 of Iwasa's discussion). Attention should be called to the unfortunate change of notation in Iwasa's discussion, in particular in eq. (8) of the discussion, which is clarified in the table below:

Item	Delleur's Notation	Iwasa's Notation
shape parameter $\frac{\delta^*}{\theta}$	$\frac{1}{k}$	H
critical depth	H	h_c
$\frac{\delta^*}{\delta}$	m	no symbol
Power of $\frac{u_1\delta^*}{\nu}$ in (7)	no symbol	m
	$-\frac{1}{4}$ in eq. (7)	
$\frac{\text{width}}{\text{critical depth}}$		no symbol
$\frac{\text{skin friction coefficient}}{\text{power of Reynolds No. in (7)}}$	no symbol	λ

Among the experimental data presented by Mr. Iwasa, fig. 4 of Iwasa's discussion is of special interest because it compares the values of the development obtained by experiment and analytically by means of Blasius 7th power law.

It is not agreed, as stated by Prof. Hom-ma, that the discharge through the depth h - δ_* is $q - \Delta q$, but simply q as derived in (10). It is true,

however, that there is a flow from the main flow into the boundary layer, and this is considered in the derivation[3] of the boundary layer momentum equation (4).

REFERENCE

A. Rouse, H., "Verteilung der hydraulischen Energie bei einem lotrechten Abstrus, Oldenburg, 1933.

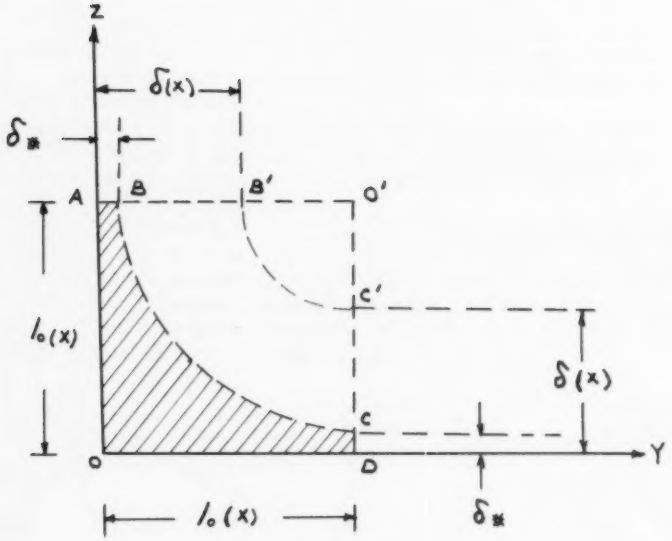

Fig. D-1. Corner of Channel

A PRESSURE LINE CONCEPT FOR INELASTIC BENDING[a]

Closure by Frank Baron

FRANK BARON,[1] M. ASCE.—Thanks are given to Mr. Hribar for his discussion and for his pertinent questions in regard to the pressure line concept for inelastic bending.

Mr. Hribar agrees that the pictorial procedure can be useful in quickly estimating the effects of plasticity on the behavior of structural elements subjected to axial and flexural loads. He also indicates that an estimate is frequently all that is desired in studies of the inelastic behavior of structural frameworks. The writer wishes to add that the degree of accuracy desired can depend on the needs and demands of an analyst. It is observed that the needs of an analyst are not always the same and that they do not always warrant "exact" solutions to problems. This is particularly true in the various stages of a design.

The statement is made by Mr. Hribar that the procedure results in only an estimate unless an analyst is experienced in the method and has a keen sense of judgment in balancing statics pictorially. Fortunately, little experience and almost no judgment are required in satisfying the requirements of statics. The only judgment required is to observe that the correction diagram as defined in the paper vanishes or balances. The diagram is balanced when the positive areas equal the negative areas and the centroid of the positive areas coincides with the centroid of the negative areas. This requirement is so simple that in most cases it can be judged by eye. However, as an aid to judgment, a numerical check can be made of any given estimate.

Several important attributes of the procedure need to be emphasized. In the theory of plasticity, the requirements of statics, geometry, and properties of materials are immediately apparent when stated pictorially and when compared to the results of the elementary theory of mechanics. In this way, every relationship can be observed including the relationship of the theory of plasticity to the elementary theory of mechanics.

Concerning the specific questions raised by Mr. Hribar, not all members are made of steel with idealized stress-strain curves nor are all cross-sections of members sufficiently simple to lend themselves to algebraic formulation. However, if an algebraic formulation is desired for a given stress-strain curve and a given shape of cross-section, the concept presented in the paper can be used with the same ease as present methods. At times, it can even be used with greater ease. For example, consider a parabolic stress-strain curve and a simple rectangular cross-section. Now determine by means of the pressure line concept the value of the reduced modulus, E_b,

---

a. Proc. Paper 1157, January, 1957, by Frank Baron.

1. Prof. of Civ. Eng., Univ. of California, Berkeley, Calif.

for any combination of axial load and moment about a principal axis of the section. The answer is obvious when the properties of a parabola are recognized.

As to the determination of ultimate loads, the same statements apply here as above. Mr. Hribar agrees that as the cross-section or the stress-strain curve becomes more unwieldy the pressure line concept becomes more powerful. No further comments are required by the author.

In conclusion, the writer is grateful to Mr. Hribar for the opportunity to emphasize certain aspects of the pressure line concept.

DEFLECTIONS OF STRUCTURES IN THE INELASTIC RANGE[a]

Discussion by John H. Percy

JOHN H. PERCY.[1]—Mr. Gerstle's paper may be considered in two parts, namely the computation of suitable coefficients to describe the behavior of elements of a structure and the use of charts showing these coefficients to determine deflections in any particular case. The second part holds no matter what shape the curves take (provided always that the coefficients are single valued). The treatment would therefore be more general if the charts could readily be drawn for any section shape and any stress-strain relationship.

If ϕ is the curvature of a member subjected to a bending moment M the relationship between the two will, in general, have the form shown nondimensionally in figure (a).

For figure 1 of the paper, taking the origin at A and measuring X along the beam, geometry gives

$$\delta_{AB} = \int_0^L \phi\, x\, dx \quad ; \quad \theta_{AB} = \int_0^L \phi\, dx \,.$$

From these it follows, using

$$\frac{M}{M_{yp}} = h - \left(\frac{h-k}{L}\right) x$$

that

$$\delta_{AB} = \frac{M_{yp} L^2}{EI} \cdot \frac{1}{(h-k)^2} \int_{\frac{M}{M_{yp}}=k}^{h} \frac{EI\phi}{M_{yp}} \left(h - \frac{M}{M_{yl}}\right) d\left(\frac{M}{M_{yp}}\right) = C_1 \frac{M_{yp} L^2}{EI}$$

$$\theta_{AB} = \frac{M_{yp} L}{EI} \cdot \frac{1}{(h-k)} \int_{\frac{M}{M_{yp}}=k}^{h} \frac{EI\phi}{M_{yp}}\, d\left(\frac{M}{M_{yp}}\right) = C_2 \frac{M_{yp} L}{EI}$$

a. Proc. Paper 1290, January, 1957, by Kurt H. Gerstle.

1. Lecturer in Civ. Eng., Univ. of Auckland, New Zealand.

where C_1, C_2 are the coefficients shown in figures 2 and 3 of the paper.

Now, if gMyp is any bending moment and if, in figure (a), Pg is the area and Qg the first moment of area about the ϕ axis of the region OAB it follows immediately that

$$C_1 = \frac{h(Q_h - Q_k) - (P_h - P_k)}{(h-k)^2}$$

$$C_2 = \frac{Q_h - Q_k}{h - k} .$$

A similar analysis for figure 5 of the paper does not lead to such straightforward results for θAC and δAC but it can be shown that

$$\delta_{AC} = C_1 \frac{M_{yf} L^2}{EI} \text{ where } C_1 = \frac{1}{2\sqrt{n-\kappa}} \int_{\frac{M}{M_{yp}}=k}^{n} \frac{EI\phi}{M_{yp}} \frac{d\left(\frac{M}{M_{yf}}\right)}{\sqrt{n - \frac{M}{M_{yf}}}} - \frac{1}{2(n-k)} \int_{\frac{M}{M_{yf}}=\kappa}^{n} \frac{EI\phi}{M_{yp}} d\left(\frac{M}{M_{yf}}\right)$$

$$\delta_{CA} = C_1 \frac{M_{yf} L^2}{EI} \text{ where } C_1 = \frac{1}{2(n-k)} \int_{\frac{M}{M_{yp}}=k}^{n} \frac{EI\phi}{M_{yf}} d\left(\frac{M}{M_{yp}}\right)$$

$$\theta_{AC} = C_2 \frac{M_{yf} L}{EI} \text{ where } C_2 = \frac{1}{2\sqrt{n-k}} \int_{\frac{M}{M_{yf}}=k}^{n} \frac{EI\phi}{M_{yf}} \frac{d\left(\frac{M}{M_{yf}}\right)}{\sqrt{n - \frac{M}{M_{yf}}}} .$$

(It is worth noting the rather surprising result that δ_{CA} for this case and θ_{AB} for figure 1 differ only by a constant factor $\frac{L}{2}$ for any bending moment-curvature relationship. The curves in figures 3 and 5 of the paper are therefore essentially the same.)

The coefficients of the paper may thus be calculated without difficulty for any bending moment-curvature relationship.

This is best found by direct experiment for any particular material and section shape, since the determination of the stress-strain relationship with sufficient accuracy for use in calculating flexural deformations is a precision laboratory task requiring considerable care (c.f. Roderick and Phillipps).(i) If necessary however the bending moment-curvature relationship for any section may be derived from the stress-strain relationship by methods similar to those used by Hrennikoff,(ii) Phillips,(iii) Roderick,(iv) and others.

REFERENCES

i. J. W. Roderick and I. H. Phillipps. "The carrying capacity of simply supported mild steel beams." Research; Engineering Structures Supplement. 1949. (Coltston Papers) pp. 9-47.

ii. A. Hrennikoff. "Theory of inelastic bending with reference to limit design." Trans. Am. Soc. C. E. vol. 113, 1948. pp. 213-247.

iii. A. Phillips. "A general method of calculating the $M_{\epsilon max}$ diagram in plastic bending of beams." Am. Soc. Mech. E.-Trans. (Journ. App. Mech.) vol. 18, 1951, pp. 353-358.

iv. J. W. Roderick. "The load-deflection relationship for a partially plastic rolled steel joist." British Welding Journal, vol 1, 1954. pp. 78-82.

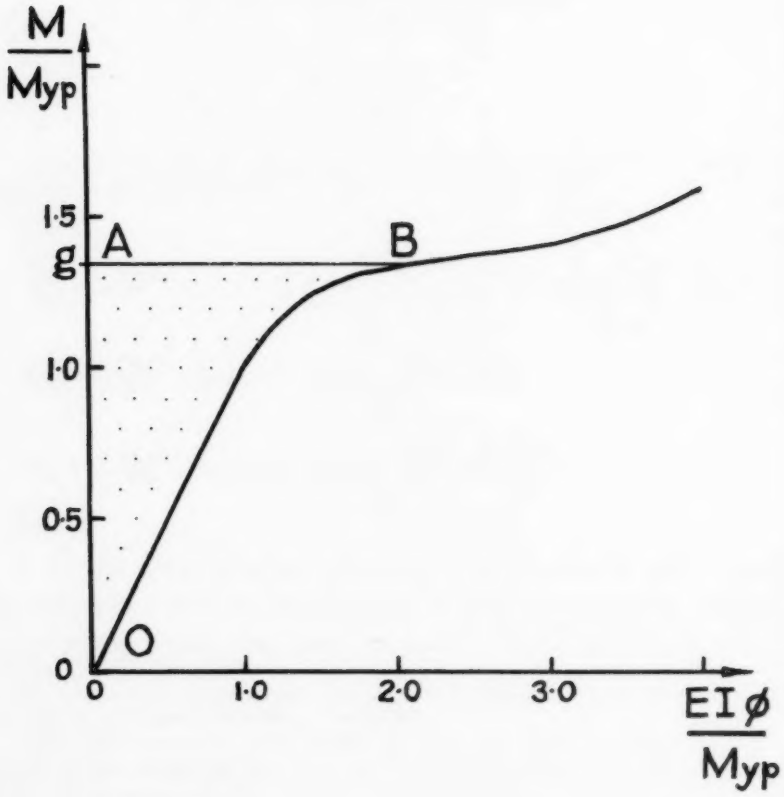

Fig. a. Relationship between Bending Moment and Curvature.

THE LATERAL RIGIDITY OF SUSPENSION BRIDGES[a]

Discussion by Arne Selberg

ARNE SELBERG.*—The paper demonstrates that the uniform distribution method is of little value for statical calculations. A short investigation will demonstrate that, for example, a triangular distribution will give a better result. However, there is little reason for using any such approximate solutions.

Theimer,(1) in 1941, has given the same solution for statical computations as given by Silverman in his Elastic Distribution Method. Theimer also used dimensionless parameters in his analysis. However, the solution as given by Silverman will be somewhat more convenient in use.

The calculated example demonstrate a slow convergence for the series when calculating moments.

Introducing (2,3)

$$z = p\left(\frac{v-u}{h}\right) = \sum H_n \sin\frac{n\pi x}{l}$$

instead of the series

$$v = \frac{l^4}{EI_v}\sum a_n \sin\frac{n\pi x}{l}$$

will improve the convergence.

The reason is that the first series is integrated twice when finding the moment, the second series has to be derivated twice.

In his investigations on the oscillations in the horizontal plane. Silverman gives what appears to be an erroneous equation (7), and all results obtained from this equation are erroneous as well. It is easily demonstrated on a model that his results are incorrect.

With the notations of Silverman, the equations for any oscillations will be:

$$EI_v v^{IV} = -z - m_s \ddot{v}$$

$$-Hu'' = z - m_c \ddot{u}$$

a. Proc. Paper 1292, July, 1957, by I. K. Silverman.

* Prof. of Theory of Structures, Norwegian Technical Univ., Trondheim, Norway.

m_S and m_C being mass of suspended structure and cables respectively. Table III demonstrate clearly that m_S and m_C both are of importance.

From these equations it is impossible to get eq. (7) given by Silverman. Introducing

$$Z = p\left(\frac{v-u}{h}\right) = \sum A_n \sin\frac{n\pi x}{l} \cdot \sin\omega t$$

and

$$v = v_0 \cdot \sin\omega t \; ; \; u = u_0 \cdot \sin\omega t$$

we get

$$EI_v v_0^{IV} - m_s\omega^2 v_0 = -Z_0 = -\sum A_n \sin n\pi\frac{x}{l}$$

$$-H u_0'' - m_c\omega^2 u_0 = Z_0 = \sum A_n \sin n\pi\frac{x}{l}$$

These equations yield

$$v_0 = \sum \frac{-A_n}{EI_v\frac{\pi^4}{l^4}n^4 - m_s\omega^2} \cdot \sin n\pi\frac{x}{l}$$

$$u_0 = \sum \frac{A_n}{H\frac{\pi^2}{l^2}n^2 - m_c\omega^2} \sin n\pi\frac{x}{l}$$

The coefficients A_n are given by the equation

$$Z_0 = \frac{p}{h}(v_0 - u_0) = \sum A_n \sin n\pi\frac{x}{l}$$

The easiest solution is obtained by requiring that this equation shall be satisfied for distinct values of x. A somewhat better solution is given by requiring:

$$\int_0^l p(v_0 - u_0)\sin r\pi\frac{x}{l}\,dx = \int_0^l \left(\sum A_n \sin n\pi\frac{x}{l}\right)h \cdot \sin r\pi\frac{x}{l}\,dx$$

Both methods give a set of linear equations for A_n, and ω^2 is given by $|D| = 0$.

With only one term

$$Z_0 = A_1 \sin\pi\frac{x}{l}$$

we have with the two methods:

Method 1.

$$\left[\frac{1}{EI_v\frac{\pi^4}{l^4}-m_s\omega^2}+\frac{1}{H\frac{\pi^2}{l^2}-m_c\omega^2}\right]=-\frac{\eta_s-\eta_c}{p}$$

requiring $\frac{p}{n}(v_o-u_o)=z_o$ at the middle of the span.

Method 2.

$$\left[\frac{1}{EI_v\frac{\pi^4}{l^4}-m_s\omega^2}+\frac{1}{H\frac{\pi^2}{l^2}-m_c\omega^2}\right]=-\frac{\eta_s-\left(\frac{2}{3}+\frac{2}{\pi^2}\right)\eta_c}{p}$$

The difference in results of the two methods are insignificant for most bridges.

Both equations usually give two values of ω_1 e.g. cable and truss oscillating in same or opposite direction, only the first one is of special interest to bridge designers.

As the horizontal oscillations of a suspension bridge is of secondary importance for the designer it will be little reason for using more than one or two terms in an actual calculation.

For Tacoma Narrows (1940) the 2 formulas give

$$\omega_1 = 0{,}44\ (5{,}3) \quad \text{and} \quad N_1 = 4{,}2\ \text{min}^{-1}\ (50{,}6)$$

or

$$\omega_1 = 0{,}42\ (2{,}1) \quad \text{and} \quad N_1 = 4{,}0\ \text{min}^{-1}\ (20{,}1)$$

respectively.

A solution with two terms A_1; A_3 give:

$$N_1 = 4.1\ \text{min}^{-1}\ (22.9) \quad \text{and} \quad N_3 = 16.1\ \text{min}^{-1}\ (36.5)$$

The difference in N_1 is insignificant. The number in parentheses is for cable and truss oscillating in opposite direction. Silverman give $N_1 = 9{,}9$ min^{-1} for this bridge.

BIBLIOGRAPHY

1. O. F. Theimer: Der Bauingenieur 1941.
2. A. Selberg: Der Stahlbau 1941.
3. A. Selberg: Publications V. 7. Int. Ass. f. Bridge and Structural Eng. 1943/44.

ANALYSIS OF CONTINUOUS BEAMS[a]

Discussion by S. J. Medwadowski

S. J. MEDWADOWSKI,[1] A.M. ASCE.—Two principal advantages, achieved at a presumably slight loss of accuracy, are claimed by the author for the use of the Fourier series technique in the analysis of problems of continuous beams of constant bending rigidity. These are:

a. the possibility of representing deflection, and related quantities, by means of a single expression valid for $0 \leqslant x \leqslant \ell$;

b. the numerical work being reduced to a minimum.

The first of these advantages results also by employing classical methods leading to a closed form solution if use is made of the Heaviside unit function.[2] The closed form solution yields exact (within the assumptions of the theory) results; in addition it possesses the advantage of yielding directly closed form expressions for bending moments and shears, as well as slope, by formally differentiating the expression for deflection. Because of poor convergence of the series involved these expressions have to be found by a separate, indirect procedure if the Fourier series representation is used, as pointed out by the author on p. 7 of the paper.

Any saving in the numerical work involved in calculating the unknown reactions R_i must occur in the calculation of the coefficients of Eqs. (15), in particular in calculating the coefficients D_{ij}, defined in Eqs. (17). Written in a somewhat more compact notation the definition is:

$$D_{ij} = \sum_{n=1}^{\infty} (1/n^4) \sin(n\pi a_i) \sin(n\pi a_j); \qquad (A)$$

It is easy to show that the closed form solution leads to the following, essentially equivalent, definition:

$$D'_{ij} = a_j (1 - a_i) \left[a_i (2 - a_i) - a_j^2 \right]; \qquad (i \geqslant j) \qquad (B)$$

a. Proc. Paper 1399, October, 1957, by Seng-Lip Lee.

1. Head, Structural Dept., John A. Carollo, Cons. Engrs., Berkeley, Calif.

2. A popular yet clear and concise presentation is given in "The Application of Heaviside's Step-Function to Beam Problems," by John E. Goldberg, Proc. ASCE, Separate No. 202, 1953.

In both cases $D_{ij} = D_{ji}$. It is readily seen that the numerical work of calculating D_{ij} from Eq. (A) involves eleven operations (if only two terms of the series are retained), while the use of Eq. (B) results in six operations only and yields an exact value of the coefficient.

Thus it would appear that the advantages claimed by the author for the Fourier series representation are in fact illusory.

The system of Eqs. (15) of the paper is usually derived directly from Eq. (11) by substituting in it the prescribed deformations $y(a_i') = - d_i$. It would be of interest to learn the author's reasons for making use of Castigliano's theorem instead, a somewhat lengthier procedure.

It is well known that a formal application of the Fourier series expansion technique often yields solution of a physical problem, even though some of the series involved in the process may be divergent. Bending of continuous beams is such a problem. However, the author's statement of p. 3 of the paper, to the effect that a function may be "approximated" by a Fourier series, is incorrect.

The application of the Fourier series representation to problems of static bending of continuous beams may be considered a particular case of the problem of dynamic bending, treated by Saibel and D'Appolonia.[3] It is hoped that a more complete list of references will be provided by the author in his closing discussion.

3. "Forced Vibrations of Continuous Beams," by Edward Saibel and Elio D'Appolonia, Proc. ASCE, Separate No. 100, 1951.

AMERICAN SOCIETY OF CIVIL ENGINEERS

OFFICERS FOR 1954

PRESIDENT

LOUIS R. HOWSON

VICE-PRESIDENTS

Term expires October, 1954:
FRANCIS S. FRIEL
NORMAN R. MOORE

Term expires October, 1955:
WALDO G. BOWMAN
SAMUEL B. MORRIS

DIRECTORS

Term expires October, 1954:
JOHN P. RILEY
GERRY H. BROWN
MASON G. PRICHARD
ROBERT E. SHERLOCK
R. ROBINSON ROWE
LOUIS T. RYDELL
CLARENCE L. ECKEL

Term expires October, 1955:
CLINTON D. HANOVER, Jr.
E. LELAND DORKEE
HOWARD F. PECKWORTH
FINLEY B. LAVERTY
WILLIAM J. HEDLEY
RANDLE B. ALEXANDER

Term expires October, 1956:
PHILIP C. RUTLEDGE
WESTON S. EVANS
TILTON E. SHELBURNE
CRAIG P. SICKLER
DONALD H. MATTERN
JOHN E. RINNE

PAST PRESIDENTS

Members of the Board

ENOCH R. NEEBLES — MASON G. LOCKWOOD

EXECUTIVE SECRETARY
WILLIAM H. WISELY

TREASURER
CHARLES E. TROUT

ASSISTANT SECRETARY
E. LAWRENCE CHANDLER

ASSISTANT TREASURER
CARLTON S. PROCTOR

PROCEEDINGS OF THE SOCIETY

HAROLD T. LARSEN
Manager of Technical Publications

PAUL A. PARISI
Editor of Technical Publications

FRANCIS J. SCHNELLER, JR.
Assistant Editor of Technical Publications

COMMITTEE ON PUBLICATIONS

HOWARD F. PECKWORTH, *Chairman*
PHILIP C. RUTLEDGE, *Vice-Chairman*

E. LELAND DORKEE
TILTON E. SHELBURNE

R. ROBINSON ROWE
LOUIS T. RYDELL